Geometry and Physics of Entanglement

A dissertation presented

by

Kumar Shivam

to

The Department of Physics
in fulfillment of the requirements
for the degree of
Doctor of Philosophy
in the subject of

Physics
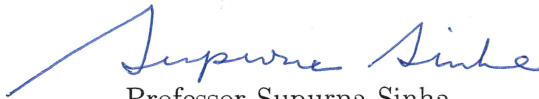
Raman Research Institute
Bangalore, India
April 2018

Dedicated to my mother Snehlata

Declaration

I, hereby, declare that this thesis is composed independently by me at Raman Research Institute, Bangalore, India, under the supervision of Prof. Supurna Sinha. The subject matter presented has not been previously formed the basis of the award of any degree, diploma, associateship, fellowship or another similar title in any other university. I also declare that I have run it through the *Turnitin* plagiarism software.

Professor Supurna Sinha

Theoretical Physics
Raman Research Institute
Bangalore - 560080
India.

Kumar Shivam

Certificate

This is to certify that the thesis entitled "**Geometry and Physics of Entanglement**" submitted by Kumar Shivam for the award of the degree of doctor of philosophy of Jawaharlal Nehru University is his original work. This has not been published or submitted to any other University for any other Degree or Diploma.

Professor Ravi Subrahmanyam

(Center Chairperson)

Director

Raman Research Institute

Bangalore - 560080

India.

Professor Supurna Sinha

(Thesis Supervisor)

Thesis Advisor   Author

Supurna Sinha   **Kumar Shivam**

Geometry and Physics of Entanglement

Synopsis

In this thesis, the issue of quantum entanglement is studied from a geometrical perspective. We have explored the geometry of the quantum state space and relativistic space-time structure to study the condition for detecting quantum entanglement in bipartite quantum systems.

The issue of entanglement is then explored in the context of quantum measurement. In all quantum measurement process, the observable to be measured is coupled to a suitable pointer degree of freedom. This coupling establishes an entanglement between state of the system and the pointer state. By reading the pointer variable we obtain information about the observable. The extent of entanglement between the pointer state and the system state then sets a limit on the amount of information that can be obtained by reading the pointer variable. We have used this concept in the analysis of the Stern-Gerlach experiment and explored the concept of coarse measurement in the quantum phase space.

Later, we investigated the role of quantum entanglement in distinguishing two quantum states. We explored the geometry of quantum state space and looked at a couple of the Riemannian metrics (namely the BH and the BKM metrics) that can be defined on these space. We give a geometrical picture of the space of density matrices analogous to that of MacAdam ellipses on the space of colours. Some of these metrics can better distinguish between two neighbouring quantum states if we use entanglement between the copies of states. We also explore the thermodynamic

meaning of the metric and establish a relation between the fluctuations in the free energy with the BKM-metric.

Finally, we prove a theorem which states that any two parameters (location-μ and scaling-σ) sub-manifold of a classical probability distribution is isomorphic to the Poincaré half plane.

The thesis is structured as follows. In chapter 1, we present an overview of the subject matter and discuss some of the earlier work on quantum entanglement and measurement. In chapter 2, we discuss a space-time approach of detecting quantum entanglement, where we show with a few examples how this criterion works using a Mathematica program. Chapter 3 discusses the Lorentzian Singular Value decomposition and gives the details and the proofs related to the entanglement test proposed in chapter 2. In chapter 4 we discuss the role of entanglement in a quantum measurement, where we calculate the entanglement entropy between the spin and the center of mass of the silver atom and argue that when there is sufficient entanglement between them coarse-graining the Wigner function can give some information about the spin of the atom. In chapter 5, we discuss how entanglement can lead to better discrimination of quantum states. We give an operational meaning to the BKM- metric on the quantum statistical manifold and discuss its relation with the fluctuation in the free energy. In chapter 6, we state and prove a theorem stating that any two parameter sub-manifold of a classical probability space is isomorphic to the Poincaré half plane. Finally, in chapter 7, we end the thesis with some concluding remarks and discuss future directions.

Contents

Citations to Previously Published Work

Large portions of Chapter 2 appeared in the following:

"Detecting qubit entanglement : an alternative to the PPT test", Joseph Samuel, Kumar Shivam,Supurna Sinha
arXiv:1712.06801 [quant-ph]

Chapter 3 in the following paper:

"Lorentzian geometry of qubit entanglement", Joseph Samuel, Kumar Shivam, Supurna Sinha
Annals of Physics Volume 396, September 2018, Pages 159-172

Chapter 4 in the following paper:

"Coarse Quantum Measurement-An analysis of Stern-Gerlach experiment", Anirudh Reddy, Joseph Samuel, Kumar Shivam, Supurna Sinha
Physics Letters A Volume 380, Issues 1112, 11 March 2016, Physics Letters A

and Chapter 5 in the following paper:

"Geometry and Entropy of Quantum States", Kumar Shivam, Anirudh Reddy, Joseph Samuel, Supurna Sinha
International Journal of Quantum Information, World Scientific Publishing, Vol. 16, No. 04, 1850032 (2018)

Acknowledgments

Doing a Ph.D. at Raman Research Institute is one of the most beautiful experiences of my life. A better understanding of the working of the physical world around me has been a priceless experience at RRI. The vibrant green floral campus gives an amazingly pleasant working environment which will always remain close to my heart.

I like to thank Prof. Supurna Sinha for her constant valuable guidance in completing this work. I have learned a lot from her. I admire her ability to express an idea very clearly. She always keeps a constant flow of good ideas in our group which kept us motivated. I would also like to thank her for teaching us how to write good papers, give good talks and posters. She also gave necessary push whenever I needed. It was an enjoyable experience working with her.

I am grateful to Prof. Joseph Samuel for educating us with his insights in quantum mechanics, probability theory, algebraic and differential geometry. Sam has always kept us wondering with his very insightful yet straightforward reasoning using elementary geometry, calculus, and algebra. He always kept us motivated and focused with his ability to cut through mathematical clutter and see useful results. It was a wonderful and very enriching experience working with him.

I would also like to thank all the other faculty members of the institute especially, Prof. Sanjib Sabhapandit, Prof. Sumati Surya, Prof. Sadiq Rangwala, Prof. Avinash Deshpande, Prof. Yashodhan Hatwale, Prof. Urbasi Sinha, Prof. Shiv Sethi, for exciting and stimulating discussions on various topics related to physics, mathematics, society and politics. I was very fortunate to be a part of those informal discussions. It gave me a wider perspective and understanding of things happening around. I also thank Anirudh Reddy for his valuable discussions on two of the joint projects that

we have done. He has a very useful quality of making good guesses. We make a good team as we have complementary strengths.

I would also like to thank our group secretary Manjunath for his constant assistance in all administration related work. He has been a great friend too. At times, he gave valuable suggestions which helped me maintain my composure and patience. He was always up for a quick chat, which acted as a very good stress-buster for me.

I thank all my colleagues, Sujit Kumar Nath, Siman Raj, Niranjan, Deepak, Shantanu, Nomaan, Abhishek, Vardhan for making my stay in this institute very productive. I am definitely going to miss our *tea time physics* discussions.

I also thank all the staff of TP (Mahadeva, Sashi), Library (Manju, Meera) for the help in completing the printing, binding and doing the plagiarism check for the thesis. I thank Radha, Marisa and Vidya, Subramanian V. G. from the administration for all the help and support. I thank our IT department especially Jacob, Krishnamurthy and Karthik for helping me a number of times with my desktop issues.

I would like to extend my thanks to all the seniors Chaitra, Prasad, Suman, batch mate, Raj, Debshankar, Sushil, and juniors Sanjay, Amit, Jaanki, with whom I had a wonderful time. I would also like to thank all my cricket and football buddies at RRI, Shafi, Marichandran, Swaminathan, Jagadish, Anindya, Ashutosh who contributed indirectly to my physical and mental well being.

Finally, I would like to thank my lady-love Sakshi, my mother Snehlata, father Prabhat and brother Harshit for all their support and affection. I would also like to thank all my family members and friends Anjali, Rajani, Indu, Hema, Anu, Onkar, Lakshminath, Anand, Pushpam, Pratyush, Adarsh, SB Dixit, Vidyanand Chaudhary,

Milind, Deepak, Avinash, Rakesh, Anurag, for their love and support.

Chapter 1

Introduction

1.1 Entanglement: A useful resource

Quantum entanglement is one of the most important quantum resources which has no classical counterpart. Subsystems comprising a quantum system are considered to be entangled if it is not possible to ascribe states to the individual subsystems comprising the full quantum system. For example, consider a spin singlet state of a pair of electrons $|\Psi_{AB}\rangle = 1/\sqrt{2}(|\uparrow_A\rangle |\downarrow_B\rangle - |\downarrow_A\rangle |\uparrow_B\rangle)$, where $|\uparrow\rangle$ and $|\downarrow\rangle$ represent spin "up" and "down" along z-axis and A and B label the two electrons. Clearly, this state can't be written in the form $|\psi_A\rangle |\psi_B\rangle$ where $|\psi_A\rangle$ and $|\psi_B\rangle$ are the states of the individual electrons. The subsystems of a bipartite quantum system are correlated in such a way that measurement on one of the subsystems determines the possible state of the other. This means that when we measure the state of one of the subsystems, the measurement affects the possible result that one could obtain when measuring the other subsystem.

Quantum entanglement is not just an interesting mathematical concept which is a subject of philosophical debate, it has also been put to real life applications. It is a resource which can be utilized to perform tasks that are not possible to do classically. For example, Bennett etal. have shown that sharing a pair of entangled states and communicating classically it is possible to teleport[1] a quantum state. Entanglement turns out to be a useful resource in teleportation.

1.1.1 Quantum Teleportation

In order to see how it is used as a resource (which doesn't have any classical counterpart) in teleportation[2] of a quantum state, consider two parties Alice and Bob sharing a *maximally entangled* state $\left|\phi_{AB}^{+}\right\rangle = \frac{1}{\sqrt{2}}(\left|\uparrow_A\uparrow_B\right\rangle+\left|\downarrow_A\downarrow_B\right\rangle)$ where A and B refer to Alice's and Bob's qubit respectively. Alice wants to teleport a quantum state $\left|\psi_S\right\rangle = \frac{1}{\sqrt{2}}(\alpha\left|\uparrow_S\right\rangle + \beta\left|\downarrow_S\right\rangle)$ to Bob. To this end Alice performs a joint measurement (in the Bell basis $\{\left|\phi_{AS}^{+}\right\rangle, \left|\phi_{AS}^{-}\right\rangle, \left|\psi_{AS}^{+}\right\rangle, \left|\psi_{AS}^{-}\right\rangle\}$) on both the qubits in her possession; one which is entangled with Bob's qubit and the one she wants to teleport. This immediately collapses Bob's qubit to one of the following states respectively $\{\alpha\left|\uparrow_B\right\rangle+ \beta\left|\downarrow_B\right\rangle, \alpha\left|\uparrow_B\right\rangle-\beta\left|\downarrow_B\right\rangle, \beta\left|\uparrow_B\right\rangle+\alpha\left|\downarrow_B\right\rangle, \beta\left|\uparrow_B\right\rangle-\alpha\left|\downarrow_B\right\rangle\}$. If Alice communicates to Bob her measurement outcome over a classical channel, then Bob can apply an appropriate local unitary transformation on his qubit to prepare the desired output. For example, let Alice obtain $\left|\psi_{AS}^{+}\right\rangle$ as the outcome of her measurement and communicate it to Bob. Bob will know with certainty that the state of his qubit is $\beta\left|\uparrow_B\right\rangle + \alpha\left|\downarrow_B\right\rangle$ so he will apply a σ_z operation on his qubit and transform his quantum state to exactly $\left|\psi_S\right\rangle$. Alice has successfully teleported her quantum state to Bob. We must note here two

things. First, energy or matter is not teleported in this protocol, only the state of a quantum system(Alice's quantum state $|\psi_S\rangle$) has been teleported. Second, the need for a classical communication channel, over which Alice needs to send the information of her measurement outcome. Unless she communicates(classically) her measurement result to Bob, she will not be able to teleport her quantum state. Hence, it doesn't violate Special Relativity. The other thing to be noticed is the role of sharing an entangled qubit (e-bit). The teleportation protocol necessarily requires sharing a maximally entangled e-bit, in the absence of which it is not possible to teleport a quantum state. Teleportation is secure against eavesdropping. If an eavesdropper intercepts the classical communication between Alice and Bob, she/he will not be able to produce the quantum state since it requires sharing an e-bit between the sender and the receiver.

One of the other domains where entanglement is used extensively as a valuable resource is quantum cryptography[3, 4]. In a typical cryptographic problem, a sender (say Alice) encrypts a message for an intended recipient (say Bob) then she shares a key through a secure channel so that the intended recipient can decrypt the message. The security of the communication then depends on the security of the channel used for sharing the key.

1.1.2   Quantum Key Distribution Protocol: E-91

In this protocol, maximally entangled pairs of photons are shared between two parties say Alice and Bob. These entangled photons can be created either by Alice or Bob or any other third party such that both Alice and Bob get one photon from

each entangled pair say $\left|\phi_{AB}^{+}\right\rangle = 1/\sqrt{2}(|+,-\rangle - |-,+\rangle)$. The reliability of the key distribution is guaranteed by the following two properties of entanglement.

I. The measurement outcomes of a pair of entangled states are perfectly correlated. That is to say if Alice performs a measurement on her qubit and finds her state to be $|-\rangle$ then if Bob chooses a compatible basis he will obtain $|+\rangle$ with 100% certainty. Instead, if Bob chooses an incompatible basis, his result will be random.

II. An attempt to measure one of the subsystems will introduce local realism to the system and will destroy the quantum correlation.

The first step of the protocol involves measuring the entangled photon in some set of pre agreed bases say $\{A_0, A_{\pi/4}, A_{\pi/2}\}$ for Alice and $\{B_{\pi/4}, B_{\pi/2}, B_{3\pi/4}\}$ for Bob where A_θ, B_θ are the bases obtained by rotating $|+\rangle$ by an angle θ about z-axis[5]. Both the parties randomly choose measurement basis for each entangled pair and the order of choice of bases is kept secret till the end of the protocol. Consider the following correlation coefficient of the measurement along A_θ and B_ϕ

$$E(A_\theta, B_\phi) = P_{++}(A_\theta, B_\phi) + P_{--}(A_\theta, B_\phi) - P_{+-}(A_\theta, B_\phi) - P_{-+}(A_\theta, B_\phi) \qquad (1.1)$$

Where $P_{+-}(A_\theta, B_\phi)$ denotes the probability of obtaining spin $+1$ along A_θ and -1 along B_ϕ and other quantities are defined analogously. Using quantum mechanics one can show $E(A_\theta, B_\phi) = -A_\theta.B_\phi$. If Alice and Bob use compatible bases for the measurements on their entangled photon, they will obtain a perfectly anti-correlated measurement outcome which will be the case roughly with a probability of 2/9. When

Alice and Bob use different measurement bases then the following correlation coefficient:

$$S = E(A_0, B_{\pi/4}) + E(A_{\pi/2}, B_{\pi/4}) + E(A_{\pi/2}, B_{3\pi/4}) - E(A_0, B_{3\pi/4})$$

must respect the CHSH(Clauser Horne Shimony Holt) inequality i.e $S \leq 2\sqrt{2}$. A classical communication channel is needed in the second step where Alice and Bob communicate with each other about the sequence of their measurement bases for successive entangled pairs. This will divide the measurement outcome into two sets, one being the set of perfectly anti-correlated outcomes which will be the case when they use same bases for their measurement and the second when they use different bases for measurement. They can announce the second set of outcomes and must find for this set S saturates the CHSH inequality. If there is an eavesdropper trying to get information either by manipulating the source that creates entanglement or by doing measurement on any of the two qubits he/she will introduce a local realism. In that case $S \leq 2$. Artur Ekert highlights the security of the protocol[4] in the following lines :

> The eavesdropper cannot elicit any information from the particles while in transit from the source to the legitimate users, simply because there is no information encoded there. The information "comes into being" only after the legitimate users perform measurements and communicate in public afterwards

Entanglement can be used to perform other interesting and useful tasks which are otherwise impossible to do. For example, the complexity of a communication can be reduced using entangled states [6]. A pair of entangled states shared between two spatially separated parties can be used to synchronize atomic clocks [7]. Entanglement has given a better understanding of phenomena like high-temperature

superconductivity[8] and it has been shown that macroscopic entanglement can exist at high temperatures[9].

1.2 Detecting Entanglement

Detecting entanglement in a general quantum system is a NP(non-deterministic polynomial time) hard problem[10]. However, it is an easy and achievable task for a given class of bipartite quantum states. For example, we will see in the rest of this Section that it is feasible to detect entanglement in an arbitrary pure state and some low dimensional mixed bipartite states.

1.2.1 Entanglement in pure bipartite systems

I. Pure separable states have *pure* sub-systems

The state of a composite pure bipartite system consisting of two parts A and B is a vector in the Hilbert space $\mathcal{H}^{AB} = \mathcal{H}^A \otimes \mathcal{H}^B$ which has a *tensorial structure*. The easiest way to check if a bipartite quantum state ρ_{AB} is entangled or not is to look at the subsystem density matrix ρ_A (or ρ_B) that can be obtained by partially tracing out B(or A) from the composite system. If the subsystem density matrix ρ_A turns out to be a pure density matrix, then the system is separable else it is entangled. To see this let us consider a pure bipartite quantum state $|\Psi_{AB}\rangle = |\psi_A\rangle |\psi_B\rangle$. The density operator for this state is $\rho_{AB} = |\psi_A\rangle \langle\psi_A| \otimes |\psi_B\rangle \langle\psi_B|$. Let us now calculate the subsystem density matrix say $\rho_A = \mathbf{tr}_B [\rho_{AB}]$ where $\mathbf{tr}_B [.]$ represents partial trace over the subsystem B. In order to perform partial trace over B let $\{|i_B\rangle\}$ be an

orthonormal basis for $\mathcal{H}^B$. Then,

$$\rho_A = \mathbf{tr}_B\left[\rho_{AB}\right]$$

$$= \sum_{i_B} |\psi_A\rangle\langle\psi_A| \otimes \underbrace{\langle i_B|\left(|\psi_B\rangle\langle\psi_B|\right)|i_B\rangle}_{=1}$$

$$= |\psi_A\rangle\langle\psi_A|$$

is a one dimensional projector corresponding to the pure state of the subsystem A.

Hence for a pure separable state individual subsystems are also pure.

Example:

Consider a two level bipartite quantum state $|\psi_+\rangle = \frac{1}{\sqrt{2}}(|0_A 0_B\rangle + |1_A 1_B\rangle)$. The density operator for this state is

$$\rho_{AB} = |\psi_+\rangle\langle\psi_+|$$

$$= \frac{1}{2}(|0_A 0_B\rangle\langle 0_A 0_B| + |0_A 0_B\rangle\langle 1_A 1_B| + |1_A 1_B\rangle\langle 0_A 0_B| + |1_A 1_B\rangle\langle 1_A 1_B|)$$

The matrix form of the state in the basis $\{|0_A 0_B\rangle, |0_A 1_B\rangle, |1_A 0_B\rangle, |1_A 1_B\rangle\}$ looks like

$$\rho_{AB} = \begin{pmatrix} \frac{1}{2} & 0 & 0 & \frac{1}{2} \\ 0 & 0 & 0 & 0 \\ 0 & 0 & 0 & 0 \\ \frac{1}{2} & 0 & 0 & \frac{1}{2} \end{pmatrix}$$

If we trace over the first subsystem A i.e. $\mathbf{tr}_A\left[\rho_{AB}\right] = \sum_{i=0}^{1}\langle i_A|\rho_{AB}|i_A\rangle$ then the reduced density operator turns out to be

$$\rho_B = \frac{1}{2}(|0_B\rangle\langle 0_B| + |1_B\rangle\langle 1_B|)$$

$$= \begin{pmatrix} \frac{1}{2} & 0 \\ 0 & \frac{1}{2} \end{pmatrix}$$

which is not a pure state density operator for the subsystem B as $\mathbf{tr}\left[\rho_B^2\right] = \frac{1}{2} < 1$, hence the density operator represents an entangled state. Notice here that if a composite quantum system is in an entangled state, then the best possible knowledge of the composite system doesn't offer us the best possible knowledge of the subsystems. This feature is special to quantum systems. In contrast, there is no classical counter part of this feature.

II. Pure separable states have *unit* Schmidt rank

A commonly used concept in the detection and quantification of entanglement is the Schmidt decomposition. If $|\Psi_{AB}\rangle$ is a pure state of a bipartite system in $\mathcal{H}^{AB}$ then there exist orthonormal bases $\{|s_A\rangle\}$, $\{|s_B\rangle\}$ for $\mathcal{H}^A$ and $\mathcal{H}^B$ respectively such that

$$|\Psi_{AB}\rangle = \sum_s \sqrt{p_s} \, |s_A\rangle \, |s_B\rangle \tag{1.2}$$

where p_s are non-negative real numbers and $\sum_s p_s = 1$. The decomposition of the form (1.2) is known as the Schmidt decomposition and $\sqrt{p_s}$ are the Schmidt coefficients. The Schmidt rank r is defined as $min\{dsup.(\rho_A), dsup.(\rho_B)\}$, where $dsup.(\rho_A)$ represents the dimension of the support of ρ_A. A given state is separable[11] if and only if $r = 1$, which is easy to see as, if any state has only one term in the Schmidt decomposition then the reduced density matrix $\rho_A = |s_A\rangle \langle s_A|$ or $\rho_B = |s_B\rangle \langle s_B|$ will have only one non-zero eigenvalue, which means that the subsystem is in the pure state and hence the given state is separable.

Example:

Consider a bipartite pure state $|\Psi\rangle = \frac{1}{2}(|00\rangle + |01\rangle + |10\rangle + |11\rangle)$. We find the Schmidt

bases to be

$$\{\underbrace{\frac{1}{\sqrt{2}}(|0\rangle + |1\rangle)}_{|0_A\rangle}, \underbrace{\frac{1}{\sqrt{2}}(-|0\rangle + |1\rangle)}_{|1_A\rangle}\} \quad \text{and} \quad \{\underbrace{\frac{1}{\sqrt{2}}(|0\rangle + |1\rangle)}_{|0_B\rangle}, \underbrace{\frac{1}{\sqrt{2}}(|0\rangle - |1\rangle)}_{|1_B\rangle}\}$$

for $\mathcal{H}^A$ and $\mathcal{H}^B$ respectively and $\{p_1 = 1, p_2 = 0\}$. Clearly, the Schmidt decomposition for $|\Psi\rangle$ has only one term,

$$|\Psi\rangle = \frac{1}{\sqrt{2}}(|0\rangle + |1\rangle) \otimes \frac{1}{\sqrt{2}}(|0\rangle + |1\rangle)$$

which means it has *unit* Schmidt rank and hence it is a separable state.

1.2.2   Entanglement in mixed bipartite systems

It is harder to detect entanglement in mixed states. An impure bipartite quantum system is separable, if and only if it can be written in the following form

$$\rho_{AB} = \sum_i p_i \rho_A^i \otimes \rho_B^i \tag{1.3}$$

where ρ_A^i, ρ_B^i are the orthogonal projectors on $\mathcal{H}^A$ and $\mathcal{H}^B$ respectively, otherwise the state is an entangled state. There are several operational and non-operational ways to detect entanglement in mixed bipartite quantum systems.

I. Entanglement Witness

The set of separable quantum states forms a convex set(See Figure 1.1). This means that any convex combination of separable states is also a separable state. Using a theorem in functional analysis which goes by the name Hahn-Banach theorem Horodecki[12] proved the following theorem for separable quantum systems.

Theorem 1 (**Entanglement Witness Theorem (EWT)**). *A given density matrix* $\rho \in \mathcal{H}^A \otimes \mathcal{H}^B$ *is entangled if and only if, there exists a Hermitian operator* $\mathcal{O}$, *such that*

$$\boldsymbol{tr}\left[\mathcal{O}\rho\right] \leq 0 \qquad and \qquad \boldsymbol{tr}\left[\mathcal{O}\sigma\right] \geq 0 \qquad \forall \quad \sigma \in \mathcal{H}^{AB}_{separable} \qquad (1.4)$$

where $\mathcal{H}^{AB}_{separable}$ *denotes the separable subspace of the composite space* $\mathcal{H}^A \otimes \mathcal{H}^B$.
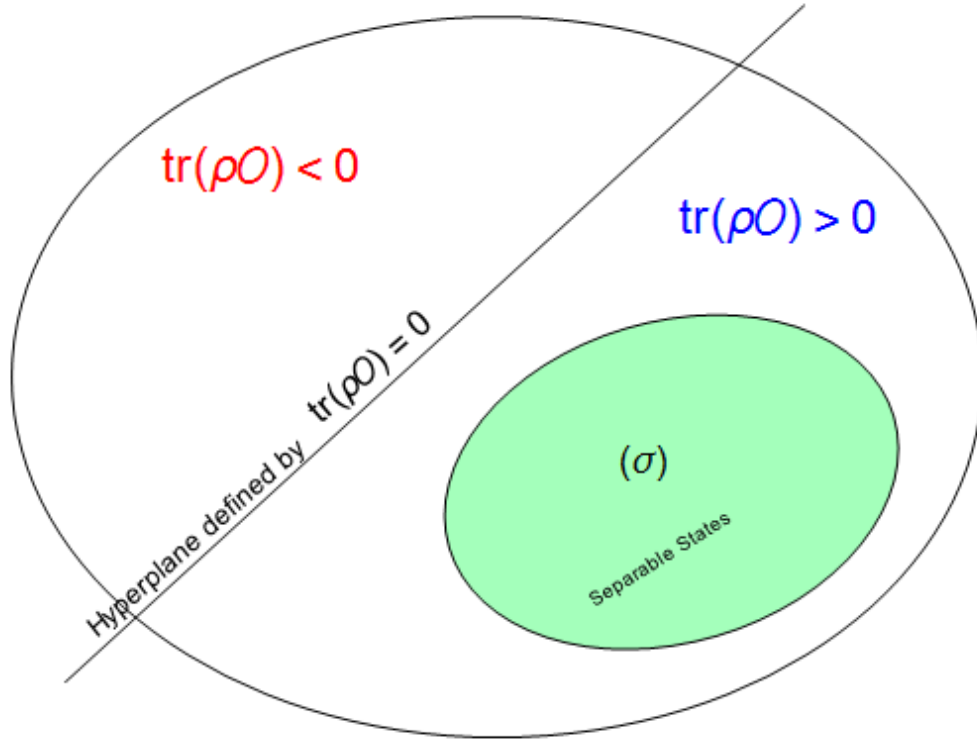
Figure 1.1: Set of separable states (σ) forms a convex set. Any non separable state ρ can be identified by a suitable witness operator $\mathcal{O}$ which will give $\mathbf{tr}\left[\rho\mathcal{O}\right] < 0$.

The negative expectation value of $\mathcal{O}$ in any state ρ_{AB} "detects" entanglement and the operator is called the entanglement witness. Horodecki et. al. have shown that there exists an entanglement witness[13] for every entangled state.

II. Positive Partial Transpose Test

Another very useful and a more general way to detect entanglement in bipartite systems is the *partial transpose test*. It is based on the theory of completely positive maps. Any positive but not completely positive (CP) map will detect entanglement. A transposition is a positive map i.e. to say that this map takes a positive matrix to another positive matrix. When we apply this map to one of the subsystems the resulting matrix is not necessarily a positive matrix and hence detects entanglement in the system.

1.3   Entanglement Measures

We have seen in Section 1.1 that entanglement is a vital resource which can be used to perform tasks that are either impossible or very difficult otherwise. Also in Section 1.2 we have seen how this resource can be detected in pure and mixed bipartite systems. In this Section we will discuss some of the measures that are commonly used for the quantification of the entanglement. Entanglement is a "correlation" exhibited by quantum systems. These correlations are different (non-local!) from classical correlations in the sense that they can't be generated using local operations and classical communications (**LOCC**) alone. For example Alice and Bob can't generate entanglement between their qubits by performing local operations on their subsystems and communicating classically the outcomes of their operations. In fact, we define classical correlations as those correlations that can be generated using just LOCC. It has been shown that an arbitrary separable state can be converted into any

other separable state just by using LOCC[12]. However, we have seen that nonlocal operations on two parties(teleportation, key distribution, superdense coding etc.) can be implemented, by using only LOCC *and* shared entanglement. In order to quantify entanglement let us look at some of the important properties that any good measure of entanglement must possess[14]

I. Any measure of entanglement must be a function from the space of quantum states to positive real numbers i.e.

$$E : \rho \rightarrow \mathbb{R}^+$$

II. For any separable state ρ_{sep}, it must vanish i.e.

$$E(\rho_{sep}) = 0$$

III. It must not increase under any LOCC protocol i.e.

$$\sum_i p_i E \left(\frac{K_i \rho K_i^\dagger}{\mathbf{tr} \left[K_i \rho K_i^\dagger \right]} \right) \leq E(\rho)$$

where $\{K_i\}$ represents a set of Kraus operators that describes a LOCC protocol and p_i is the probability of occurrence of the ith outcome[15].

Any measure satisfying all the three conditions is commonly known as *entanglement monotone*. Let us look at some of the entanglement monotones in detail.

1.3.1   Entanglement Entropy

The simplest entanglement monotone for a bipartite pure state (say ρ_{AB}) is the von Neumann entropy of the subsystem density matrix(ρ_A orρ_B) that we obtain after

tracing out the other subsystem.

$$E(\rho_{AB}) = \mathbf{tr}\left[\rho_A \log \rho_A\right] \tag{1.5}$$

It is easy to see that this measure satisfies all the properties of an entanglement monotone[16].

Example

Consider a pure bipartite state $|\Psi_{AB}\rangle = \sqrt{\mu}\,|00\rangle + \sqrt{1-\mu}\,|11\rangle$. The density matrix in the basis $\{|00\rangle, |01\rangle, |10\rangle, |11\rangle\}$ looks like

$$|\Psi_{AB}\rangle\langle\Psi_{AB}| = \begin{pmatrix} \mu & 0 & 0 & \sqrt{\mu(1-\mu)} \\ 0 & 0 & 0 & 0 \\ 0 & 0 & 0 & 0 \\ \sqrt{\mu(1-\mu)} & 0 & 0 & 1-\mu \end{pmatrix}$$

If we now compute the reduced density matrix we obtain

$$\rho_A = \rho_B = \mu\,|0\rangle\langle 0| + (1-\mu)\,|1\rangle\langle 1|$$

and if we compute the von Neumann entropy of the subsystem we get

$$E(\rho) = -\mu \log \mu - (1-\mu)\log(1-\mu)$$

It is interesting to note that $E(\rho) = 0$ for $\mu = 0$ and $\mu = 1$, which corresponds to a pure separable bipartite state and attains a maximum of $\log 2$ for $\mu = \frac{1}{2}$ for maximally entangled state(See Figure 1.2).

1.3.2 Concurrence

The concurrence is one of the widely used measures of entanglement which are defined for both pure and mixed states.
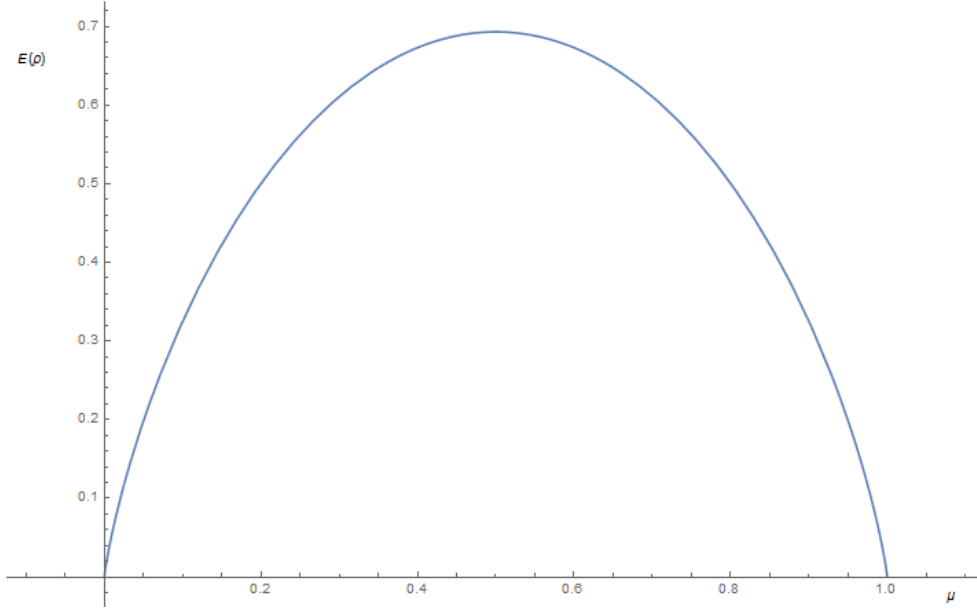
Figure 1.2: A plot showing the variation of the entanglement entropy $E(\rho)$ versus μ.

I. Concurrence of a pure state

Let $|\Psi\rangle$ be a pure bipartite 2-qubit state, then the concurrence $\mathcal{C}(|\Psi\rangle)$ is defined as the magnitude of the inner product of $|\Psi\rangle$ with its spin flipped state $|\tilde{\Psi}\rangle$.

$$\mathcal{C}(|\Psi\rangle) = |\langle\Psi|\tilde{\Psi}\rangle| = \langle\Psi\,|\,\sigma_y \otimes \sigma_y\,|\,\Psi^*\rangle$$

where $|\Psi^*\rangle$ denotes complex conjugate of $|\Psi\rangle$.

Example

If a pure bipartite state is $|\Psi\rangle = \alpha\,|00\rangle + \beta\,|01\rangle + \gamma\,|10\rangle + \delta\,|11\rangle$ then concurrence of this state turns out to be

$$\mathcal{C}(|\Psi\rangle) = 2|\alpha\delta - \beta\gamma|$$

In fact, it is easy to show that a pure bipartite state is separable if and only if $|\alpha\delta - \beta\gamma| = 0$.

II. Concurrence of a mixed bipartite state

The concurrence of a mixed state is defined as the average concurrence of the ensemble decomposition which represents the given mixed state, minimized over all possible pure state decomposition[16].

$$\mathcal{C}(\rho) = \min_{\{p_i, \ |\Phi_i\rangle\}} \left\{ \sum_i p_i \mathcal{C}(\Phi_i) \right\} \tag{1.6}$$

In general, this definition involves optimising over all bases and therefore not very computable. However, an explicit formula for the concurrence exists for a 2-qubit state which is given by[16] $\mathcal{C}(\rho) = \min\{0, \lambda - \lambda_2 - \lambda_3 - \lambda_4\}$ where λ_is are the square roots of the eigenvalues of the matrix $\rho\tilde{\rho}$ in decreasing order, and $\tilde{\rho} = (\sigma_y \otimes \sigma_y)\rho^*(\sigma_y \otimes \sigma_y)$ is the "spin flipped" version of the density matrix.

In this thesis, we investigate some of the geometrical aspects of entanglement detection and quantification. We also discuss some of its application in quantum measurement and state discrimination. The thesis is organized as follows . Chapter 2 explores the geometry of quantum state space making a correspondence between qubits and the special relativistic Minkowski geometry. We find a separability criterion for a bipartite density matrix based on the geometrical interpretation. In chapter 3 we discuss in detail how this separability criteria works and give the separable form whenever it exists. Chapter 4 explores the role of entanglement in a *coarse quantum measurement*. In particular, we study entanglement entropy of the spin and the center of mass of a silver atom in the Stern Gerlach experiment in some detail. Chapter 5 then explores how entanglement can be used as a resource in discrimination between quantum states. In the context of the Bures-Helstrom metric n-copies don't give any advantage in state discrimination over a single copy of the given quantum

state. In contrast, the BKM (Bogoliubov-Kubo-Mori) metric gives an entanglement advantage in state discrimination when we consider n-copies of the quantum state. In chapter 6, we study the geometry of statistical manifolds, in particular we focus on the issue of distinguishability of probability distributions and prove a theorem related to the emergence of the Poincaré metric on a two parameter sub-manifold. Finally, in chapter 7 we end with some concluding remarks and future directions. There are two appendices. Appendix A consists of the mathematica programs and Appendix B gives a brief introduction to the energy conditions in general relativity.

Chapter 2

Detecting qubit entanglement

The state space of a two-level quantum system is the Poincare ball, where points on the surface of the sphere correspond to pure states whereas points inside the ball which are convex combinations of points on the sphere correspond to mixed states. In this chapter we will look at some of the properties of pure and mixed states and will take a geometrical look at entanglement in a bipartite system.

2.1   A Two Level System

A two level system refers to a quantum system which has only two eigenstates. Such systems are ubiquitous in nature. For example, polarization states of a photon, a spin-$\frac{1}{2}$ particle in a magnetic field are examples of two state systems. We will talk about these system in a more general context which takes into account not only the pure states but also the mixed ones. A mixed state of a quantum system can be thought of as an ensemble of normalized pure states with a probability distribution

defined on it $\{p_i, |\psi_i\rangle\}$. To represent this ensemble we use a density matrix which is written as

$$\rho = \sum_i p_i |\psi_i\rangle \langle \psi_i|$$

The following properties of the density matrix immediately follow from the expression

- *Normalization:* $\mathbf{tr}[\rho] = 1$

- *Hermiticity:* $\rho^\dagger = \rho$, that it is Hermitian.

- *Positivity:* $\rho > 0$, that it is an operator with positive eigenvalues.

- *Purity:* $\mathbf{tr}[\rho^2] \leq 1$

2.1.1 State of a Two Level System as a Point in the Bloch Ball

Any quantum state of a two level system can be represented by a 2×2 unit trace positive Hermitian matrix known as the density matrix. The space of density matrices is a *strictly convex space*. An often convenient and useful choice of basis for this vector space is the set of four Pauli matrices[11], $\mathbb{1}, \sigma_x, \sigma_y, \sigma_z$. Any density matrix which represents a quantum state of a two level system can now be associated with a point $\boldsymbol{X}$ where

$$\rho = \frac{\mathbb{1} + \boldsymbol{X}.\boldsymbol{\sigma}}{2} \tag{2.1}$$

Hermiticity of ρ requires $\boldsymbol{X}(x^1, x^2, x^3)$ to be real, and positivity requires

$$\sqrt{(x^1)^2 + (x^2)^2 + (x^3)^2} = |\boldsymbol{X}| \leq 1$$

The set of points satisfying the above two conditions forms a spherical ball of unit radius commonly known as Bloch ball(see Figure 2.1) and has a one to one correspondence with the space of quantum states[17]. States with purity defines as,
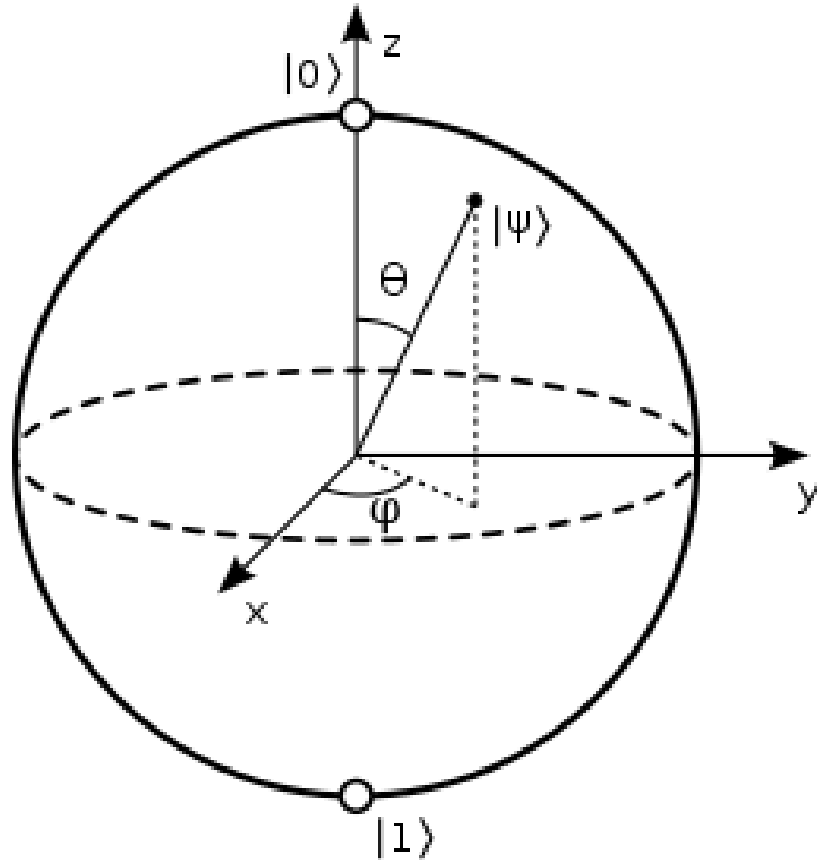
Figure 2.1: A Bloch ball (Picture taken from Wikipedia). A point on the sphere can be associated with a pure quantum state, whereas a point inside the sphere can be thought of as representing a mixed state

$$\gamma = \mathbf{Tr}[\rho^2] \tag{2.2}$$

are pure and forms the boundary of the ball whereas the interior constitutes the mixed states with $\gamma < 1$.

2.1.2 State of a Two Level System as a Future-Pointing 4-Vector

Mathematically, a state (vector) of a two-level quantum system is an element $\boldsymbol{s}$ of a two dimensional complex Hilbert space and transforms according to certain transformation laws. Such a complex vector is a **rank-1 spinor**. A density matrix$(\rho = \boldsymbol{s}\boldsymbol{s}^{\dagger})$ which is formed by taking the outer product of rank-1 spinors —an unit trace positive Hermitian matrix— is thus a standard contravariant rank-2 spinor [18] which can in general be written in the form (2.1). In this section we are going to bring out the properties of the associated vector $x^i(1, x^1, x^2, x^3)$.

Pure States

A pure state $\rho = |\xi\rangle \langle\xi|$ in the light of equation (2.1) can be associated with a vector $\boldsymbol{X}(1, x^1, x^2, x^3)$ whose components are given by the following relation:

$$x^i = \mathbf{tr}\left[\rho\sigma^i\right] = \langle\xi|\,\sigma^i\,|\xi\rangle \tag{2.3}$$

Such a state with purity

$$\gamma = \frac{1 + |\boldsymbol{X}|^2}{2} = 1 \qquad \implies \qquad 1 - (x^1)^2 - (x^2)^2 - (x^3)^2 = 0$$

can formally be viewed as a null 4-vector with components $(1, x^1, x^2, x^3)$.

Mixed States

Mixed states with purity

$$\gamma = \frac{1 + |\boldsymbol{X}|^2}{2} < 1 \qquad \implies \qquad 1 - (x^1)^2 - (x^2)^2 - (x^3)^2 > 0$$

can be thought of as a timelike 4-vector.

Consider a two level quantum system. Its evolution can be described by a set of transformations acting on the spinor s —*an element of a two dimensional complex Hilbert space*— given by $s' = As$. The density matrix thus in turn transforms as $\rho' = s's'^{\dagger} \longrightarrow A\rho A^{\dagger} = Ass^{\dagger}A^{\dagger}$. There are two useful classes of transformations that are commonly used to describe the dynamics of the quantum system. First being the set of unitary transformations SU(2), which describes the evolution of isolated quantum systems. These operations preserve the purity γ of a quantum state $(\text{Tr}[\rho^2])$. These transformations map a pure state to a pure and a mixed state to a mixed state. For example, a $SU(2)$ operation on a density matrix ρ corresponds to a spatial rotation of the 4-vector x^i associated with the state. Another interesting class of transformations are $SL(2, C)$ and are used to describe the dynamics of a quantum system which is interacting with another quantum system. These set of transformations preserve the $det(\rho) = (1 - |\boldsymbol{X}|)/4$ of a density matrix. Let us briefly look at the determinant preserving condition:

$$det(\rho') = det(A\rho A^{\dagger}) \Longrightarrow det(A) = e^{i\theta}$$

Since phase acts trivially on the density matrix, we can restrict ourselves to the set of transformations with *unit* determinant. Clearly the matrices A which are 2×2 matrices with determinant equal to 1 form a group $SL(2, C)$, the Lorentz group. As noted in section 2.2, a state ρ —a rank-2 spinor— can be associated with a 4-vector x^i and determinant preserving transformation A —a $SL(2, C)$ matrix— can be associated with a Lorentz transformation acting on the 4-vector. A particularity

interesting one[19] is $\exp\{-\boldsymbol{n}\boldsymbol{\sigma}\}$ which corresponds to a Lorentz boost in the direction $\boldsymbol{n}$ on the 4-vector x^i.

2.2 A Bipartite System

A bipartite quantum system is one which consists of two(say A and B) interacting subsystems. The simplest example is a pair of interacting spin-$\frac{1}{2}$ particles.

2.2.1 Entanglement in a bipartite quantum system

In this section we will be interested only in describing the entanglement between the spin states of a bipartite composite system (for a discussion on bipartite entanglement see section 1.2). However entanglement can be established between any number of degrees of freedom of the same or different systems by turning on the coupling between these degrees of freedom. For example we can create entanglement between spin and positional degrees of freedom of a spin-$\frac{1}{2}$ particle by turning on a magnetic field, which will be the topic of discussion of the next chapter.

We consider a bipartite quantum system consisting of two qubits. Let the state of the system be ρ_{AB}. In general this can be a pure or a mixed state of the composite system. How can we tell if there exists an entanglement between the sub-systems? In other words we would like to see if we can assign a state—ρ_A and ρ_B— to each of the subsystems. The state ρ_{AB} is separable if and only if it can be written in the following form

$$\rho_{AB} = \sum_i p_i \rho_A^i \otimes \rho_B^i \tag{2.4}$$

We have seen that a density matrix is a positive semi-definite Hermitian matrix and transposition preserves the spectrum of the matrix. If we transpose the matrix ρ_{AB} we again obtain a Hermitian positive semi-definite matrix.

2.2.2   Positive Maps but not Completely Positive Maps

Let $\mathcal{B}(\mathcal{H})$ be a set of positive operators defined on the Hilbert space $\mathcal{H}$. Λ is said to be a positive map if it takes a positive operator to another positive operator. Consider an extended map $\Lambda \otimes \mathbb{1}$ which acts on positive operators defined on $\mathcal{H}_A \otimes \mathcal{H}_B$. Let us consider the action of $\Lambda \otimes \mathbb{1}$ on a positive operator which can be written in the form of Equation (2.4) i.e. a separable state,

$$
\begin{aligned}
\tilde{\rho}_{AB} &= \Lambda \otimes \mathbb{1} \left(\sum_i p_i \rho_A^i \otimes \rho_B^i \right) \\
&= \sum_i p_i \Lambda(\rho_A^i) \otimes \mathbb{1}(\rho_B^i)
\end{aligned}
\tag{2.5}
$$

It is straightforward to see that $\tilde{\rho}_{AB}$ is also a positive operator, since p_i is a positive number, $\Lambda(\rho_A^i)$ and $\mathbb{1}(\rho_B^i)$ are positive operators[14], hence each term of the above sum has a positive expectation value. All extended maps of the form $\Lambda \otimes \mathbb{1}$ (where Λ is a positive map) will yield a positive operator when applied on a separable state.

Notice that the positivity of $\tilde{\rho}_{AB}$ under the extended map $\Lambda \otimes \mathbb{1}$ hinges on the decomposition of ρ_{AB} in the form (2.4). Conversely if any expectation value of $\tilde{\rho}_{AB} = (\Lambda \otimes \mathbb{1})(\rho_{AB})$ fails to be positive for "some" positive map Λ then the assumption that we made about ρ_{AB} is no longer true and ρ_{AB} will then be an entangled state. A positive map Λ is said to be a *completely positive map* (CP-map) if the extended map $\Lambda \otimes \mathbb{1}$ is also positive for an arbitrary operator ρ_{AB}. A suitable positive, but *not*

completely positive map can thus detect a mixed entangled state.

Partial transposition in low dimensions (2×2 or 2×3) is one such suitable map. An arbitrary positive map for 2×2 or 2×3 dimensions can be written as,

$$\Lambda = \Lambda_{CP}^1 \circ T + \Lambda_{CP}^2 \qquad (2.6)$$

where Λ_{CP}^1, Λ_{CP}^2 are two CP-maps, T is transposition and '$\circ$' represents composition of maps. Let us apply this map to an arbitrary separable state,

$$\tilde{\rho}_{AB} = (\Lambda \otimes \mathbb{1})\rho_{AB} > 0$$

$$(\Lambda_{CP}^1 \otimes \mathbb{1}) \circ (T \otimes \mathbb{1})\rho_{AB} + (\Lambda_{CP}^2 \otimes \mathbb{1})\rho_{AB} > 0 \qquad (2.7)$$

$$(\Lambda_{CP}^1 \otimes \mathbb{1})[\rho_{AB}]^{T_A} + (\Lambda_{CP}^2 \otimes \mathbb{1})\rho_{AB} > 0$$

where $[\rho_{AB}]^{T_A}$ represents partial transposition with respect to subsystem A. If we demand $\tilde{\rho}_{AB}$ to be a positive operator then $[\rho_{AB}]^{T_A}$ must be a positive operator. Hence for a separable state of a bipartite system of two qubits or a qubit and a qutrit the partially transposed density matrix must be a positive semi-definite matrix.

2.2.3 Positivity condition for associated tensor A_{ij}

As discussed in the previous sections positivity of a density matrix plays an important role in detecting the entanglement of bipartite 2×2 and 2×3 systems. We are going to look at these criteria in terms of the associated rank-2 tensor. We are going to use a slightly different notation for later convenience. A two-qubit density matrix is a rank-4 spinor with index structure $\rho^{p_1}{}_{q_1}{}^{p_2}{}_{q_2}$ where p_1, q_1 and p_2, q_2 correspond to spinor index of 1st and 2nd system respectively. We relate this 4-spinor with a second

rank tensor using σ matrices.

$$\rho^{p_1}{}_{q_1}{}^{p_2}{}_{q_2} = A_{ij}\sigma^{ip_1}{}_{q_1}\sigma^{jp_2}{}_{q_2} \tag{2.8}$$

Positivity of a density matrix means that any expectation value of the density operator must be positive. Mathematically,

$$\langle\psi|\,\rho^{p_1}{}_{q_1}{}^{p_2}{}_{q_2}\,|\psi\rangle \geq 0 \qquad \forall \quad |\psi\rangle \in \mathcal{H}_1 \otimes \mathcal{H}_2$$

An arbitrary state of a two qubit system(a vector in a 4-dimensional complex Hilbert space) can be written using spinors[20] in the following form:

$$\psi = \kappa_1^{A_1}\kappa_2^{A_2} + D\kappa_1^{A_2}\kappa_2^{A_1} \tag{2.9}$$

where κ_1, κ_2 are two rank-1 spinors. Using equations (2.8),(2.9) and (2.3) the positivity condition can be written as,

$$f(D) \equiv \sum_{i,j}(DD^*\underbrace{A_{ij}n^il^j}_{a} + D\underbrace{A_{ij}\overline{m}^im^j}_{b} + D^*\underbrace{A_{ij}m^i\overline{m}^j}_{b^*} + \underbrace{A_{ij}l^in^j}_{c} \geq 0 \tag{2.10}$$

where $\boldsymbol{l}, \boldsymbol{n}$ are two real null vectors, $\boldsymbol{m}$ is a complex null vector and $\overline{\boldsymbol{m}}$ is its complex conjugate. This corresponds to the *dominant energy condition*[21] on A_{ij}. In order to find the minimum value of $f(D)$ we set

$$\frac{\partial f}{\partial D} = 0$$

and obtain $D = -\frac{b^*}{a^*}$ and $D^* = -\frac{b}{a}$. Substituting these values in f we obtain

$$f_{min} = \frac{ac - b^*b}{a}.$$

Taking

$$l = \frac{t+z}{\sqrt{2}} \qquad ; \qquad n = \frac{t+z}{\sqrt{2}} \qquad ; \qquad \overline{m} = \frac{x+\iota y}{\sqrt{2}} \qquad ; \qquad m = \frac{x-\iota y}{\sqrt{2}}$$

we obtain

$$a = \frac{1}{2}[(A_{00} + A_{33}) + (A_{03} - A_{30})]$$

$$c = \frac{1}{2}[(A_{00} + A_{33}) - (A_{03} - A_{30})]$$

$$b = \frac{1}{2}[(A_{11} + A_{22}) + \iota(A_{12} - A_{21})]$$

Then the condition for positivity in terms of components of tensor A_{ij} reads:

$$\tau \equiv (A_{00} + A_{33})^2 - (A_{03} - A_{30})^2 - (A_{11} + A_{22})^2 - (A_{12} - A_{21})^2 \geq 0 \qquad (2.11)$$

Werner State[1]

A Werner state is a mixed quantum state. We obtain a Werner state when a maximally entangled (say a singlet) state is "corrupted" by a maximally mixed state. The degree of entanglement depends on the parameter $\alpha \in (0, 1)$. For $0 < \alpha < \frac{1}{3}$ the state is separable and for any other value of α it is entangled.

$$\rho^{Werner} = \frac{1}{4} \begin{pmatrix} 1-\alpha & 0 & 0 & 0 \\ 0 & \alpha+1 & -2\alpha & 0 \\ 0 & -2\alpha & \alpha+1 & 0 \\ 0 & 0 & 0 & 1-\alpha \end{pmatrix} \Rightarrow \left[A_{ij}^{Werner} \right] = \begin{pmatrix} 1 & 0 & 0 & 0 \\ 0 & -\alpha & 0 & 0 \\ 0 & 0 & -\alpha & 0 \\ 0 & 0 & 0 & -\alpha \end{pmatrix}$$

$$(2.12)$$

In a computer program we randomly choose the null vectors $\boldsymbol{n}, \boldsymbol{l}, \boldsymbol{m}, \overline{\boldsymbol{m}}$ and contract with A_{ij}^{Werner} to obtain the scalar τ for a Werner state($\alpha = 0.7$) as in Eq.(2.10). Figure 2.2 shows the values of [2]$sign(\tau)$ obtained for 10,000 such random choices.

---

[1]$\rho^{Werner} = \alpha\,|singlet\rangle \langle singlet| + (1-\alpha)\frac{1}{4}$

[2]$sign(x) = \begin{cases} 1, & \text{for } x > 0 \\ 0, & \text{for } x = 0 \\ -1, & \text{for } x < 0 \end{cases}$

Figure 2.3 shows $sign(\tau)$ for the partially transposed density matrix of the Werner state $\tilde{A}_{ij}^{Werner}$. A negative value of $sign(\tau)$ indicates entanglement.

Partial Lorentz transformation (*A completely positive map*): A two-qubit
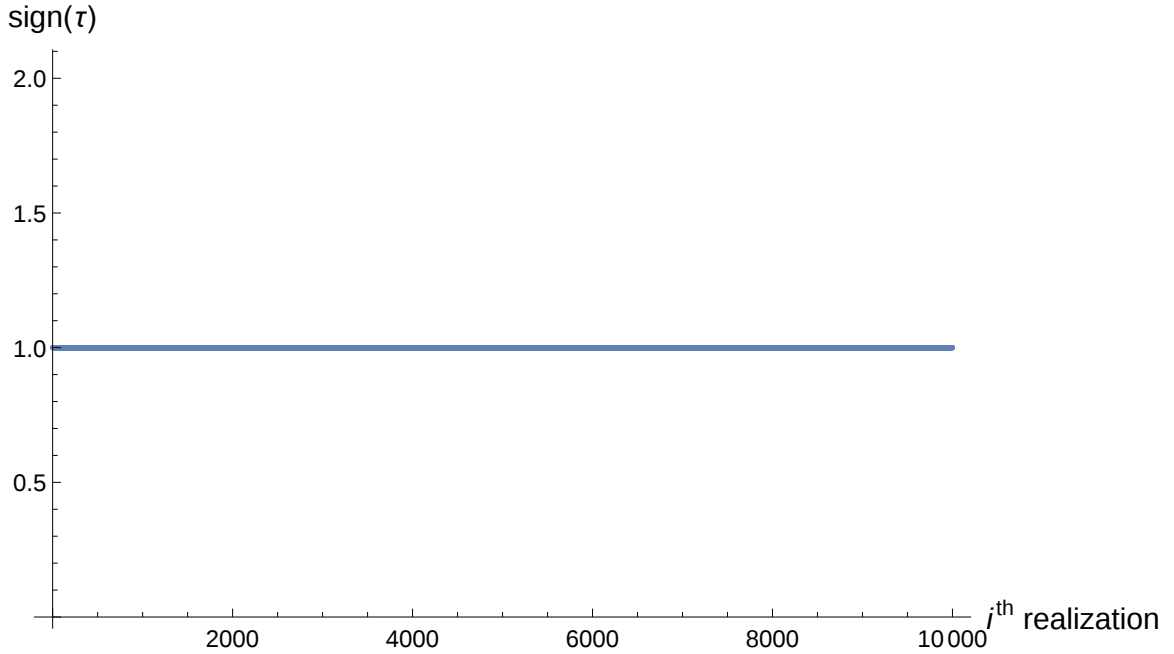
Figure 2.2: A plot of $sign(\tau)$ (see Eq.(2.11)) for A_{ij}^{Werner} for 10000 random choices of null bases.

state can be represented by a 4 × 4 positive semidefinite Hermitian matrix ρ (a rank 4-spinor) or equivalently by a rank 2-tensor (A_{ij})[22]. As seen in Section 2.1.2 that a Lorentz transformation of the 4-vector associated with a qubit is equivalent to a $SL(2,C)$ transformation on ρ. In particular a pure rotation of the 4-vector is equivalent to a $SU(2)$ operation on the qubit and a pure boost on the 4-vector is equivalent to a $SL(2,C)$ operation on the qubit. We demonstrate with a computer program that a Lorentz transformation of the tensor associated with a two level system is a positive map (See Appendix A). In fact, it can be shown that it is a
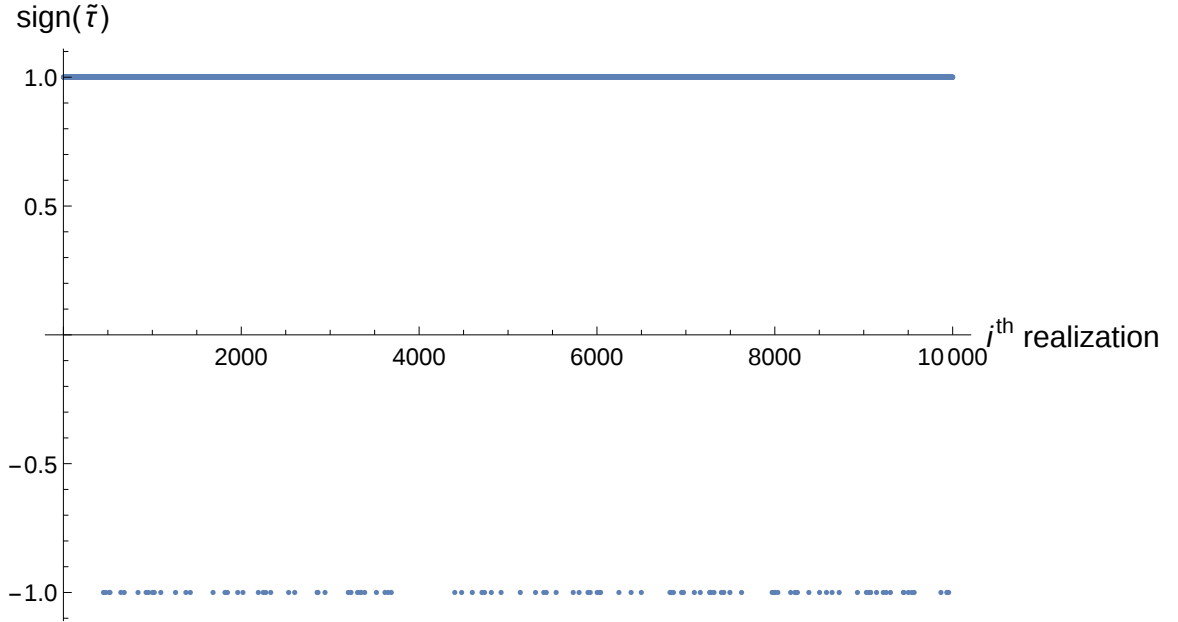
Figure 2.3: A plot of $sign(\tau)$ for $\tilde{A}_{ij}^{Werner}$ for 10000 random choices of null bases.

completely positive map.

An arbitrary Lorentz transformation can be written as[23]

$$\mathcal{L} = \mathcal{R}(\mathbf{u})\Lambda(\eta)$$

Where Λ is a pure boost in some direction and $\mathcal{R}$ represents a pure rotation about some direction($\mathbf{u}$). We will construct a rank-2 tensor associated with a two-qubit density matrix in the next section. In order to generate a partial Lorentz transformation we proceed as follows. On the tensor A_{ij} we apply a Lorentz transformation only on one of the indices i.e. only on the one of the subsystems as,

$$A'_{ij} = \mathcal{L}_i{}^\mu A_{\mu j}$$

We randomly choose a Lorentz matrix $\mathcal{L}$ and transform A_{ij} to A'_{ij}. This A'_{ij} corresponds to a positive semi-definite operator(see Figure 2.4).
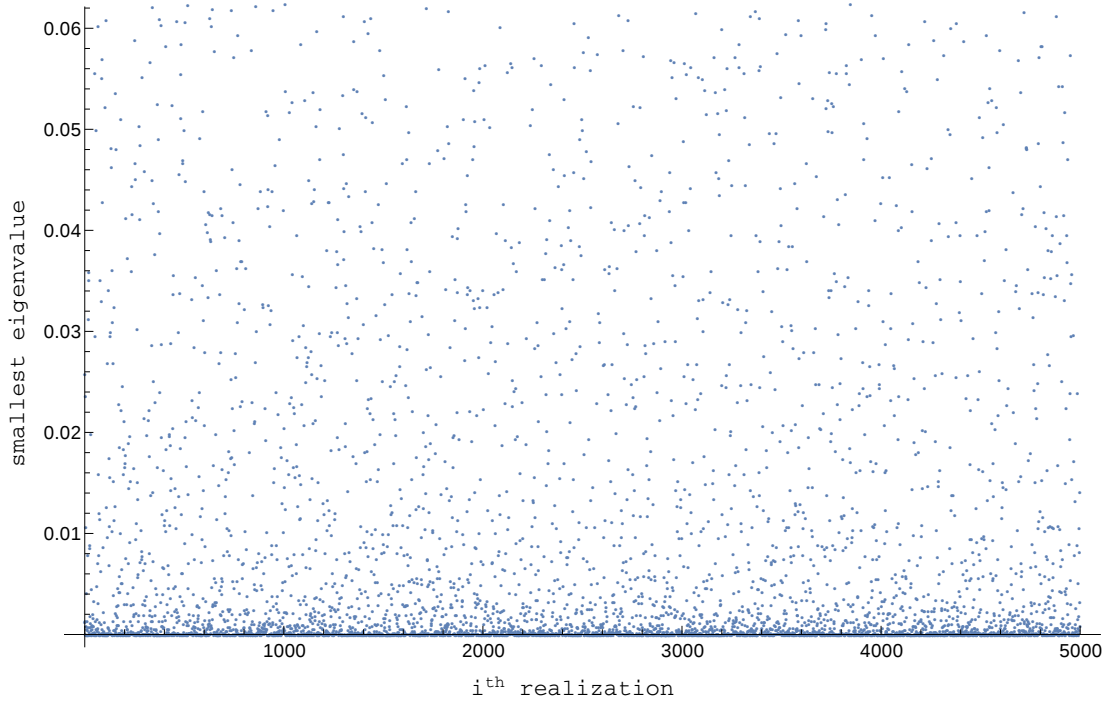
Figure 2.4: On the vertical axis we plot the smallest eigenvalue of the partially Lorentz transformed density matrix for 5000 randomly chosen Lorentz matrices. Notice that the smallest eigenvalue is positive, indicating that a partial Lorentz transformation is a positive map.

2.3 Entanglement Test for Two Qubits

Let ρ be a density matrix of a two qubit system. If ρ can be expressed in the form (τ^1 and τ^2 are 1-qubit density matrices)

$$\rho = \sum_i w_i \, \tau_i^1 \otimes \tau_i^2 \qquad w_i > 0 \tag{2.13}$$

we say that ρ is separable, else ρ is entangled. We assume ρ is positive ($\rho \geq 0$) and Hermitian ($\rho^\dagger = \rho$). In our treatment, we will not need to normalize ρ. One can expand the density matrix ρ as

$$\rho = \frac{1}{4} A^{\mu\nu} \sigma_\mu \otimes \sigma_\nu \tag{2.14}$$

where $\sigma_\mu = (\mathbb{I}, \ \sigma_1, \ \sigma_2, \ \sigma_3)$ are the identity and the Pauli matrices. $A^{\mu\nu}$ can be calculated from

$$A_{\mu\nu} = \mathrm{Tr}(\rho\sigma_\mu \otimes \sigma_\nu). \tag{2.15}$$

Let us consider $B^\mu_{\ \nu} = A^{\mu\alpha}g_{\alpha\beta}A^{\sigma\beta}g_{\sigma\nu}$ where $g = \mathrm{diag}(1, -1, -1, -1)$ is the Minkowski metric. Now,

$$B^\mu_{\ \nu} = A^\mu_{\ \alpha}A_\nu^{\ \alpha}. \tag{2.16}$$

Notice that $B^{\mu\nu}$ is symmetric i.e. $B^{\mu\nu} = B^{\nu\mu}$. It can be shown[24] that the eigenvalues of B (3.9) are non-negative and so we can define $\mu_a = \sqrt{\lambda_a}$ to be real where $a = 0, 1, 2, 3$.

Our claim is that, the necessary and sufficient condition for separability is

$$T(\mu_a) = \mu_0 - (\mu_1 + \mu_2 + \mu_3) \geq 0. \tag{2.17}$$

Violation of this inequality signals entanglement. This is our Partial Lorentz Transformation (PLT) test for entanglement of two qubits. The PLT test is an alternative to the PPT test which is widely known and used in this field.

2.4 Detection of entanglement: A few examples

In this section we consider some specific families of states to illustrate the use of our criterion for detecting entanglement. We first consider the Werner state.

2.4.1 Example-I

The Werner state is a two qubit mixed state given by $\rho^W = \frac{1-\alpha}{4}\mathbb{I} + \alpha \left|\mathcal{S}\right\rangle \left\langle\mathcal{S}\right|$ where $\left|\mathcal{S}\right\rangle = \frac{\left|\uparrow\downarrow\right\rangle - \left|\downarrow\uparrow\right\rangle}{\sqrt{2}}$ is a spin singlet state and $0 \leq \alpha \leq 1$. The PPT test shows that this

state is separable for $0 \leq \alpha \leq 1/3$ and entangled for $1/3 < \alpha \leq 1$. Let us first construct $A_{\mu\nu} = \text{Tr}\left[\rho^W \sigma_\mu \otimes \sigma_\nu\right]$.

$$A_{\mu\nu} = \begin{pmatrix} 1 & 0 & 0 & 0 \\ 0 & -\alpha & 0 & 0 \\ 0 & 0 & -\alpha & 0 \\ 0 & 0 & 0 & -\alpha \end{pmatrix}. \tag{2.18}$$

From $A_{\mu\nu}$ we can construct matrix B:

$$B^\mu{}_\nu = \begin{pmatrix} 1 & 0 & 0 & 0 \\ 0 & \alpha^2 & 0 & 0 \\ 0 & 0 & \alpha^2 & 0 \\ 0 & 0 & 0 & \alpha^2 \end{pmatrix} \tag{2.19}$$

The eigenvalues of B are $\lambda_0 = 1$ and $\lambda_1, \lambda_2, \lambda_3 = \alpha^2$. They are positive as claimed earlier and hence we can take the positive square-root of these eigenvalues to obtain the μs. We now apply the test by computing $T(\alpha) = \sqrt{\lambda_0} - \sqrt{\lambda_1} - \sqrt{\lambda_2} - \sqrt{\lambda_3}$. A state is entangled iff $T(\alpha) < 0$, which gives

$$1 - 3\alpha < 0 \qquad \Rightarrow \qquad \alpha > \frac{1}{3}$$

Hence, we correctly obtain the condition $1/3 < \alpha \leq 1$ for ρ to be entangled (See Figure 2.5).
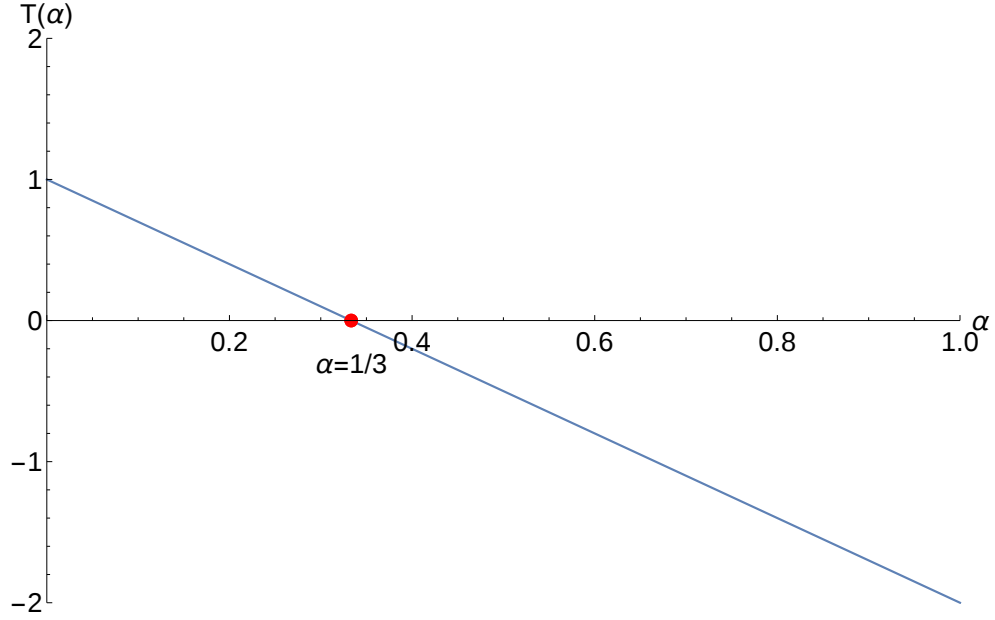
Figure 2.5: A figure showing the variation of $T(\alpha)$ with α. We see that for $\alpha > 1/3$, $T(\alpha)$ is negative and the state is therefore entangled.

2.4.2   Example-II

Another interesting example is the state given by[25]

$$\rho = \quad \frac{1}{4} \quad ((r - s + 1)\sigma_3 \otimes \sigma_3 + r(\sigma_3 \otimes \mathcal{I}) + s(\mathcal{I} \otimes \sigma_3)$$

$$+ \quad t(\sigma_1 \otimes \sigma_1) - t(\sigma_2 \otimes \sigma_2) + \mathcal{I} \otimes \mathcal{I}). \tag{2.20}$$

ρ is a two qubit density matrix for the parameter range

$$s - r \quad \geq \quad 0$$

$$|r| \quad \leq \quad 1$$

$$|s| \quad \leq \quad 1$$

$$t^2 \quad \leq \quad (1 - s)(1 + r) \equiv h^2. \tag{2.21}$$

Applying the partial transpose test to ρ we find that the state is entangled[25] for

$|t| \neq 0$ and separable for $|t| = 0$. Let us apply the PLT test on ρ. Following the same recipe as in the previous example we find,

$$A_{\mu\nu} = \begin{pmatrix} 1 & 0 & 0 & s \\ 0 & t & 0 & 0 \\ 0 & 0 & -t & 0 \\ r & 0 & 0 & r-s+1 \end{pmatrix} \tag{2.22}$$

$$B^{\mu}{}_{\nu} = \begin{pmatrix} 1-s^2 & 0 & 0 & (s-r)(1-s) \\ 0 & t^2 & 0 & 0 \\ 0 & 0 & t^2 & 0 \\ -(s-r)(1-s) & 0 & 0 & -(2r-s+1)(s-1) \end{pmatrix} \tag{2.23}$$

and the eigenvalues of B are (h^2, h^2, t^2, t^2). The last inequality of the state condition(2.21) implies that the dominant eigenvalue of the matrix B is h^2. Then the PLT condition for separability requires,

$$|h| \geq |h| + 2|t| \implies |t| \leq 0 \implies t = 0.$$

Hence, we find that the state ρ is separable for $t = 0$ and entangled otherwise which is in agreement with the PPT test.

The computable cross norm (CCN) test proposed in [25] doesn't detect entanglement for all states. It only works if the reduced density matrices of the individual systems are maximally disordered ($r = 0$ and $s = 0$ in Example II)[25]. For instance, it does not work for the the state ρ given by (2.20) for the parameters $r = 1/4$ and $s = 1/2$, $t = 1/16$. However, we notice that the PLT gives $T(t) = -4\sqrt{2/5}\,|t|$ showing that the state is not separable for any non-zero value of t (See Figure 2.6) in agreement with the PPT test.
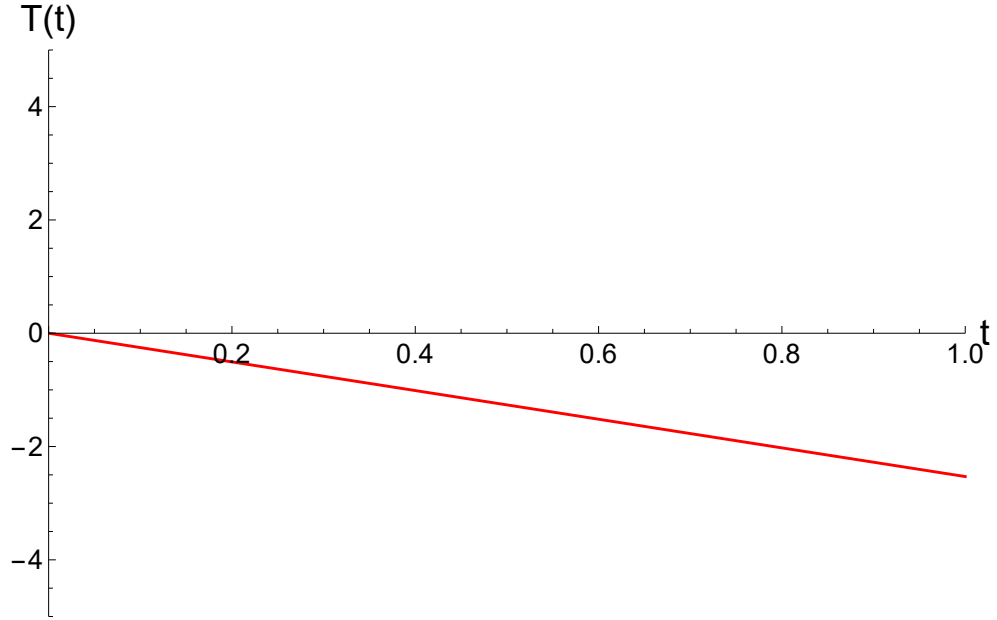
Figure 2.6: A figure showing the variation of $T(t)$ with t. We see that for all $t \in (0, 1]$ $T(t)$ is negative, indicating non-separability.

2.4.3 Example-III

Now, we apply this test to a set of states which are incoherent mixtures of the singlet state and the maximally polarized state[26].

$$\rho = x \left| \mathcal{S} \right\rangle \left\langle \mathcal{S} \right| + (1 - x) \left| \uparrow\uparrow \right\rangle \left\langle \uparrow\uparrow \right| \tag{2.24}$$

where $\left| \mathcal{S} \right\rangle$ is the singlet state and $0 \leq x \leq 1$. We compute the matrices A and B and find

$$A_{\mu\nu} = \begin{pmatrix} 1 & 0 & 0 & 1 - x \\ 0 & -x & 0 & 0 \\ 0 & 0 & -x & 0 \\ 1 - x & 0 & 0 & 1 - 2x \end{pmatrix} \tag{2.25}$$

$$B^{\mu}{}_{\nu} = \begin{pmatrix} -(x-2)x & 0 & 0 & 2(x-1)x \\ 0 & x^2 & 0 & 0 \\ 0 & 0 & x^2 & 0 \\ -2(x-1)x & 0 & 0 & x(3x-2) \end{pmatrix}. \tag{2.26}$$

The eigenvalues of B are $(x^2,\ x^2,\ x^2,\ x^2)$, which are all positive. These states turn out to be entangled since $T(x) = -2x < 0$ for all values of the parameter $x \in (0,1]$ in agreement with the PPT test.

2.4.4 Example-IV

Finally, we present the results of a numerical study in support of the claims made in this chapter. A Mathematica program (see Appendix A) generates random density matrices of a two qubit system. The states are then tested for entanglement using the PLT test and the PPT test. In *all* cases, we find that the two tests agree. The program also shows by numerical evidence that the eigenvalues of B (3.9) are positive.

2.5 Conclusion

We have presented a necessary and sufficient criterion, to detect two qubit entanglement. This criterion is distinct from the celebrated PPT test and thus serves as an alternative method for detection of entanglement. We have explicitly demonstrated that this test works for some specific cases. More generally, we numerically generate random density matrices and show that the PLT test agrees with the PPT test in all cases (See Appendix A).

Expressions similar to T have appeared before in [27], which studies the entanglement of formation for two qubit systems. However our work goes beyond this, in proposing an explicit test for detection of two qubit entanglement, which serves as an alternative to the PPT test.

In Ref[25] a separability criterion called the computable cross norm (CCN) is proposed. Example-II is taken from [25] and shows that the CCN test fails to detect entanglement, while the PPT and PLT succeed. Thus the PLT test is a more discriminating test for detection of entanglement compared to the CCN test and just as good as the PPT test. It is worth noting that the use of a Lorentzian metric is the crucial ingredient that leads to the sucess of the PLT test. We expect that this framework for detection of entanglement can be extended to higher dimensional examples beyond two qubits. This test is of relevance to the area of Quantum Information where entanglement is viewed as an important resource.

Chapter 3

Lorentzian geometry of qubit entanglement

3.1 Introduction

Detecting entanglement is one of the outstanding problems in Quantum Information Theory. In two qubit systems, the Positive Partial Transpose (PPT) criterion [26, 13, 14] gives a simple, computable criterion for detecting entanglement. The criterion gives a necessary and suficient condition for a state to be separable.

In chapter 2, we proposed a new test based on Partial Lorentz Transformation(PLT) of individual qubits. It turns out that like the PPT test, the PLT criterion is necessary and sufficient in the two qubit case. In chapter 2, the PLT test was given as a recipe, a form that could be directly used by those who want to apply the test. The purpose of this chapter is to describe the theoretical framework behind the PLT test. In addition to showing why the test works, our Lorentzian approach yields an

explicit separable form of the density matrix, when such a form exists. It also permits a complete elucidation of the state space using a Lorentzian version of the Singular Value Decomposition. The PLT test uses ideas borrowed from the space-time physics of Special Relativity.

The chapter is organized as follows. In Section 3.2 we discuss Partial Lorentz Transformations (PLT). Section 3.3 describes the Lorentzian Singular Value Decomposition which provides the theoretical basis for the PLT test. Section 3.4 gives necessary and sufficient conditions on the singular values to define a state and expresses the state in separable form, under certain conditions on the singular values. We also show that these conditions are necessary for separability. We then discuss a simple three dimensional representation of the two-qubit state space in Section 3.5. Section 3.6 deals with non generic states. We finally end the chapter with some concluding remarks in Section 3.8.

We use a Lorentzian metric of signature mostly minus: $g = diag(1, -1, -1, -1)$. Spacetime Lorentz indices μ, ν range over $0, 1, 2, 3$, as also do Frame indices $a, b, ...$ Both these indices are raised and lowered by the Minkowski metric and we use the Einstein summation convention. All causal (timelike or lightlike 4-vectors) are pointing into the future. Throughout this chapter, by "Lorentz group", we mean its proper, orthochronous subgroup, which preserves time orientation as well as the spatial orientation.

3.2 Lorentz Transformations

The states of a qubit can be expressed in space-time form by using $\sigma_\mu = (\mathbb{1}, \sigma_x, \sigma_y, \sigma_z)$, the identity and the Pauli matrices

$$\tau = u^\mu \sigma_\mu \tag{3.1}$$

u^μ is a real future pointing 4-vector and satisfies

$$u^\mu u^\nu g_{\mu\nu} > 0 \tag{3.2}$$

for impure states and

$$u^\mu u^\nu g_{\mu\nu} = 0 \tag{3.3}$$

for pure states. Impure states have time-like u and pure states have lightlike u. In both the cases $u^0 > 0$, the 4-vector u^μ is future pointing. If we were to fix the "normalization" by $\text{Tr}(\rho) = 2$, $u^0 = 1$, the impure states can be represented in the Bloch ball $\vec{u}.\vec{u} < 1$ and the pure states on the Bloch sphere $\vec{u}.\vec{u} = 1$. The Lorentzian nature of the state space is already evident. Under Lorentz Transformations

$$u^\mu \mapsto u'^\mu = S^\mu{}_\nu u^\nu$$

where $S^\mu{}_\nu S^\alpha{}_\beta g_{\mu\alpha} = g_{\nu\beta}$. The Lorentz Transformation maps states to states. The group action has two orbits: the pure states constitute one orbit and the impure states another.

Partial Lorentz Transformations: Let ρ be a density matrix of a two qubit system. We assume ρ is non negative ($\rho \geq 0$), Hermitian ($\rho^\dagger = \rho$). In our treatment, we will not need to normalize ρ, but we suppose ρ does not vanish identically. One can

expand the density matrix ρ as

$$\rho = \frac{1}{4}A^{\mu\nu}\sigma_\mu \otimes \sigma_\nu \tag{3.4}$$

where $A^{\mu\nu}$ can be calculated from

$$A_{\mu\nu} = \text{Tr}(\rho\sigma_\mu \otimes \sigma_\nu). \tag{3.5}$$

Consider doing a Lorentz Transformation on just the first subsystem

$$\sigma_\mu \mapsto \sigma_\mu{}' = \sigma_\alpha L^\alpha{}_\mu. \tag{3.6}$$

This results in a new state $\rho' = \frac{1}{4}L^\mu{}_\alpha A^{\alpha\nu}\sigma_\mu \otimes \sigma_\nu$, so

$$A'^{\mu\nu} = L^\mu{}_\alpha A^{\alpha\nu}. \tag{3.7}$$

We refer to this as a Partial Lorentz Transformation since it acts only on the first subsystem. Similarly one can perform a Partial Lorentz Transformation on the second subsystem

$$A''^{\mu\nu} = A^{\mu\alpha}R^\nu{}_\alpha. \tag{3.8}$$

Partial Lorentz Transformations act on A by left (L) and right (R) actions. It is elementary to check that PLT s are completely positive[14] maps on the state space. They also have the important property that they preserve separability of states. The PLT of a separable state is separable. The PLT of an entangled state is entangled. This is the key property of the Partial Lorentz Transformation group that we exploit here.

3.3 Lorentzian Singular Value Decomposition

Let us now consider the action of left and right PLTs [See Equation 3.7 and 3.8] on the state space. The space of (unnormalized) density matrices is 16 dimensional. The left and the right PLTs generate orbits which are generically $6 + 6 = 12$ dimensional. Thus the 16 dimensional state space splits into a 4 parameter family of 12 dimensional fibers. (There are also isolated points where the isotropy subgroup is larger and the fiber smaller). Each fiber is either entirely separable or entirely entangled. Thus we can reduce the problem to the 4 dimensional space of orbits. In order to characterize the orbits, consider

$$B^{\mu}{}_{\nu} = A^{\mu}{}_{\alpha} A_{\nu}{}^{\alpha}. \tag{3.9}$$

$B^{\mu\nu}$ is symmetric i.e $B^{\mu\nu} = B^{\nu\mu}$. It is easily checked that $\text{Tr}(B^n)$ is invariant under both left and right PLTs. Generically we would expect the four eigenvalues of $B^{\mu}{}_{\nu}$ to characterise the orbits.

Just as we constructed B from a state A, we can also similarly define D

$$D^{\mu}{}_{\nu} = A^{\alpha\mu} A_{\alpha\nu}. \tag{3.10}$$

B and D have the same four eigenvalues since from the cyclicity of the trace we have $\text{Tr}(B^n) = \text{Tr}(D^n)$ for all integer n. These common eigenvalues determine the singular values of A. The relation

$$A_{\beta}{}^{\mu} A^{\beta}{}_{\alpha} A_{\nu}{}^{\alpha} = D^{\mu}{}_{\alpha} A_{\nu}{}^{\alpha} = A_{\beta}{}^{\mu} B^{\beta}{}_{\nu} \tag{3.11}$$

shows that A is an intertwining operator[28] relating the eigenspaces of B and D. The eigenspaces of B and D are then used to bring A to its Lorentzian singular value

decomposition (LSVD) form.

Dominant Energy Condition: The non-negativity of ρ implies that $\text{Tr}\rho(\tau_1 \otimes \tau_2) \geq 0$, where $\tau_1 = n^\mu \sigma_\mu$ and $\tau_2 = m^\mu \sigma_\mu$ are pure 1-qubit states of two subsystems. We conclude that

$$A_{\mu\nu} n^\mu m^\nu \geq 0 \tag{3.12}$$

for all lightlike n^μ, m^ν. This implies that the linear transformation $A^\mu{}_\nu$ maps causal vectors to causal vectors (see Figure 3.1). More explicitly, $A^\mu{}_\nu n^\nu$ is causal if n^ν is. This is also true of the transpose of A ($A_\mu{}^\nu n^\mu$ is causal for n^μ causal) and the composite maps B and D. This property of mapping the light cone into itself is usually demanded of stress energy tensors in Relativity, where it is called (see Appendix B) the Dominant Energy Condition (DEC)[21].
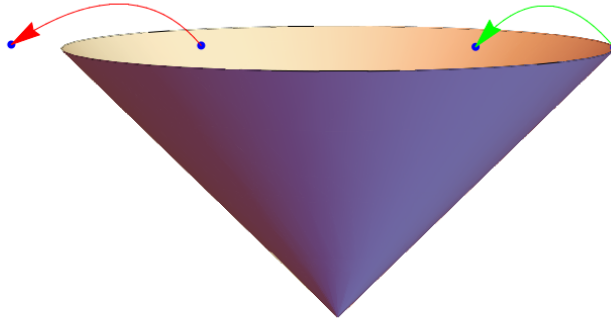
Figure 3.1: A representation depicting causal vectors getting mapped to causal vectors (green arrow on the right). The reverse map of a timelike vector going to a space like vector is not allowed (red arrow on the left) by the Dominant Energy Condition.

The dominant energy condition imposes restrictions on the forms that B can take. Hawking and Ellis [21] give a classification of the canonical forms taken by a symmetric tensor in a Lorentzian space. There are four types, of which only Type-I

and Type-II are relevant for us, since the others do not satisfy the DEC. Let λ_0 be the dominant eigenvalue of B (and D).

Type-I States: These states are defined by the condition that B admits a timelike eigenvector e_0 ($B^\mu_{\ \nu} e_0^\nu = \lambda_0 e_0^\mu$) with $\lambda_0 > 0$. From Eq. (3.11) it follows that $A_\nu^{\ \alpha} e_0^\nu$ is an eigenvector E_0^α of D with the same eigenvalue λ_0. Computing $E_0.E_0 = \lambda_0 e_0.e_0$ we see that E_0 is timelike, since e_0 is. Normalising these eigenvectors, we can write (with $\mu_0 > 0$),

$$\mu_0 E_0^\mu = A^\mu_{\ \alpha} e_0^\alpha. \tag{3.13}$$

Squaring (3.13) we find that

$$\lambda_0 = \mu_0^2. \tag{3.14}$$

Let us define

$$b^\mu_{\ \nu} = B^\mu_{\ \nu} - \lambda_0 e_0^\mu e_\nu^0$$

b is symmetric and spatial ($b_{\mu\nu} = b_{\nu\mu}$, $b_{\mu\nu} e_0^{\ \nu} = 0$) and can therefore be diagonalized by an $SO(3)$ transformation. We thus have a diagonal form for B.

The orthonormal frame which diagonalises B, (e_a^μ) gives us a Lorentz tetrad, whose inverse is e_μ^a. In this frame B has the form:

$$B^\mu_{\ \nu} = e_a^\mu B^a_{\ b} e_\nu^b. \tag{3.15}$$

where $B = diag(\lambda_0, \lambda_1, \lambda_2, \lambda_3)$. Similarly

$$D^\mu_{\ \nu} = E_a^\mu D^a_{\ b} E_\nu^b. \tag{3.16}$$

$D = diag(\lambda_0, \lambda_1, \lambda_2, \lambda_3)$. Applying A to e_a^ν we have

$$A^\mu_{\ \nu} e_a^\nu = \mu_a \delta_a^b E_b^\mu = T_a^{\ b} E_b^\mu \tag{3.17}$$

or equivalently

$$A^\mu{}_\nu = E^\mu_b T^b{}_a e^a_\nu, \tag{3.18}$$

where $T^a{}_b$ is diagonal with the form

$$T^a{}_b = \begin{pmatrix} \mu_0 & 0 & 0 & 0 \\ 0 & \mu_1 & 0 & 0 \\ 0 & 0 & \mu_2 & 0 \\ 0 & 0 & 0 & \mu_3 \end{pmatrix} \tag{3.19}$$

The μ s are the singular values of A and $e_a{}^\mu$ and $E^b{}_\nu$ the left and right Partial Lorentz Transformations that bring A to the LSVD (Lorentzian Singular Value Decomposition) form (3.19). Since the eigenvalues of B are the squares of the singular values of A, it follows that λs are positive. At this stage μ_1, μ_2, μ_3 can all have either sign. By Partial Lorentz transformations (e.g by rotation by π in the $x - y$ plane) it is possible to reverse the signs of two of μ_1, μ_2, μ_3. By such transformations it is possible to arrange for all of μ_1, μ_2, μ_3 to have the same sign. μ_0, of course, is positive (3.14).

3.4   States and Separability

The DEC is a necessary condition for ρ to be a state (have non negative eigenvalues). From the LSVD form (3.19) it is easy to write down sufficient conditions on

the μs to ensure that ρ is positive. The diagonal form (3.19) leads to a state,

$$\rho = \begin{pmatrix} \mu_0 - \mu_3 & 0 & 0 & \mu_2 - \mu_1 \\ 0 & \mu_3 + \mu_0 & -\mu_1 - \mu_2 & 0 \\ 0 & -\mu_1 - \mu_2 & \mu_3 + \mu_0 & 0 \\ \mu_2 - \mu_1 & 0 & 0 & \mu_0 - \mu_3 \end{pmatrix} \tag{3.20}$$

with eigenvalues

$$\mu_1 - \mu_2 - \mu_3 \;+\; \mu_0$$

$$-\mu_1 + \mu_2 - \mu_3 \;+\; \mu_0$$

$$-\mu_1 - \mu_2 + \mu_3 \;+\; \mu_0$$

$$\mu_1 + \mu_2 + \mu_3 \;+\; \mu_0$$

$$\tag{3.21}$$

Requiring that the eigenvalues of ρ are positive gives us the conditions

$$-\mu_1 + \mu_2 + \mu_3 \;\leq\; \mu_0$$

$$\mu_1 - \mu_2 + \mu_3 \;\leq\; \mu_0$$

$$\mu_1 + \mu_2 - \mu_3 \;\leq\; \mu_0$$

$$\mu_1 + \mu_2 + \mu_3 \;\geq\; -\mu_0$$

$$\tag{3.22}$$

The form of $T^a{}_b$ gives us a way to express it in separable form, provided $T^a{}_b$ (See also the Appendix B) satisfies the strong energy condition [21]:

$$\mu_1 + \mu_2 + \mu_3 \leq \mu_0.$$

Let us define an orthonormal frame T^a, X^a, Y^a, Z^a in which $T^a_{\ b}$ is diagonal. Suppose first that μ_1, μ_2, μ_3 are all non negative.

$$T^a_{\ b} = \mu_1 X^a X_b + \mu_2 Y^a Y_b + \mu_3 Z^a Z_b + \mu_0 T^a T_b \tag{3.23}$$

Let us also define lightlike vectors $X_\pm = (T \pm X)/\sqrt{2}$ and similarly $Y_\pm$ and $Z_\pm$. From the identity

$$X^a_+ X_{+b} + X^a_- X_{-b} = X^a X_b + T^a T_b \tag{3.24}$$

we can write $T^a_{\ b}$ as

$$
\begin{aligned}
T^a_{\ b} = \quad & \mu_1 (X^a_+ X_{+b} + X^a_- X_{-b}) \\
+ \ & \mu_2 (Y^a_+ Y_{+b} + Y^a_- Y_{-b}) \\
+ \ & \mu_3 (Z^a_+ Z_{+b} + Z^a_- Z_{-b}) \\
+ \ & (\mu_0 - \mu_1 - \mu_2 - \mu_3) T^a T_b
\end{aligned}
\tag{3.25}
$$

T is explicitly in separable form provided

$$\mu_0 \geq \mu_1 + \mu_2 + \mu_3,$$

i.e. the Strong Energy Condition(SEC) is satisfied.

If μ_1, μ_2, μ_3 are all non positive, they automatically satisfy (3.22) $|\mu_1| + |\mu_2| + |\mu_3| \leq \mu_0$. The identity

$$X^a_+ X_{-b} + X^a_- X_{+b} = -X^a X_b + T^a T_b \tag{3.26}$$

gives us

$$
\begin{aligned}
T^a_{\ b} = \quad & |\mu_1|(X^a_+ X_{-b} + X^a_- X_{+b}) \\[6pt]
+ \quad & |\mu_2|(Y^a_+ Y_{-b} + Y^a_- Y_{+b}) \\[6pt]
+ \quad & |\mu_3|(Z^a_+ Z_{-b} + Z^a_- Z_{+b}) \\[6pt]
+ \quad & (\mu_0 - |\mu_1| - |\mu_2| - |\mu_3|)T^a T_b,
\end{aligned}
\tag{3.27}
$$

which is in separable form.

Conversely, if A represents a separable state, we can write

$$
A_{\mu\nu} = \sum_i w_i \, n^i_\mu m^i_\nu
$$

where $w_i > 0$ are positive weights and n^i and m^i are future pointing causal vectors. Without loss of generality we can suppose n, m to be lightlike (since time-like vectors are convex combinations of lightlike ones) and further absorb w_i into the vectors n, m. Computing

$$
\begin{aligned}
A_{xx} + A_{yy} + A_{zz} &= \sum_i \vec{n}_i . \vec{m}_i \;\leq\; \sum_i |n_i||m_i| \\
&= \sum_i n_{i0} m_{i0} \\
&= A_{00}
\end{aligned}
\tag{3.28}
$$

Applying this argument to the LSVD diagonal form T, we see that separable states satisfy the SEC. Thus we have shown that the SEC is necessary and sufficient for separability. If the SEC is satisfied we find an explicit decomposition of $T^a_{\ b}$ (and therefore of A) into separable form.

3.5 Three dimensional representation of the two-qubit state space

As we discussed earlier, the 16 dimensional space of un-normalized density matrices undergoes a reduction to a 4 parameter family of twelve dimensional fibers under the action of left and right Partial Lorentz Transformations. In fact, the 4 parameter $(\mu_0, \mu_1, \mu_2, \mu_3)$ representation can be further reduced to a 3 parameter representation since only the ratios are relevant. Since we have assumed $\lambda_0 \neq 0$ we have $\mu_0 \neq 0$. By scaling let us set $\mu_0 = 1$ and plot a simple three dimensional representation of the state space. From the DEC, it follows that $0 \leq |\mu_{\hat{a}}| \leq 1, \hat{a} = 1, 2, 3$, so the states lie within the cube of side 2 whose body diagonal connects $\tilde{\mathbf{P}} = \{-1, -1, -1\}$ to $\mathbf{P} = \{1, 1, 1\}$.

As mentioned earlier, we can suppose that μ_1, μ_2, μ_3 have the same sign. Instead of the eight octants spanned by the cube above, we need only restrict ourselves to two of the eight octants: the positive octant and the negative octant. This results in the figure shown in Figure 3.2.

The region shaded blue is the set of separable states. All states in the negative octant are separable and form the convex hull $S^- = H(\mathbf{O}, -\mathbf{i}, -\mathbf{j}, -\mathbf{k})$ of the origin $\mathbf{O}$ and the tips of the unit vectors $-\mathbf{i}, -\mathbf{j}, -\mathbf{k}$. The plane passing through $-\mathbf{i}, -\mathbf{j}, -\mathbf{k}$ divides μs satisfying the state conditions (3.22) from those that don't. In the positive octant, the separable states form the convex hull $S^+ = H(\mathbf{O}, \mathbf{i}, \mathbf{j}, \mathbf{k})$ of the origin $\mathbf{O}$ and the tips of the unit vectors $\mathbf{i}, \mathbf{j}, \mathbf{k}$. The plane passing through $\mathbf{i}, \mathbf{j}, \mathbf{k}$ divides the separable states from the entangled states. All states "above" this plane (Figure 3.2)
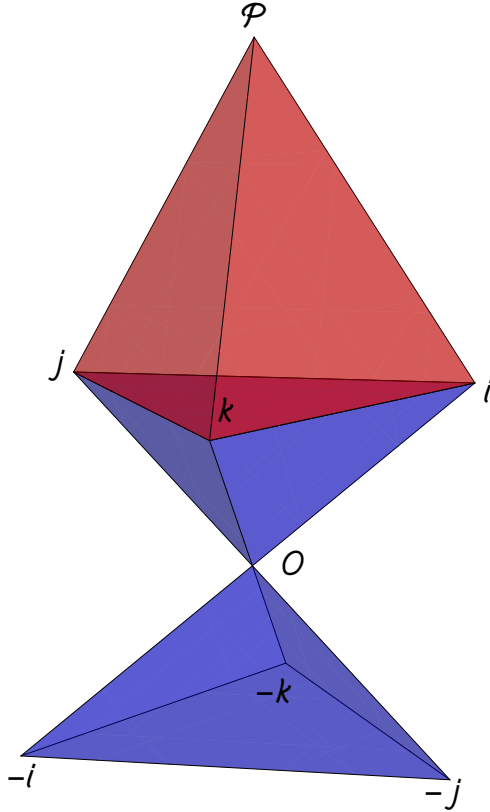
Figure 3.2: A three dimensional representation of the state space of μ_1, μ_2, μ_3 for Type-I states. The red tetrahedron ($\{\mathbf{P}, \mathbf{i}, \mathbf{j}, \mathbf{k}\}$) represents the set of entangled states and the blue tetrahedra ($\{\mathbf{O}, \mathbf{i}, \mathbf{j}, \mathbf{k}\}$ and $\{\mathbf{O}, -\mathbf{i}, -\mathbf{j}, -\mathbf{k}\}$), the set of separable states. The boundary between these two sets is defined by a plane passing through the tips of the unit vectors $\mathbf{i}, \mathbf{j}, \mathbf{k}$.

are entangled and shown in red.

Note also that under inversion, (reversing the sign of all of μ_1, μ_2, μ_3), the separable states S^+ and S^- exchange places, but the entangled states are mapped to regions outside the state space. In fact, inversion $\mathcal{I}$ in the $\vec{\mu}$ space is identical to the partial transpose (and to the partial inversion). As expected from the PPT test, the entangled states (in red in Figure 3.2) are mapped outside the state space by the
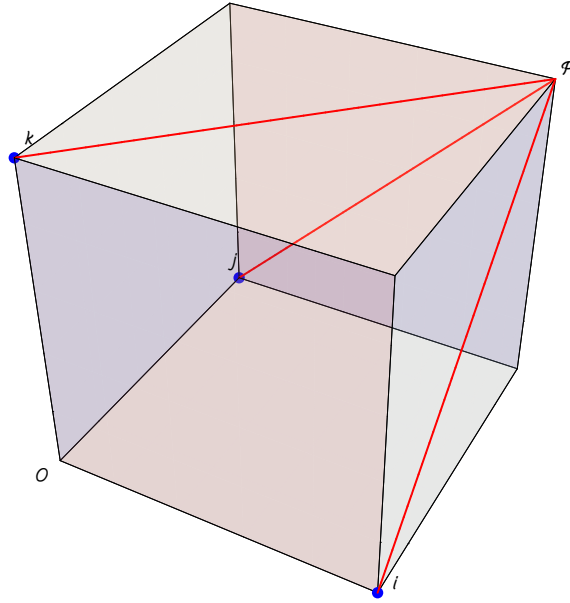
Figure 3.3: A three dimensional representation of the state space for Type-II states.The three blue dots at $\{\mathbf{i}, \mathbf{j}, \mathbf{k}\}$ represent separable states and the three red lines $\{\mathbf{i}, \mathbf{P}\}$, $\{\mathbf{j}, \mathbf{P}\}$, $\{\mathbf{k}, \mathbf{P}\}$ represent entangled states.

partial transpose operation.

Finally we remark that the states on the boundary of S^+ and S^-, where one or more μ s vanishes have to be identified with their images under inversion. With this identification, Figure 3.2 gives a complete elucidation of the generic state space. Each point in the state space of Figure 3.2 represents an equivalence class of states, all of which are related by partial Lorentz transformations.

The generic state space includes most of the states of the two qubit system, including all strictly positive density matrices. The non generic states are characterised by the absence of a timelike eigenvector for B (D). We deal with these in the next section titled exceptional states[29].

3.6 Exceptional States

There are some states which do not admit a timelike eigenvector for B (D). For this to happen, the dominant eigenvalue λ_0 has to be degenerate.

Type-II States:

These states are characterised by the fact that B (D) has a repeated lightlike eigenvector with positive eigenvalue. The dominant eigenvector can be chosen to be $= X_+$. For Type-II states, the LSVD matrix $T^a_{\ b}$ is not diagonal but only in Jordan form. The basis which achieves this form is not a standard Lorentz frame $\{T, X, Y, Z\}$ but a null frame $\{X_+, X_-, Y, Z\}$. The Jordan form is

$$
T^a_{\ b} = \begin{pmatrix} \mu_0 & 0 & 0 & 0 \\ x & \mu_0 & 0 & 0 \\ 0 & 0 & \mu_2 & 0 \\ 0 & 0 & 0 & \mu_3 \end{pmatrix}
\tag{3.29}
$$

where $x > 0$. (DEC guarantees $x \geq 0$, but if x vanishes, A is of Type-I, since B has *two* distinct lightlike eigenvectors X_+, X_-.) We have arbitrarily selected μ_1 degenerate with μ_0. Since $\mu_1 = \mu_0$ is positive, we can arrange for μ_2, μ_3 also to be positive and we have

$$
\begin{aligned}
T^a_{\ b} = \quad & \mu_0(X^a_- X_{+b} + X^a_+ X_{-b}) \\
+ \quad & \mu_2(Y^a_+ Y_{+b} + Y^a_- Y_{-b}) \\
+ \quad & \mu_3(Z^a_+ Z_{+b} + Z^a_- Z_{-b}) \\
+ \quad & x X^a_+ X_{+b}
\end{aligned}
\tag{3.30}
$$

The condition that A is defined from a state (Equation (3.22)) requires $\mu_2 = \mu_3$. From the argument at the end of section 3.4, we see that these states are entangled if $\mu_2 = \mu_3 > 0$.

If $\mu_2 = \mu_3 = 0$, then

$$T^a_{\ b} = \mu_0(X^a_- X_{+b} + X^a_+ X_{-b}) + xX^a_+ X_{+b}.$$

(3.31)

These states are clearly in separable form. The Type-II states are shown in Figure 3.3. The blue dots represent the separable states and the red lines the entangled ones. By switching the roles of B and D, we also have states where the Jordan form is the transpose of (3.29).

Type-II0 States:

Finally, we address the possibility that the dominant eigenvalue λ_0 vanishes. As described in the appendix, these states come in three families (t is a timelike vector and x is positive):

1. Type-II0a: $A^\mu_{\ \nu} = xt^\mu l_\nu$. B vanishes identically.

2. Type-II0b: $A^\mu_{\ \nu} = xl^\mu t_\nu$. D vanishes identically.

3. Type-II0c: $A^\mu_{\ \nu} = xl_1^{\ \mu} l_{2\nu}$. Both B and D vanish.

These states are separable and because they have vanishing μ_0, do not find a place in either Figure 3.2 or Figure 3.3. The form of the stress tensor for Type-II0c is $T^a_{\ b} = xX_+^{\ a}X_{+b}$. Such a form for the stress tensor appears in Relativity where it is known as a null fluid or null dust[21]. It represents radiation which is all travelling in the same direction.

To summarise our classification (which is explained in more detail in the appendix),

1. Type-I: $\lambda_0 > 0$ and B (and D) admit a timelike eigenvector.

2. Type-II: $\lambda_0 > 0$ and B (and D) has a repeated lightlike eigenvector.

3. Type-II0: $\lambda_0 = 0$. B or D (or both) vanish.

3.7 Classification of States

In the text, the division of states into different types is only briefly described with a reference to Hawking and Ellis [21]. Ref.[21] gives four possible types for the stress tensor. Of these, Type-III and Type-IV violate the weak energy condition and therefore also the dominant energy condition. These types are irrelevant to our present context, since *all* states satisfy the DEC. Here we describe briefly our classification of states into Type-II0, Type-I and Type-II. Our Type-II0 is contained in Hawking's Type-II. We separate it from Type-II because it does not fit into the graphical representation for Type-II states.

To classify the states, we look at the action of $A^\mu{}_\nu$ on lightlike vectors (which corresponds to a pure state of a quantum system). Are there lightlike vectors which are mapped to the zero vector? If the answer is yes, the state is

Type-II0: This is further divided into three classes as follows.

Type-II0a: A takes some lightlike vector l^ν to zero. $A^\mu{}_\nu l^\nu = 0$. Contracting with an arbitrary timelike covector α_μ, and noting that $\alpha_\mu A^\mu{}_\nu$ is causal and orthogonal to l^ν

we see that A must take the form

$$A^\mu_{\ \nu} = xt^\mu l_\nu \tag{3.32}$$

where x is positive, t timelike and l, t normalised by $t.t = l.t = 1$. This form is Type-II0a. In this case B vanishes and $D^\mu_{\ \nu} = x^2 l^\mu l_\nu$.

Type-II0b: The transpose of A takes some lightlike vector l^ν to zero. $A_\mu^{\ \nu} l^\mu = 0$. Contracting with an arbitrary timelike covector α_ν, and noting that $\alpha_\nu A_\mu^{\ \nu}$ is causal and orthogonal to l^μ we see that A must take the form

$$A_\mu^{\ \nu} = x l_\mu t^\nu \tag{3.33}$$

where x is positive, t timelike and l, t normalised by $t.t = l.t = 1$. In this case D vanishes and $B^\mu_{\ \nu} = x^2 l^\mu l_\nu$.

Type-II0c: Both A and the transpose of A takes some lightlike vector to zero. $A^\mu_{\ \nu} l_1^\nu = 0$ and $A_\mu^{\ \nu} l_2^\mu = 0$. Arguing similarly, we see that A must take the form

$$A^\mu_{\ \nu} = x l_2^\mu l_{1\nu} \tag{3.34}$$

where x is positive, l_1 and l_2 lightlike and l_1, l_2 normalised by $l_1.l_2 = 1$. This form is Type-II0c. In this case both B and D vanish.

If no lightlike vectors are mapped to zero by A or its transpose, we ask how many lightlike vectors mapped by A (or its transpose) to lightlike vectors. If the answer is exactly one, the state is of

Type-II: We have

$$A^\mu_{\ \nu} l^\nu = \mu_0 n^\mu \tag{3.35}$$

with $\mu_0 > 0$. It follows that the transpose of A maps n to l

$$A_\nu^{\ \mu} n^\nu = \mu_0 l^\mu \tag{3.36}$$

and that D and B have a single lightlike eigenvector

$$D^{\mu}{}_{\nu}l^{\nu} = \mu_0^2 l^{\mu} \tag{3.37}$$

$$B^{\mu}{}_{\nu}n^{\nu} = \mu_0^2 n^{\mu} \tag{3.38}$$

In this case B and D can only be brought to Jordan form (3.29).

Type-I If A maps two (or more) distinct lightlike vectors l_1^{μ} and l_2^{μ} to lightlike vectors n_1^{μ} and n_2^{μ}, the same argument shows that B has *two* (or more) *distinct* lightlike eigenvectors with the same eigenvalue. If B (D) has two *distinct* lightlike eigenvectors X_+ and X_- with the same eigenvalue λ_0, B also admits a timelike eigenvector $X_- + X_+$ and thus is Type-I.

If there are no lightlike vectors mapped to lightlike vectors by A, $A^{\mu}{}_{\nu}l^{\nu}$ is strictly timelike for all lightlike l. We have a strict version of the DEC.

$$l^{\mu}A_{\mu\nu}n^{\nu} > 0 \tag{3.39}$$

This implies that A, its transpose and the composites B and D map lightlike vectors to timelike vectors. To classify the remaining states, let us consider the function $f(l, n)$ defined on the space of distinct lightlike directions determined by the lightlike vectors l and n. $(l.l = n.n = 0)$

$$f(l, n) := \frac{B_{\mu\nu}l^{\mu}n^{\nu}}{l.n} \tag{3.40}$$

By construction $f(l, n)$ depends only on the lightlike directions of l, n. By (3.39), the numerator is positive and the function $f(l, n)$ approaches positive infinity as l approaches n. The global minimum of f occurs at l_0, n_0 with l_0 and n_0 linearly independent lightlike vectors, which we can normalise by $l_0.n_0 = 1$. By considering

the first variation of f around its minimum, we see that the l_0, n_0 plane is mapped to itself by B:

$$Bl_0 = \alpha l_0 + \beta n_0 \tag{3.41}$$

$$Bn_0 = \gamma l_0 + \alpha n_0, \tag{3.42}$$

where $\alpha = B(l_0, n_0), \beta = B(l_0, l_0), \gamma = B(n_0, n_0)$ are all strictly positive by (3.39). It is easily seen that B has dominant eigenvalue $\lambda_0 = \alpha + \sqrt{\beta\gamma}$ and dominant eigenvector $l_0 + (\sqrt{\beta/\gamma})n_0$, whose norm $2\sqrt{\beta/\gamma}$ is strictly positive. The dominant eigenvector is timelike and the state is Type-I. This is in fact the generic case and most of the states of the two qubit system fall in this category. In fact, all the interior states where the eigenvalues of ρ are strictly positive fall into Type-I.

3.8 Conclusion

We have presented a necessary and sufficient criterion to detect two qubit entanglement. In addition our approach reveals a separable form of the density matrix if it exists. Our approach is based on Lorentzian geometry, in particular a Lorentzian Singular Value Decomposition. The LSVD has also been described by Avron et al [29]. They also notice the relevance of the Dominant Energy Condition that all states must satisfy and go on to give a three dimensional graphical representation of the state space. However, Avron et al [29] do not propose an entanglement test, as we have done. Neither do they comment on the relevance of the strong energy condition to entanglement. Our graphical representation, though related to [29], is simpler, because we reduce the picture from eight octants to two. There has also been work

[30] which proposes an entanglement test based on a standard Singular Value Decomposition. However, this test only works on a restricted class of states: the reduced density matrices of each subsystem have to be maximally disordered. We go beyond earlier work in providing an explicit construction of a separable state for the density matrix in those cases where it exists.

Our focus in this chapter is entirely on quantum entanglement. There are other quantum correlations like discord described for example in [31], which are not considered here. Ref.[31] studies the so-called X states, which have nonzero entries on the diagonal and the anti-diagonal. The focus of Ref.[31] is the study of quantum discord for two qubit X states, with a view to understanding the relation between quantum discord, classical correlations and entanglement. They observe that these are independent measures of correlation.

Ref. [32] also addresses X states and quantum discord. Just as we do here, Ref. [32] also makes use of Lorentzian structures. However, the local operations considered are local unitary transformations (six parameters in all) and the canonical forms used are X states, which are characterised by essentially five parameters. As a result the total dimension of the state space explored is generically eleven, which falls short of the dimension of fifteen, for normalised states. In contrast, our use of local (or partial) Lorentz transformations provides twelve parameters, which along with the four eigenvalues of the canonical diagonal form provides a complete characterisation of the sixteen dimensional unnormalised state space. It is interesting to note that our Equation (3.20) represents an X state, but the number of parameters appearing is only four. In our treatment, not all X states are required to produce the general

state by local Lorentz transformations.

There appears to be a rich Lorentzian structure hidden within the theory of quantum entanglement. The relation is probably best appreciated using spinors, which have been studied by relativists like Penrose, Newman etc[33]. In this exposition, we have deliberately avoided the use of spinor language since this is not widely used in the general physics community. The key property of Partial Lorentz Transformations used here is that they map states to states, separable states to separable states and entangled states to entangled states. This allows us to decompose the total set of states into equivalence classes. Any two elements from the same equivalence class are related by Partial Lorentz Transformations and are either both separable or both entangled. To decide whether a particular equivalence class is entangled or separable, we can choose any element from the class. By choosing the canonical form given by the LSVD decomposition, we are able to easily determine if the class is separable or entangled.

Although the test proposed in [34] relies only on the eigenvalues of B (D), it is important to realise that the *state* depends both on the eigenvalues and the eigenvectors of B (D). While a knowledge of the eigenvalues is enough to determine if a state is separable, one needs also the eigenvectors to explicitly write out the separable form.

By setting quantum states in correspondence with tensors in Minkowski space, we were naturally led to a formalism combining Quantum Information Theory with Relativity. While the analogy at this level is a purely formal one, it may contain the seeds of some future amalgamation of Relativity with Quantum Information Theory.

For instance one can consider physical realisations of PLT s by forming two qubits in an entangled state, separating the qubits and acclerating one of them adiabatically to a new Lorentz frame. One would expect the states to transform according to the formulae of this chapter.

How does this theory work in higher dimensional quantum systems? It would appear that one has to find a maximal group of transformations which takes states to states and separable states to separable states. These would be the appropriate generalisation of PLT s to the higher dimensional case. Once such a group of entanglement preserving transformations is identified the dimensionality of the problem can be drastically reduced. We hope to interest the quantum information community in this new approach to the problem of detecting quantum entanglement.

Chapter 4

Role of Entanglement in a Coarse Quantum Measurement

An observer plays an active role in a quantum measurement process. Unlike measurements in classical systems where the act of measurement merely "reveals" the value of the observable being measured without actually perturbing the system, the act of observation in quantum mechanics forces the quantum system to "collapse" into one of the possible alternative measurement outcomes. Entanglement plays a key role in all measurement processes. In order to obtain any information about a dynamical variable from a quantum system, an observer establishes a coupling between the system and the measuring apparatus. This coupling entangles the state corresponding to each alternative outcome of the system to a unique state of the measuring apparatus. By observing the state of the measuring device one then infers the state of the quantum system. This is the general scheme of the measurement process in a quantum system. In this chapter, we will take a closer look at the

measurement process in the context of the Stern-Gerlach experiment. In particular, we will investigate the effect of the extent of entanglement on measurement. We will also study the idea of a coarse-grained measurement and see its effect on the Wigner matrix associated with the system density matrix.

4.1 The measurement process

Let us summarize the measurement process in quantum mechanics. Our system is initially in a coherent superposition of states $|S\rangle = \sum_i c_i |S_i\rangle$ in an orthonormal basis which diagonalises the quantity being measured. To begin with, the system plus apparatus is in the product state $|\psi\rangle = |S\rangle|A\rangle$, in which the system and the apparatus are unentangled. It is useful to logically break up the measurement process into three steps. The first step in the measurement process entails coupling between the quantum system and the measuring apparatus so that the total state evolves unitarily to an entangled state $U|\psi\rangle = \sum_i c_i |S_i\rangle|A_i\rangle$[1]. This state can be represented as a pure density matrix

$$\rho = |\psi\rangle\langle\psi| = \sum_{ij} c_j^* c_i |S_i\rangle|A_i\rangle\langle S_j|\langle A_j| \tag{4.1}$$

After the first step, the density matrix of the system takes the impure form

$$\tilde{\rho} = \sum_i |c_i|^2 |S_i\rangle\langle S_i| \tag{4.2}$$

which is interpretable as a classical mixture of states. Finally, the impure diagonal density matrix (4.2) goes over to a pure state $c_i |S_i\rangle\langle S_i| c_i^*$. The first step can

---

[1]We note that in general, the $|A_i\rangle$ s need not be orthonormal.

be explained entirely in terms of unitary evolution and therefore is not controversial. The final step, sometimes called "collapse", has been debated extensively as the "quantum measurement problem". This singling out of one outcome from many possibilities is not addressed here. Let us note that, even in classical probability theory, there is a singling out of one from several outcomes (only one horse wins the race). We address here the second step; the transition from quantum superpositions to classical mixtures. This is the focus of the chapter. In this chapter, we investigate the Stern-Gerlach experiment from the perspective of a coarse quantum measurement (CQM), in which we recognize the fact that all experiments are constrained by bounded resources. We model these constraints by using a screen whose size and spatial resolution are fixed. The spatial resolution of the screen is given by the pixel size and the size of the screen determines the total number of pixels. Experimentally one can only say that an atom was incident on our screen somewhere within a pixel. Fixing these resources imposes ultraviolet as well as infrared cutoffs on the experimental probes. In this Chapter we are more concerned with the short distance cutoff.

4.2 The Stern-Gerlach set up

Let us consider a Stern Gerlach (**SG**) type experiment for measuring the spin of a silver atom. In a typical SG setup a beam of silver atoms produced in an oven is made to pass through an inhomogeneous magnetic field and later detected on a screen placed at a distance in the direction of the propagating beam (see Figure 4.1). We will consider the spin of the silver atom as our quantum system and the
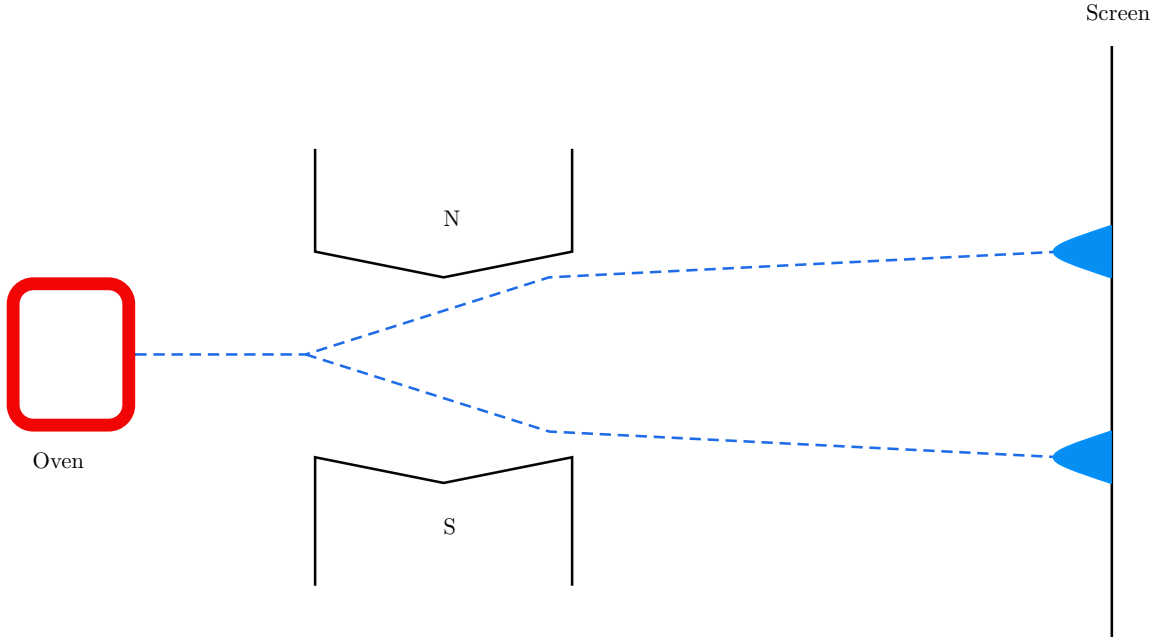
Screen

Figure 4.1: Figure shows a typical Stern-Gerlach setup. A beam of silver atoms is produced in the oven. This beam then travels through an inhomogeneous magnetic field. Finally, they are detected on the screen.

center of mass as the measuring apparatus. Following the general scheme of the

measurement we establish a coupling between the spin(quantum system) and the

center of mass of the silver atom(measuring apparatus) by allowing it to pass through

an inhomogeneous magnetic field of the form $\vec{B} = (B_0 y, B_0 x, 0)^2$. The system and

the measuring apparatus evolves with the Hamiltonian:

$$\hat{H} = \frac{1}{2m}(p_x^2 + p_z^2) - xF\sigma_y \qquad \text{where} \qquad F = g\mu_B \frac{\hbar}{2} B_0 \tag{4.3}$$

with g the Landé g factor and μ_B the Bohr magneton. Let the initial state of the

spin and the center of mass of the silver atom be $|\Psi(0)\rangle = \psi(x,0) \otimes |\chi(0)\rangle$ where

---

[2]This field is both divergence and curl free i.e.

$$\boldsymbol{\nabla} \times B = 0 \quad \text{and} \quad \boldsymbol{\nabla} \cdot B = 0$$

$\psi(x,0) = \left(\frac{2}{\pi\sigma^2}\right)^{1/4} \exp\left(-\frac{x^2}{\sigma^2}\right)$ is the initial Gaussian wave packet associated with the position of the center of mass of the silver atom and $|\chi(0)\rangle = \frac{1}{\sqrt{2}}\left(|+\rangle + |-\rangle\right)$ is the spin part[3] of the silver atom. Notice that at this point of time there is *no entanglement* between the system(spin) and the measuring apparatus(the position of the center of mass), as the total wave function corresponding to the composite state (system and measuring apparatus) is *separable*. We will later see that as the system and the apparatus interact entanglement will set in. In order to time evolve this initial wave packet $|\Psi(0)\rangle$, we first need to find the propagator for the interaction of the system and the apparatus. The time evolved state $|\Psi(t)\rangle$ can then be obtained by "folding" the initial Gaussian with the propagator matrix.

4.3　Propagator for the Stern-Gerlach Hamiltonian

We will use the path-integration technique for calculating the propagator of the Hamiltonian (4.3). The propagator K between initial and final points $x(0) = x_i$ and $x(t) = x$ will be given by[35],

$$K(x,t;x_i,0) = \int_{x_i}^{x} \exp\left(\frac{1}{\hbar}S[x(t)]\right)\mathcal{D}[x(t)] \qquad (4.4)$$

The Lagrangian for the problem can be written as

$$\mathcal{L} = \frac{1}{2}m\dot{x}\dot{x} + xF$$

where F is the constant force acting on the particle such that $a = F/m$. Since the potential is of the form $V(x) = a + bx + cx^2 + d\dot{x} + ex\dot{x}$ the exact propagator can

---

[3] $|+\rangle, |-\rangle$ are the eigenstates of σ_y

be obtained by just considering the action along the classical path[36]. Let us now calculate the action along the classical path with the condition $x(0) = x_i$, $\dot{x}(0) = \left(x - x_i - \frac{1}{2}at^2\right)/t$; $x(t) = x$, $\dot{x}(t) = \left(x - x_i + \frac{1}{2}at^2\right)/t$.

$$S_{classical} = \int_0^t \left(\frac{1}{2}m\dot{x}\dot{x} + xF\right)dt = \left[\frac{m}{2}(x\dot{x})\right]_0^t - \underbrace{\frac{m}{2}\int_0^t (\ddot{x} - a)dt}_{=0} + \frac{m}{2}\int_0^t (ax)dt$$

Substituting the values of $x(t), \dot{x}(t), x(0), \dot{x}(0)$ we obtain

$$S_{classical} = \frac{m}{2t}(x - x_i)^2 + \frac{Ft}{2}(x + x_i) - \frac{F^2t^3}{24m}$$

so the propagator is,

$$K^{++}(x, t \;;\; x_i, 0) = A(t)\exp\left(\frac{i}{\hbar}\left(\frac{m}{2t}(x - x_i)^2 + \frac{Ft}{2}(x + x_i) - \frac{F^2t^3}{24m}\right)\right)$$

where $A(t)$ is the normalization which can be obtained by using the fact that as $t \to 0$, $K^{++} \to \delta(x - x_i)$. On comparison we obtain $A(t) = \sqrt{\frac{m}{2i\pi\hbar t}}$. We can obtain $K^{--}(x, t \;;\; x_i, 0)$ by replacing $F \longrightarrow -F$. Hence,

$$K^{++}(x, t \;;\; x_i, 0) = \sqrt{\frac{m}{2i\pi\hbar t}}\exp\left(\frac{i}{\hbar}\left(\frac{m}{2t}(x - x_i)^2 + \frac{Ft}{2}(x + x_i) - \frac{F^2t^3}{24m}\right)\right) \quad (4.5)$$

$$K^{--}(x, t \;;\; x_i, 0) = \sqrt{\frac{m}{2i\pi\hbar t}}\exp\left(\frac{i}{\hbar}\left(\frac{m}{2t}(x - x_i)^2 - \frac{Ft}{2}(x + x_i) - \frac{F^2t^3}{24m}\right)\right) \quad (4.6)$$

$$K^{+-}(x, t \;;\; x_i, 0) = 0 \quad (4.7)$$

$$K^{-+}(x, t \;;\; x_i, 0) = 0 \quad (4.8)$$

4.3.1 Energy eigenstates of the SG-Hamiltonian

The time independent Schrödinger Equation for the Hamiltonian (4.3) mentioned above is:

$$\left[-\frac{\hbar^2}{2m}\left(\frac{\partial^2}{\partial x^2} + \frac{\partial^2}{\partial z^2}\right) - xF\sigma_y\right]\phi(x, z) = E\phi(x, z) \quad (4.9)$$

where $\phi(x, z)$ is a two component Pauli spinor. We assume without loss of generality, a solution of the form $\phi(x, z) = \theta(x, z)e^{ikz}$ where $\frac{\hbar^2 k^2}{2m} = E$. Then the above equation becomes

$$-\frac{\hbar^2}{2m}\frac{\partial^2 \theta(x, z)}{\partial x^2} - \frac{\hbar^2}{2m}\left(\frac{\partial^2 \theta(x, z)}{\partial z^2} + 2ik\frac{\partial \theta(x, z)}{\partial z} - k^2\theta(x, z)\right) - xF\sigma_y\theta(x, z) = E\theta(x, z)$$

Furthermore if we assume $\frac{\partial^2 \theta(x,z)}{\partial z^2} \ll \frac{\partial \theta(x,z)}{\partial z}, \frac{\partial^2 \theta(x,z)}{\partial x^2}$ (the paraxial approximation) then equation (4.9) reduces to

$$\frac{\hbar^2}{2m}\frac{\partial^2 \theta(x, z)}{\partial x^2} + \frac{ik\hbar^2}{m}\frac{\partial \theta(x, z)}{\partial z} - xF\sigma_y\theta(x, z) = 0. \tag{4.10}$$

We choose to work in the σ_y basis so that equation (4.10) becomes a pair of uncoupled differential equations with solutions $\theta_+(x, z)$ and $\theta_-(x, z)$ corresponding to eigenvalues +1 and -1 for σ_y. We will first solve for $\theta_+(x, z)$ and then replace F with $-F$ to get the other solution $\theta_-(x, z)$. The equation for $\theta_+(x, z)$ then reads

$$\frac{\hbar^2}{2m}\frac{\partial^2 \theta_+(x, z)}{\partial x^2} + \frac{ik\hbar^2}{m}\frac{\partial \theta_+(x, z)}{\partial z} - xF\theta_+(x, z) = 0 \tag{4.11}$$

In order to solve Eq(4.11) we take the Fourier transform of the above equation with respect to x and get:

$$\frac{ik\hbar^2}{m}\frac{\partial \Theta_+(p, z)}{\partial z} = i\hbar F\frac{\partial \Theta_+(p, z)}{\partial p} - \frac{p^2}{2m}\Theta_+(p, z) \tag{4.12}$$

where $\Theta_+(p, z)$ is the Fourier transform of $\theta_+(x, z)$. This equation can now be solved using a separation of variables of the form $\Theta_+(p, z) = \zeta(z)\xi(p)$. Using this substitution we get two ordinary differential equations (ODE)

$$\frac{ik}{m}\hbar^2\frac{1}{\zeta(p)}\frac{\partial \zeta(p)}{\partial z} = \frac{p^2}{2m} - \frac{i\hbar F}{\xi(p)}\frac{\partial \xi(p)}{\partial p} = \epsilon \ .$$
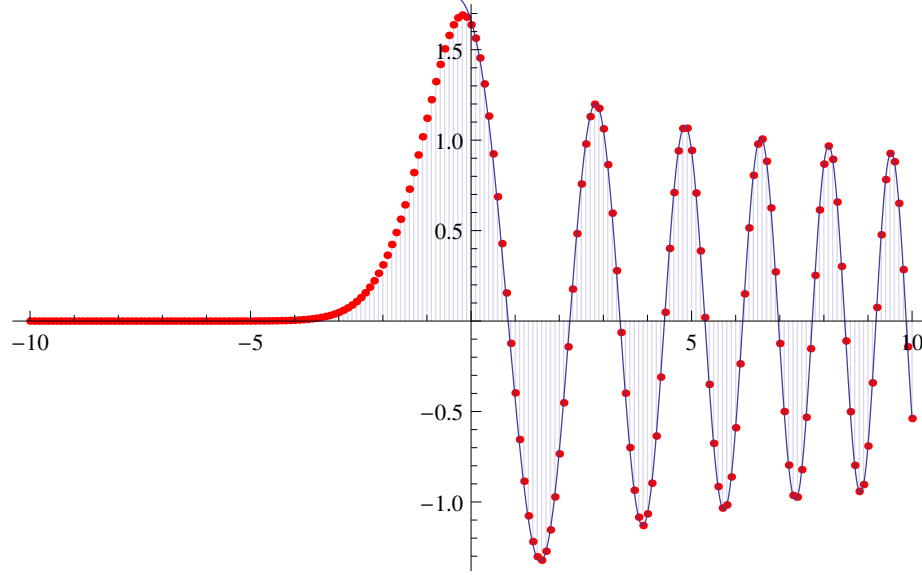
Figure 4.2: Plot of $\theta_+(x, 0)$ against x

.

Solving the above two ODE's we obtain

$$\zeta(z) = e^{-i\frac{m\epsilon}{k\hbar^2}z} \qquad \xi(p) = e^{\frac{i}{\hbar F}\left(\frac{p^3}{6m} - \epsilon p\right)} \tag{4.13}$$

In order to get $\xi(x)$ we need to take the inverse Fourier transform of $\xi(p)$.

$$\xi(x) = \frac{1}{\sqrt{2\pi\hbar}} \int_{-\infty}^{\infty} e^{\frac{i}{\hbar F}\left(\frac{p^3}{6m} - (\epsilon + xF)p\right)} dp \tag{4.14}$$

Using a stationary phase approximation to evaluate $\xi(x)$ we get[4]

$$\theta_+(x, z) = 2\left(\frac{mF^2}{2(\epsilon + xF)}\right)^{1/4} \cos\left(\frac{2\sqrt{2m}}{3\hbar F}(\epsilon + xF)^{\frac{3}{2}} - \frac{\pi}{4}\right) e^{-i\frac{m\epsilon}{k\hbar^2}z} \tag{4.15}$$

$$\theta_-(x, z) = 2\left(\frac{mF^2}{2(\epsilon - xF)}\right)^{1/4} \cos\left(\frac{2\sqrt{2m}}{3\hbar F}(\epsilon - xF)^{\frac{3}{2}} - \frac{\pi}{4}\right) e^{-i\frac{m\epsilon}{k\hbar^2}z} \tag{4.16}$$

Figure 4.2 and 4.3 shows the variation of $\theta_+(x, 0)$ and $\theta_-(x, 0)$ along the direction of the incident silver beam.

---

[4]in this case we obtain a continuous spectrum for every value of ϵ in $(-\infty, \infty)$
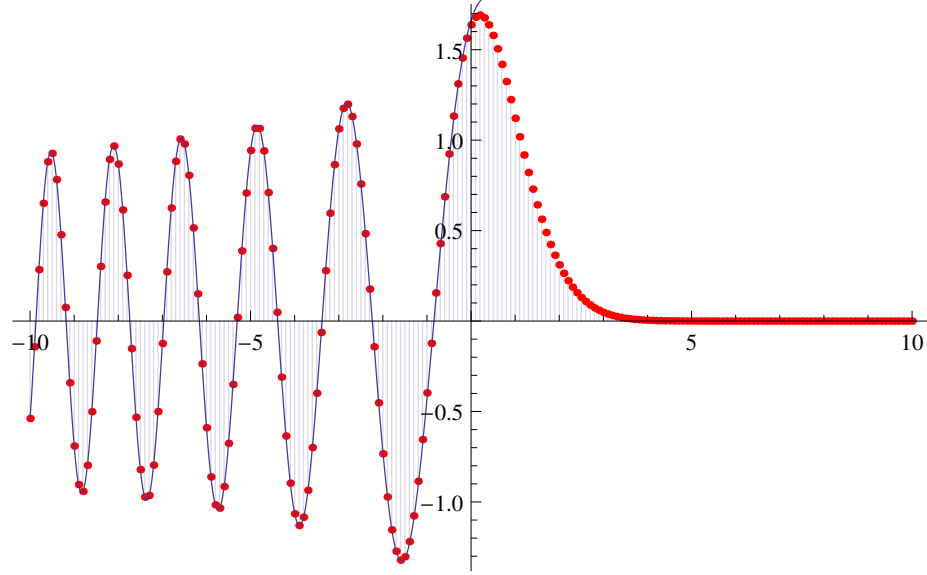
Figure 4.3: Plot of $\theta_-(x,0)$ against x

4.4   Evolution of the entanglement entropy

We now find the combined state of the system and the apparatus after t seconds of interaction. This combined state will be given by,

$$|\Psi(x,t)\rangle = \frac{1}{\sqrt{2}}\begin{pmatrix} \psi_+(x,t) \\ \psi_-(x,t) \end{pmatrix} = \frac{1}{\sqrt{2}}\int_{-\infty}^{\infty}\left[\begin{pmatrix} K^{++} & K^{+-} \\ K^{-+} & K^{--} \end{pmatrix}\begin{pmatrix} \psi_+(x_i,0) \\ \psi_-(x_i,0) \end{pmatrix}\right]dx_i \quad (4.17)$$

Using Equations (4.5) to (4.8) we easily evaluate the integral (4.17) and obtain

$$\psi_+(x,t) = \sqrt{\frac{m\sigma}{(m\sigma^2+i\hbar t)\sqrt{\pi}}}\exp\left\{-\frac{m(12x^2+\frac{a^2}{\hbar}(4im\sigma^2-\hbar t)t^3+\frac{12axt}{\hbar}(-2im\sigma^2+\hbar t))}{24(m\sigma^2+i\hbar t)}\right\}$$

(4.18)

$$\psi_-(x,t) = \sqrt{\frac{m\sigma}{(m\sigma^2+i\hbar t)\sqrt{\pi}}}\exp\left\{-\frac{m(12x^2+\frac{a^2}{\hbar}(4im\sigma^2-\hbar t)t^3-\frac{12axt}{\hbar}(-2im\sigma^2+\hbar t))}{24(m\sigma^2+i\hbar t)}\right\}$$

(4.19)

It can now be seen that the combined state of the system and the apparatus $|\Psi(x,t)\rangle$ is an *entangled* state, as this state can't be written in the form $\psi(x,t)\otimes|\chi(t)\rangle$. The

total density matrix of the system after time t is given by $\rho(x, x', \alpha, \beta) = \psi_\alpha^*(x)\psi_\beta(x')$ where α, β take the values $\{+, -\}$. The degree of entanglement can be measured by the entanglement entropy [12], which is most easily computed by tracing over the position and diagonalising the 2×2 reduced density matrix ρ_{spin} for the spin. If we trace over the position and get a reduced density matrix for the spin we have:

$$\rho_{\alpha\beta}^{spin} = \mathbf{tr}_{position}\left[\rho(x, x', \alpha, \beta)\right] \tag{4.20}$$

$$= \int_{-\infty}^{\infty} \psi_\alpha^*(x)\psi_\beta(x')dx \tag{4.21}$$

$$= \frac{1}{2}\begin{pmatrix} 1 & e^{-\frac{F^2 t^2}{4m^2\sigma^2}\left(t^2 + 4\frac{m^2\sigma^4}{\hbar^2}\right)} \\ e^{-\frac{F^2 t^2}{4m^2\sigma^2}\left(t^2 + 4\frac{m^2\sigma^4}{\hbar^2}\right)} & 1 \end{pmatrix}. \tag{4.22}$$

Now the entanglement entropy $E(\rho)$ will be given by,

$$
\begin{aligned}
E(\rho) &= -\mathbf{tr}_{position}\left[\rho \log \rho\right] \\
&= -\mathbf{tr}\left[\rho_{spin} \log(\rho_{spin})\right] \\
&= \log 2 - \frac{(1 + A(t))}{2}\log\left(1 + A(t)\right) - \frac{(1 - A(t))}{2}\log\left(1 - A(t)\right) \quad (4.23)
\end{aligned}
$$

where $A(t) = \exp\left\{-\frac{t^2(t^2 + \tau_{spread}^2)}{\tau_{separation}^4}\right\}$ and $\frac{1 \pm A(t)}{2}$ are the eigenvalues of the spin density matrix[5]. Here τ_{spread} corresponds to the time over which each of the wave-packets spreads and $\tau_{separation}$ is the time over which the centers of mass of the two wavepackets separate. Clearly, the entanglement between the spin and the center of mass of the silver atom is a function of time. In Figure 4.4 this time dependence has been shown. The entanglement entropy can also be expressed as:

$$E(\rho) = -\mathbf{tr}_{spin}\left[\rho \log \rho\right] = \int_{-\infty}^{\infty} P(x)\log P(x)dx \tag{4.24}$$

---

[5]for a discussion on $\tau_{separation}$ and τ_{spread} see section 4.5

where $P(x) = P_+(x) + P_-(x)$ and $P_\pm(x) = \psi_\pm^*(x)\psi_\pm(x)$. This is the maximum information about the spin state that can be extracted from a spatial measurement[37].

4.5 Entanglement and coarse graining

We start with an initial Gaussian wave packet of width σ for the center of mass of the silver atom then from (4.18) and (4.19) we obtain

$$|\psi_+(x,t)|^2 = \frac{1}{\sqrt{\pi(\sigma^2 + (\frac{\hbar}{m\sigma})^2 t^2)}} \exp\left(-\frac{1}{\sigma^2 + (\frac{\hbar}{m\sigma})^2 t^2}\left[x - \frac{1}{2}at^2\right]^2\right)$$

$$|\psi_-(x,t)|^2 = \frac{1}{\sqrt{\pi(\sigma^2 + (\frac{\hbar}{m\sigma})^2 t^2)}} \exp\left(-\frac{1}{\sigma^2 + (\frac{\hbar}{m\sigma})^2 t^2}\left[x + \frac{1}{2}at^2\right]^2\right)$$

This initial Gaussian wave-packet has

i) $\Delta x_{separation} = at^2$

ii) $\sigma(t) = \sqrt{\sigma^2 + \frac{\hbar^2}{m^2\sigma^2}t^2}$

Clearly, the wave-packet separates($\sim t^2$) at a faster rate than it spreads($\sim t$). We can identify two relevant time scales: $\tau_{separation} = \sqrt{\frac{2\sigma}{a}}$, the time over which the centers of mass of the two wave packets separate and $\tau_{spread} = \frac{m\sigma^2}{\hbar}$, the timescale over which each individual wave-packet spreads. We use the values $m = 1.79 \times 10^{-25}kg$, $F = 9.27 \times 10^{-22}N$ and $\sigma = 10^{-6}m$ which are experimentally reasonable. Typical values for the two time scales are $\tau_{separation} = 10^{-5}s$ and $\tau_{spread} = 10^{-3}s$. It is worth mentioning that at time $t = 11\ ms$ the separation of the wave-packet takes over the spreading. We restrict our discussion to a situation where the detection screen is placed at a location just at the point where the atom exits the magnetic field.
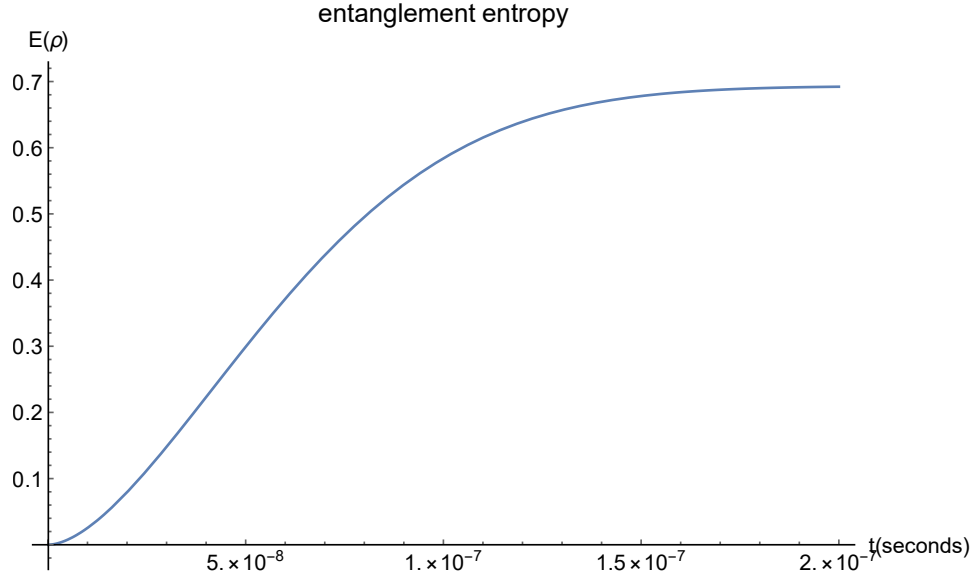
Figure 4.4: Figure shows the entanglement entropy as a function of time in seconds.

However, in general one can have a further free evolution of the separated wave-packets beyond this region in the field free space.

The entanglement entropy is plotted in Figure 4.4, which shows that $E(\rho)$, starts from zero at $t = 0$, then increases and finally settles down to an asymptotic value of $\log 2$ over a time scale of the order of $10^{-7}s$. This entanglement timescale is given by $\tau_{entanglement} = \tau_{separation}^2/\tau_{spread}$ and is shorter than the separation or spreading timescales. For $\tau_{separation} \sim t >> \tau_{entanglement}$, the entanglement is high even though the wavepackets have not cleanly separated in real space.

4.6   Visibility of the interference fringes

In order to observe the interference pattern on the screen in our setup we must have the size of the pixel of the screen smaller than the size of the successive maxima

of the interference pattern. To estimate the separation of successive maxima (say Δ_x) we compute the density matrix as shown in the next section. A brief calculation shows that for $\psi_+(x,t) = N\exp(A + iB)$ and $\psi_-(x,t) = N\exp(C + iD)$, the density matrix (4.26) has the off diagonal oscillatory term $cos(D - B)$. The separation between two maxima can thus be obtained by invoking the following condition

$$(D - B) = 2\pi \qquad \text{and hence we get} \qquad \Delta_x = \frac{2\pi\hbar}{Ft}\left(\frac{1 + \frac{\hbar^2 t^2}{m^2\sigma^4}}{2 + \frac{\hbar^2 t^2}{m^2\sigma^4}}\right) \qquad (4.25)$$

Setting $m = 1.79 \times 10^{-25}kg$, $\sigma = 10^{-6}m$ and $t = 10^{-5}s$ we get:

$$\Delta_x \leq 3.55 \times 10^{-8}m.$$

Any pixel size larger than Δ_x will wash out the interference fringes by averaging the $|\psi(x,t)|^2$ to zero due to the presence of the oscillatory term $cos(D - B)$.

4.6.1 Loss of coherence

The density matrix that corresponds to the state of the silver atom after passing through the magnetic field is given by

$$\rho(x,t) = \begin{bmatrix} |\psi_+(x,t)|^2 & \psi_+(x,t)\psi_-^*(x,t) \\ \psi_+^*(x,t)\psi_-(x,t) & |\psi_-(x,t)|^2 \end{bmatrix} \qquad (4.26)$$

In order to see the time dependence of the off-diagonal term(which captures the coherence) in the above case we integrate over the position variable and get:

$$\int_{-\infty}^{\infty} \psi_+(x,t)\psi_-^*(x,t)dx = \frac{1}{2}e^{-\frac{F^2 t^2}{4m^2\sigma^2}\left(t^2 + 4\frac{m^2\sigma^4}{\hbar^2}\right)} \qquad (4.27)$$

and also

$$\int_{-\infty}^{\infty} |\psi_+(x,t)|^2 \, dx = \frac{1}{2} \tag{4.28a}$$

$$\int_{-\infty}^{\infty} |\psi_-(x,t)|^2 \, dx = \frac{1}{2} \tag{4.28b}$$

Hence the density matrix corresponding to the spin variable in our case becomes

$$\rho(t) = \frac{1}{2} \begin{pmatrix} 1 & e^{-\frac{F^2 t^2}{4m^2\sigma^2}\left(t^2 + 4\frac{m^2\sigma^4}{\hbar^2}\right)} \\ e^{-\frac{F^2 t^2}{4m^2\sigma^2}\left(t^2 + 4\frac{m^2\sigma^4}{\hbar^2}\right)} & 1 \end{pmatrix} \tag{4.29}$$

Clearly, the off diagonal terms get exponentially suppressed with time.

4.7 Wigner function

The Wigner function corresponding to a density operator $\rho = |\psi\rangle \langle\psi|$ is defined as,

$$\mathbf{W}(x,p) := \frac{1}{2\pi\hbar} \int_{-\infty}^{\infty} dy \, e^{-i\frac{py}{\hbar}} \psi\left(x + \frac{y}{2}\right) \psi^*\left(x - \frac{y}{2}\right)$$

It is straightforward to see that the expectation value of an observable $\mathcal{O}$ in the state ρ can be obtained as,

$$\langle \mathcal{O} \rangle = \mathbf{tr}\left[\rho\mathcal{O}\right] := \int_{-\infty}^{\infty} \int_{-\infty}^{\infty} \mathbf{W}(x,p)\tilde{\mathcal{O}}(x,p) dx dp$$

where $\tilde{\mathcal{O}}(x,p)$ is the Weyl transform[6] of the operator $\mathcal{O}$. The Wigner function in quantum mechanics plays a role analogous to that of a probability distribution defined

---

[6]Weyl transform $\tilde{\mathcal{A}}(x,p)$ of an operator $\mathcal{A}$ is defined as

$$\tilde{\mathcal{A}}(x,p) := \frac{1}{2\pi\hbar} \int_{-\infty}^{\infty} dy \, e^{-i\frac{py}{\hbar}} \langle x + y/2|\mathcal{A}|x - y/2\rangle$$

on the classical phase space. However, it is strictly not a probability distribution as it can take negative values unlike a probability distribution, which is always positive. We will now show in the next section the effect of coarse-graining on the Wigner function of the full density matrix associated with the system and the apparatus.

4.8 Coarse graining in the quantum phase space

From the density matrix $\rho_{\alpha\beta}(x, x')$ we construct the Wigner matrix $\mathbf{W}(q, p)$ [38]. The matrix elements of $\mathbf{W}(q, p)$ are:

$$W_{\alpha\beta}(q, p) = \frac{1}{2\pi\hbar} \int_{-\infty}^{+\infty} \rho_{\alpha\beta}(q + y/2, q - y/2) e^{\frac{ipy}{\hbar}} dy \qquad (4.30)$$

with α, $\beta = \pm$. $\mathbf{W}(q, p)$ is a 2×2 Hermitean matrix (not necessarily positive). All components of $\mathbf{W}(q, p)$ can *in principle* be measured by having a Stern-Gerlach setup at the screen to measure $Tr[\mathbf{W}(q, p)(\mathbb{1} + \hat{n}.\vec{\sigma})/2]$. In Figures 4.5 and 4.6, we display the function $W(q, p) = \text{Tr}[\mathbf{W}(q, p)(\mathbb{1} + \sigma_x)/2]$, which shows the diagonal as well as the off diagonal terms in the $|+\rangle, |-\rangle$ basis.

We now use the fact that the detection is done *coarsely*: the phase space resolution is poor and so we integrate the Wigner matrix over volumes of phase space which are large compared to h. The coarse grained Wigner matrix $\overline{\mathbf{W}}(q, p)$ (See Section 3.6.1) has elements:

$$\overline{W}_{\alpha\beta}(q, p) = \frac{1}{\Delta\delta} \int_{-\Delta/2}^{\Delta/2} du \int_{-\delta/2}^{\delta/2} dv W_{\alpha\beta}(q + u, p + v), \qquad (4.31)$$

with Δ and δ, the pixel size in position and momentum respectively. The off diagonal term $W_{+-}(q, p)$ is oscillatory due to a term $e^{iq2\pi/d}$, which oscillates on a length scale
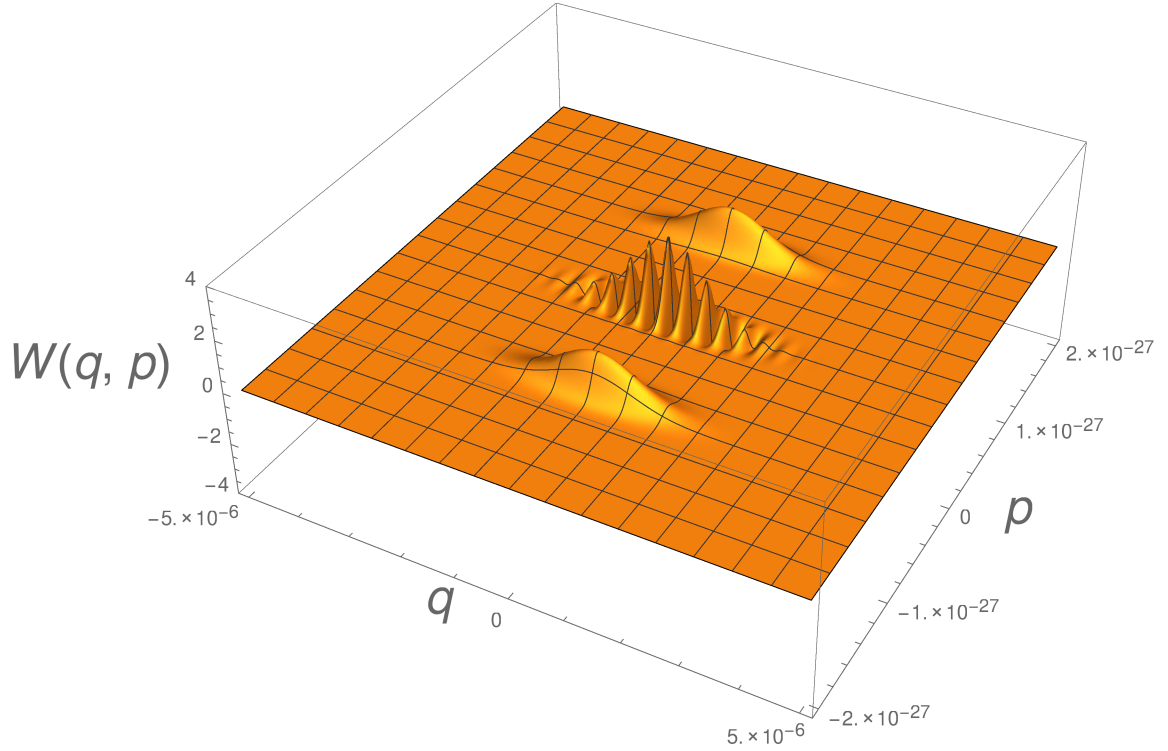
Figure 4.5: Figure shows a plot of the function $W(q, p)$ as a function of q and p at $t = 1\mu$ sec. The central hump showing oscillations is the real part of the off-diagonal element of the Wigner matrix and the others are diagonal elements. We have used typical values $m = 1.79 \times 10^{-25} kg$, $F = 9.27 \times 10^{-22} N$, $\sigma = 10^{-6} m$. The $W(q, p)$ axis has been rescaled by multiplying by a factor of 10^{-33}. q is displayed in m and p in kgm/s.

$d = \frac{\hbar}{2Ft}$ (See Section 3.9), which is about $10^{-8} m$. On a coarse scale these off-diagonal elements average to zero and we have a diagonal matrix of the form(See Appendix B):

$$\begin{pmatrix} \overline{W}_{++}(q, p) & 0 \\ & \\ 0 & \overline{W}_{--}(q, p) \end{pmatrix}$$

After the wave packets have separated, the coherence between the two wavepackets is still perceptible in the Wigner function. As is well known, the Wigner function is
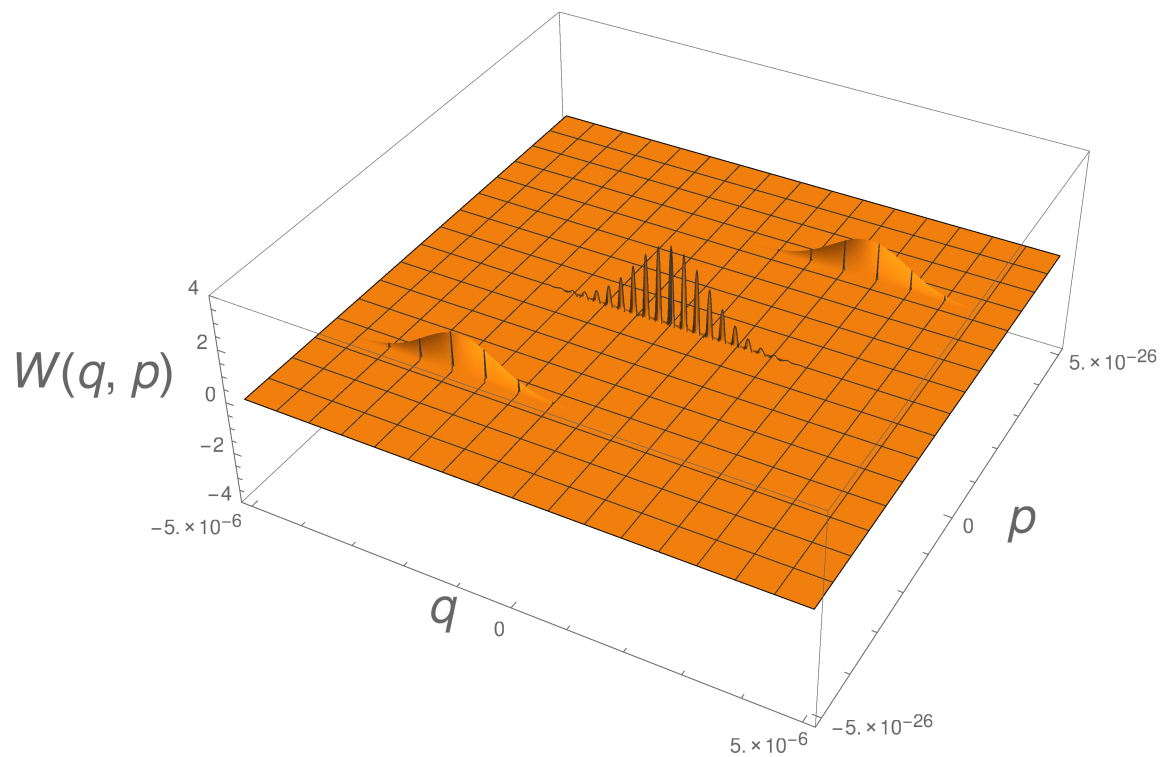
Figure 4.6: Figure shows a plot of the function $W(q, p, t)$ as a function of q and p at t=30 μ sec. The remaining parameters are as mentioned in the caption of Figure 4.5. The $W(q, p)$ axis has been rescaled by multiplying by a factor of 10^{-33}. q is displayed in m and p in kgm/s.

only a quasiprobability distribution. On coarse graining it becomes positive[39] and can be viewed as a probability distribution in the phase space of the atomic position. This constitutes a *coarse measurement.*

4.8.1 Suppression of off diagonal elements of the Wigner matrix due to coarse graining

The Wigner matrix is of the form:

$$\mathbf{W}(q,p) = \begin{pmatrix} W_{++}(q,p) & W_{+-}(q,p) \\ W_{-+}(q,p) & W_{--}(q,p) \end{pmatrix} \tag{4.32}$$

Explicitly, for instance, we have:

$$W_{++}(q,p) = \frac{1}{2\pi\hbar} \exp\left(-\frac{\frac{4p^2t^2}{m^2} - \frac{4pt(at^2+2q)}{m} + (at^2+2q)^2 + \frac{4p^2\sigma^4}{\hbar^2} - \frac{8ampt\sigma^4}{\hbar^2} + \frac{4a^2m^2t^2\sigma^4}{\hbar^2}}{4\sigma^2} \right) \tag{4.33}$$

$$W_{+-}(q,p) = \frac{1}{2\pi\hbar} \exp\left(-\left\{ \frac{(pt-mq)^2}{m^2\sigma^2} + \frac{p^2\sigma^2}{\hbar^2} + \frac{iat(pt-2mq)}{\hbar} \right\} \right) \tag{4.34}$$

Notice that $W_{+-}(q,p)$ oscillates on a spatial scale $d = \frac{\hbar}{2mat} = \frac{\hbar}{2Ft}$. The coarse grained Wigner matrix $\overline{\mathbf{W}}(q,p)$ has elements

$$\overline{W}_{\alpha\beta}(q,p) = \frac{1}{\Delta\delta} \int_{-\Delta/2}^{\Delta/2} du \int_{-\delta/2}^{\delta/2} dv W_{\alpha\beta}(q+u, p+v), \tag{4.35}$$

with Δ and δ, the pixel size in position and momentum respectively. The numerically generated plots show how the offdiagonal terms $W_{+-}(q,p)$ and $W_{-+}(q,p)$ on coarse graining average to zero due to the presence of the oscillatory term $e^{iq\frac{2\pi}{d}}$, where d is the spatial scale of oscillation. We finally get the following diagonal form for the coarse grained Wigner matrix:

$$\begin{pmatrix} \overline{W}_{++}(q,p) & 0 \\ & \\ & \\ 0 & \overline{W}_{--}(q,p) \end{pmatrix}$$

For instance, for $q = 10^{-6}m$ and $p = 0\ kgm/s$ and $t = 3 \times 10^{-5}s$ we get the following form for the coarse grained Wigner matrix, for the realistic experimental parameter values for a typical Stern Gerlach setup.

$$\overline{\mathbf{W}}(q,p) = \begin{pmatrix} 5.7 \times 10^{-2} & 0 \\ & \\ 0 & 1.6 \times 10^{-5} \end{pmatrix} \tag{4.36}$$

4.9   Conclusion

This chapter analyses the classic experiment of spin measurement, the Stern-Gerlach experiment, using the idea of coarse measurement. A coarse measurement is one performed with limited resources of resolution. In the present chapter, we have explicitly demonstrated the effect of coarse graining on the Wigner function(Section 4.8) associated with the spin and the center of mass of the silver atom by integrating the Wigner function over the volume of the phase space of size large compared to h. This leads to a diagonal Wigner matrix. We conclude that the apparent non-unitarity of the measurement process is a consequence of a *coarse measurement.*

The entanglement between the system and the measuring apparatus is a key concept in any measuring process. This quantum correlation allows us to infer the state of the system by reading the state of the measuring device. In this analysis, we have shown that the observer can learn about the state of the spin of a silver atom only when the entanglement between the spin and the center of mass of the silver

atom is saturated, which happens over a time scale(10^{-7}s) much smaller than the separation(10^{-5}s) and spreading(10^{-3}s) time scales.

The point of view that is highlighted here is very much similar in spirit to reference [40, 41], where the author argues that the notion of entropy is a subjective one. Depending on the resolution of the available resources a measurement process may appear unitary or non-unitary. When the interference between the wave packet is detectable, we must conclude that the spin is both *up* and *down* simultaneously. In a low-resolution experiment, the interference apparently gets washed out, and we can obtain the information about the spin.

The idea of measurement presented here is very different from the idea of decoherence. In the decoherence paradigm, the information about the off-diagonal terms of the system density matrix is lost due to uncontrollable interaction of the system with the environment degrees of freedom. In contrast, in a *coarse measurement* the measurement process is perceived as non-unitary due to the limitation in resolving the eigenstate of the system.

Chapter 5

Geometry and Thermodynamics of Quantum States

5.1 Introduction

Given two quantum states, how easily can we tell them apart? Consider for instance, gravitational wave detection which is of considerable interest in recent times [42, 43]. Typically, we expect a weak signal which produces a small change in the quantum state of the detector. The sensitivity of our instrument is determined by our ability to detect small changes in a quantum state. This leads to the issue of distinguishability measures on the space of quantum states [44, 45, 46, 47, 48]. In general, quantum states are represented by density matrices. In this chapter, we address this question and arrive at a natural Riemannian metric on the space of density matrices.

In fact, even in the classical domain, one encounters similar questions while con-

sidering drug trials, electoral predictions or when we compare a biased coin to a fair one. As the number of trials (or equivalently, the size of the sample) increases, our ability to distinguish between candidate probability distributions improves. Such considerations give rise in a natural and operational manner, to a metric on the space of probability distributions [49]. This metric is known as the Fisher-Rao metric and plays an important part in the theory of parameter estimation. This metric leads to the Cramer-Rao bound which limits the variance of any unbiased estimator.

Another example of the use of a Riemannian metric to measure distinguishability occurs in the theory of colours [14, 50]. The space of colours is two dimensional (assuming normal vision) and one can see this on a computer screen in several graphics softwares. The sensation of colour is determined by the relative proportion of the RGB values, which gives us two parameters. The extent to which one can distinguish neighbouring colours is usually represented by MacAdam ellipses [14, 51, 50], which are contours on the chromaticity diagram which are just barely distinguishable from the centre. These ellipses give us a graphical representation of an operationally defined Riemannian metric on the space of colours. The flat metric on the Euclidean plane would be represented by circles, whose radii are everywhere the same. As it turns out, the metric on the space of colours is not flat and the MacAdam ellipses vary in size, orientation and eccentricity over the space of colours. This analogy is good to bear in mind, for we provide a similar visualisation of the geometry of state space based on entropic considerations.

In this chapter we use Umegaki's quantum relative entropy [52] as a measure of distinguishability between quantum states. We will show that this entropy defines

a metric on state space which is the true quantum counterpart of the Fisher-Rao metric. We demonstrate that this metric suggests improved experimental strategies for discriminating between two quantum states.

5.2   KL Divergence as maximum likelihood

Let us consider a biased coin for which the probability of getting a head is $p_H = 1/3$ and that of getting a tail is $p_T = 2/3$. Suppose we incorrectly assume that the coin is fair and assign probabilities $q_H = 1/2$ and $q_T = 1/2$ for getting a head and a tail respectively. The question of interest is the number of trials needed to be able to distinguish (at a given confidence level) between our assumed probability distribution and the measured probability distribution. A popular measure for distinguishing between the expected distribution and the measured distribution is given by the relative entropy or the Kullback-Leibler divergence (KLD) which is widely used in the context of distinguishing classical probability distributions [53]. Let us consider n independent tosses of a coin leading to a string $S = \{HTHHTHTHHTTTTT......\}$. What is the probability that the string is generated by the model distribution $Q = \{q, 1 - q\}$? The observed frequency distribution is $P = \{p, 1 - p\}$. If there are n_H heads and n_T tails in a string then the probability of getting such a string is $\frac{n!}{n_H! n_T!} q^{n_H} (1 - q)^{n_T}$ which we call the likelihood function $L(n|Q)$. If we take the average of the logarithm of this likelihood function and use Stirling's approximation for large n we get the following expression:

$$\frac{1}{n} \log L(n|Q) = -D_{KL}(P\|Q) + \frac{1}{n} \log \frac{1}{\sqrt{2\pi n p(1 - p)}}, \qquad (5.1)$$

where $p = \frac{n_H}{n}$ and $D_{KL}(P\|Q) = p\log\frac{p}{q} + (1-p)\log\frac{1-p}{1-q}$. The second term in (5.1) is due to the sub-leading term $\frac{1}{2}\log 2\pi n$ of Stirling's approximation. If $D_{KL}(P\|Q) \neq 0$ then the likelihood of the string S being produced by the Q distribution decreases exponentially with n.

$$L(n|Q) = \frac{1}{\sqrt{2\pi np(1-p)}} \exp\{-\{nD_{KL}(P\|Q)\}\}.$$

Thus $D_{KL}(P\|Q)$ gives us the divergence of the measured distribution from the model distribution. The KL divergence is positive and vanishes if and only if the two distributions P and Q are equal. In this limit, we find that the exponential divergence gives way to a power law divergence, due to the subleading term in (5.1). The arguments above generalize appropriately to an arbitrary number of outcomes (instead of two) and also to continuous random variables.

5.3 Relative entropy as a metric

As we saw above, the relative entropy (or KLD) gives an operational measure of how distinguishable two distributions are, quantified by the number of trials needed to distinguish two distributions at a given confidence level. However, the KLD is not a distance function on the space of probability distributions: it is not symmetric between the distributions P and Q. One may try to symmetrize this function, but then, the result does not satisfy the triangle inequality. However, when P and Q approach one another, the relative entropy can be Taylor expanded to second order about P. The Hessian matrix does define a positive definite quadratic form at P and thus a Riemannian metric on the space of probability distributions. In classical

probability theory, this is known as the Fisher-Rao metric [49, 54] and this forms the basis of classical statistical inference and the famous χ-squared test.

5.3.1   The Fisher-Rao metric

Let us consider two distributions $p(x|\lambda^i)$ and $q(x|\lambda^i)$ close to each other such that,

$$q(x|\lambda^i) = p(x|\lambda^i) + \frac{\partial p(x|\lambda^i)}{\partial \lambda^i} d\lambda^i = p(x|\lambda^i)\left(1 + \frac{1}{p(x|\lambda^i)}\frac{\partial p(x|\lambda^i)}{\partial \lambda^i} d\lambda^i\right) \qquad (5.2)$$

where λ^is are the parameters of the distribution. We can also think of these λs as coordinates on the probability simplex. $D_{KL}(p\|q)$ would then be given by,

$$D_{KL}(p\|q) = \int_{-\infty}^{\infty} p(x|\lambda^i)\log\left(\frac{p(x|\lambda^i)}{q(x|\lambda^i)}\right)dx$$

if we substitute for $q(x|\lambda^i)$ from the Eq.(5.2) into the above expression and expand the logarithm up to the second order we obtain,

$$\begin{aligned} D_{KL}(p\|q) = \ & - \left(\int_{-\infty}^{\infty}\frac{\partial p(x|\lambda^i)}{\partial \lambda^i}dx\right)d\lambda^i \\ & + \left(\int_{-\infty}^{\infty} p(x|\lambda^i)\frac{\partial \log p(x|\lambda^i)}{\partial \lambda^i}\frac{\partial \log p(x|\lambda^j)}{\partial \lambda^j}dx\right)d\lambda^i d\lambda^j. \end{aligned} \qquad (5.3)$$

The first of the two terms on the right hand side of the above equation vanishes since the derivative and integral are with respect to different variables so can be interchanged and $\int_{-\infty}^{\infty} p(x|\lambda^i) = 1$. The second term defines what we call the Fisher-Rao metric. Commonly the partial derivatives of the logarithm of the likelihood function are called *score vectors*($\boldsymbol{l}^i$). Then the Fisher-Rao metric in terms of the score vectors are written as,

$$g_{FR} = \left\langle \frac{\partial \log p(x|\lambda^i)}{\partial \lambda^i}\frac{\partial \log p(x|\lambda^j)}{\partial \lambda^j}\right\rangle = \left\langle \boldsymbol{l}^i \boldsymbol{l}^j \right\rangle \qquad (5.4)$$

The Riemannian metric then defines a distance function, based on the lengths of the shortest curves connecting any two states P and Q. Our strategy below is to apply the same idea to Umegaki's quantum relative entropy defined on the space of quantum states [55, 56, 57, 58, 59].

Consider a density matrix ρ of an N state system, satisfying $\rho^\dagger = \rho$, $\mathbf{tr}\,[\rho] = 1$ and $\rho > 0$, where we assume ρ to be *strictly* positive, so that we are not at the boundary of state space. The quantum relative entropy of any two states parametrized by a set of parameters $\boldsymbol{\lambda}(\lambda^1, \lambda^2, \ldots, \lambda^N)$ is represented in terms of density matrices $\rho_1(\boldsymbol{\lambda_1})$ and $\rho_2(\boldsymbol{\lambda})$ and is given by:

$$S(\rho_1(\boldsymbol{\lambda_1})\|\rho_2(\boldsymbol{\lambda})) = \mathbf{tr}\,[\rho_1 \log \rho_1 - \rho_1 \log \rho_2]\,. \tag{5.5}$$

S is positive and vanishes if and only if $\rho_2 = \rho_1$ [11]. Let us consider $S(\rho_1(\boldsymbol{\lambda_1})\|\rho_2(\boldsymbol{\lambda}))$ as a function of its second argument. If the states ρ_1 and ρ_2 are infinitesimally close to each other, we can Taylor expand the relative entropy function.

$$S(\rho_1\|\rho_2) = S(\rho_1\|\rho_1) + \frac{\partial S}{\partial \lambda^i}\Delta\lambda^i + \frac{1}{2}\frac{\partial^2 S}{\partial \lambda^j \partial \lambda^i}\Delta\lambda^i \Delta\lambda^j + .. \tag{5.6}$$

Notice that $S(\rho_1\|\rho_1)$ is zero and the second term is zero because we are doing a Taylor expansion about the minimum of the relative entropy function. The third term, which is second order in $\Delta\lambda$, gives us the metric and is positive definite for $\Delta\lambda \neq 0$.

$$g_{ij} = \frac{\partial^2 S}{\partial \lambda^j \partial \lambda^i}\,. \tag{5.7}$$

As is made clear below, the Hessian actually defines a metric *tensor*.

5.3.2 Hessian as a rank-2 tensor

If we consider the relative entropy $S(\lambda^i)$ as a function of the parameters of the density matrix then the first derivative in (5.6) transforms like a tensor of rank-1 under a change of co-ordinates. To see this let us consider $A_i = \frac{\partial S}{\partial \lambda^i}$. When we make a change of coordinates from $\lambda^i \to \bar{\lambda}^i$, A_i transforms as follows:

$$\bar{A}_i = \frac{\partial \lambda^j}{\partial \bar{\lambda}^i} \frac{\partial S}{\partial \lambda^j} = T_i^j A_j. \tag{5.8}$$

Consider the second derivative term $g_{ij} = \frac{\partial^2 S}{\partial \lambda^j \partial \lambda^i} = \frac{\partial}{\partial \lambda^j} A_i$. In order to see its transformation property consider,

$$\bar{g}_{ij} = \frac{\partial}{\partial \bar{\lambda}^j} \left(\frac{\partial S}{\partial \bar{\lambda}^i} \right) = \frac{\partial}{\partial \bar{\lambda}^j} (\bar{A}_i) = \frac{\partial}{\partial \bar{\lambda}^j} (T_i^k A_k). \tag{5.9}$$

$$
\begin{aligned}
\frac{\partial}{\partial \bar{\lambda}^j} (T_i^k A_k) &= T_i^k \left(\frac{\partial A_k}{\partial \bar{\lambda}^j} \right) + \left(\frac{\partial T_i^k}{\partial \bar{\lambda}^j} \right) A_k \\
&= T_i^k T_j^l g_{kl} + \left(\frac{\partial T_i^k}{\partial \bar{\lambda}^j} \right) \frac{\partial S}{\partial \lambda^k}^{\,0}.
\end{aligned}
\tag{5.10}
$$

The last term in (5.10) vanishes identically as we are Taylor expanding the relative entropy function about a stationary point and we obtain $\bar{g}_{ij} = T_i^k T_j^l g_{kl}$. Positivity of the Hessian is guaranteed as the stationary point is *the absolute* minimum.

5.3.3 Metric for a two-level system

Consider two mixed states ρ_1 and ρ_2 of a two level quantum system commonly referred to as a qubit. These can be written as $\rho_1 = \frac{\mathbb{1} + \boldsymbol{X} \cdot \boldsymbol{\sigma}}{2}$ and $\rho_2 = \frac{\mathbb{1} + \boldsymbol{Y} \cdot \boldsymbol{\sigma}}{2}$ where $|\boldsymbol{X}|$ and $|\boldsymbol{Y}| < 1$. $\boldsymbol{X}$ and $\boldsymbol{Y}$ are three dimensional vectors with components x^i and

y^i. The relative entropy function can be written as follows:

$$
\begin{aligned}
S(\rho_1\|\rho_2) &= \mathbf{tr}\left[\left(\frac{\mathbb{1}+\boldsymbol{X}.\boldsymbol{\sigma}}{2}\right)\log\left(\frac{\mathbb{1}+\boldsymbol{X}.\boldsymbol{\sigma}}{2}\right)\right] \\
&\quad -\mathbf{tr}\left[\left(\frac{\mathbb{1}+\boldsymbol{X}.\boldsymbol{\sigma}}{2}\right)\log\left(\frac{\mathbb{1}+\boldsymbol{Y}.\boldsymbol{\sigma}}{2}\right)\right].
\end{aligned}
\tag{5.11}
$$

We can use the power series expansion of $\log(\mathbb{1}+\boldsymbol{Y}.\boldsymbol{\sigma})$ to evaluate the trace of the above expression.

$$
\log(\mathbb{1}+\boldsymbol{Y}.\boldsymbol{\sigma}) = \underbrace{\left(\sum_{m=0}^{\infty}\frac{|\boldsymbol{Y}|^{2m+1}}{2m+1}\right)}_{f_o(|\boldsymbol{Y}|)}\frac{\boldsymbol{Y}.\boldsymbol{\sigma}}{|\boldsymbol{Y}|} + \underbrace{\left(\sum_{n=0}^{\infty}\frac{|\boldsymbol{Y}|^{2n}}{2n}\right)}_{f_e(|\boldsymbol{Y}|)}\mathbb{1},
\tag{5.12}
$$

where $f_o(|\boldsymbol{Y}|)$ and $f_e(|\boldsymbol{Y}|)$ are respectively the odd and even parts of the function $f(r)=\log(1+r)$. Notice that the odd part of the expansion is traceless. Making use of the above expansion we can express $S(\rho_1\|\rho_2)$ as follows

$$
S(\rho_1\|\rho_2) = S(\boldsymbol{X}\|\boldsymbol{Y}) = f_e(|\boldsymbol{Y}|) - \frac{f_o(|\boldsymbol{Y}|)}{|\boldsymbol{Y}|}(\boldsymbol{X}.\boldsymbol{Y}).
\tag{5.13}
$$

In order to compute the Hessian of $S(\rho_1\|\rho_2)$ we compute the second derivative $\frac{\partial^2 S}{\partial y^i \partial y^j}$ with respect to y^j and then set $y^i=x^i$ and obtain the following metric [14]:

$$
\boxed{g_{ij} = \frac{\partial^2 S}{\partial x^i \partial x^j} = C(r)\frac{x^i x^j}{r^2} + D(r)\{\delta_{ij} - \frac{x^i x^j}{r^2}\}},
\tag{5.14}
$$

where $C(r)=\frac{1}{1-r^2}$, $D(r)=\frac{1}{2r}\log\left(\frac{1+r}{1-r}\right)$ and $r=|\boldsymbol{Y}|$.

The corresponding line element is given in polar coordinates by:

$$
ds^2 = \frac{dr^2}{1-r^2} + \left[\frac{r}{2}\log\left(\frac{1+r}{1-r}\right)\right](d\theta^2 + \sin^2\theta d\phi^2).
\tag{5.15}
$$

This metric has been discussed earlier by Bogoliubov, Kubo and Mori (BKM) in the context of statistical mechanical fluctuations [60, 61]. We refer to it as the BKM metric.

5.4 Non commuting limits of the Fisher-Rao metric

We notice that there are two limits involved in state discrimination namely,

1) **The thermodynamic limit:** N – the number of copies of a state available for each of the $\mathcal{N}$ measurements – goes to infinity.

2) **The infinitesimal limit:** The separation between the states is infinitesimal i.e. $d\rho = (\rho_1 - \rho_2) \to 0$.

However, these two limits do not commute in the quantum case. If we take the thermodynamic limit followed by the infinitesimal limit we get the Bures-Helstrom(BH) metric and taking the limits in the reverse order will give us the BKM-metric.

Generally, the BH-metric is defined as follows[62, 63, 64]. Let $d\rho$ be a tangent vector at ρ. Consider the equation for the unknown L:

$$d\rho = \frac{1}{2}\{\rho, L\} \tag{5.16}$$

This linear equation defines the symmetric logarithmic derivative L uniquely. Optimising the Fisher-Rao metric (5.4), $g_{FR}(\rho, d\rho) = \sum_i \langle i| \rho |i\rangle^{-1} \langle i| d\rho |i\rangle^2$ over all choices of orthonormal bases $b = \{|i\rangle, i = 1, 2, 3....d\}$ we find that [62]

i) the optimal choice is given by the basis b^* which diagonalizes L and

ii) that the optimal value is given by $g_{BH}(\rho, d\rho) = \mathbf{tr}\,[\rho L L]$ which is defined as the Bures metric.

The discussion above is general and applicable to a d state system. For a qubit we get,

$$ds^2 = \frac{dr^2}{1-r^2} + r^2 d\Omega^2 \tag{5.17}$$

We now take the thermodynamic limit. Consider N qubits with the state $\rho^{\otimes N}$. We will show that

$$\frac{1}{N} g_{BH}(\rho^{\otimes N}, d\rho^{\otimes N}) = g_{BH}(\rho, d\rho) \tag{5.18}$$

The proof is by induction. For $N = 1$ (5.18) is an identity. Assuming (5.18) for $N-1$, we note that

$$d\rho^{\otimes N} = d(\rho^{\otimes N-1} \otimes \rho) = d\rho^{\otimes N-1} \otimes \rho + \rho^{\otimes N-1} \otimes d\rho,$$

and that

$$L_N = L_{N-1} \otimes \mathbb{1} + \mathbb{1} \otimes L$$

uniquely solves (5.16). Computing $g_{BH}(\rho^{\otimes N}, d\rho^{\otimes N}) = \mathbf{tr}\left[\rho^{\otimes N} L_N L_N\right]$ and using the fact that (5.16) implies $\mathbf{tr}\left[\rho L\right] = 0$ we arrive at (5.18). The optimized Fisher-Rao metric has the same discriminating power (per qubit) for N qubits as for a single qubit. This is exactly as in the classical case. This holds true in the limit $N \to \infty$. There is no quantum advantage. Note that in the above, we have taken the infinitesimal limit first. We will see that taking the thermodynamic limit first leads to an entirely different picture.

Let us now take the "thermodynamic" limit of large N first. Given N qubits, which may be a state $\rho_1^{\otimes N}$ or $\rho_2^{\otimes N}$ we can choose a measurement basis in the Hilbert space $\mathcal{H}^{\otimes N}$. The optimization over measurement bases is now over an enlarged set. Earlier we were restricted to bases of the form $b^{\otimes N}$ which are separable in the Hilbert space $\mathcal{H}^{\otimes N}$. We now have the freedom to include *entangled bases* and this implies
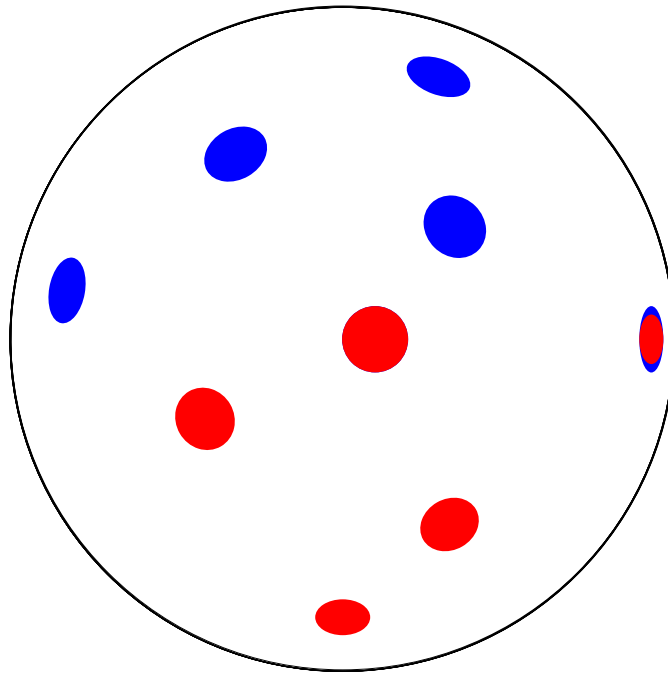
Figure 5.1: The figure represents the geometry of the qubit state space as given by the BKM metric (red ellipses in the lower half) and the BH metric (blue ellipses in the upper half). The figure shows a two dimensional slice of the three dimensional qubit state space. The geometry is invariant under rotations due to the unitary symmetry of the state space. Note that the ellipticity increases near the boundary of state space. The ellipse on the right shows both BH and BKM metrics superposed. Note that the red BKM ellipse is *inside* the blue BH ellipse.

$$\frac{S^*(\rho_1^{\otimes N} \| \rho_2^{\otimes N})}{N} \geq S^*(\rho_1 \| \rho_2). \tag{5.19}$$

In fact[65], no matter how small the separation between the distinct states ρ_1 and ρ_2, as $N \to \infty$, $\frac{1}{N} S^*(\rho_1^{\otimes N} \| \rho_2^{\otimes N}) \to S(\rho_1 \| \rho_2)$, where $S(\rho_1 \| \rho_2)$ is Umegaki's quantum relative entropy. The appropriate relative entropy to use in the thermodynamic limit is Umegaki's relative entropy.

If we now take the infinitesimal limit as $\rho_2 \to \rho_1$, we effectively pass from the quantum relative entropy to a Riemannian metric defined as the Hessian of the quantum relative entropy. The form of this metric in the case of a qubit is (see Sec. 4.3.3)

$$g_{ij} = \frac{\partial^2 S}{\partial x^i \partial x^j} = C(r) \frac{x^i x^j}{r^2} + D(r)\{\delta_{ij} - \frac{x^i x^j}{r^2}\}, \tag{5.20}$$

where $C(r) = \frac{1}{1-r^2}$, $D(r) = \frac{1}{2r} \log\left(\frac{1+r}{1-r}\right)$ and $r = |\mathbf{Y}|$.

To summarize, we find that if we consider the infinitesimal limit first and then take the thermodynamic limit we can't make use of entanglement. In contrast, if we take the thermodynamic limit first and then take the infinitesimal limit then we can make use of entanglement as a resource in distinguishing quantum states. This particular non-commutative feature is present in the quantum domain but it doesn't have a classical counterpart.

5.5 Geodesics and the scalar curvature

The scalar curvature R of the BKM metric is given by:

$$R = \frac{4r^2 - 4r(1+r^2)\log\left(\frac{1+r}{1-r}\right) + (1 + 2r^2 - 3r^4)[\log\left(\frac{1+r}{1-r}\right)]^2}{2r^2(1-r^2)[\log\left(\frac{1+r}{1-r}\right)]^2}. \tag{5.21}$$
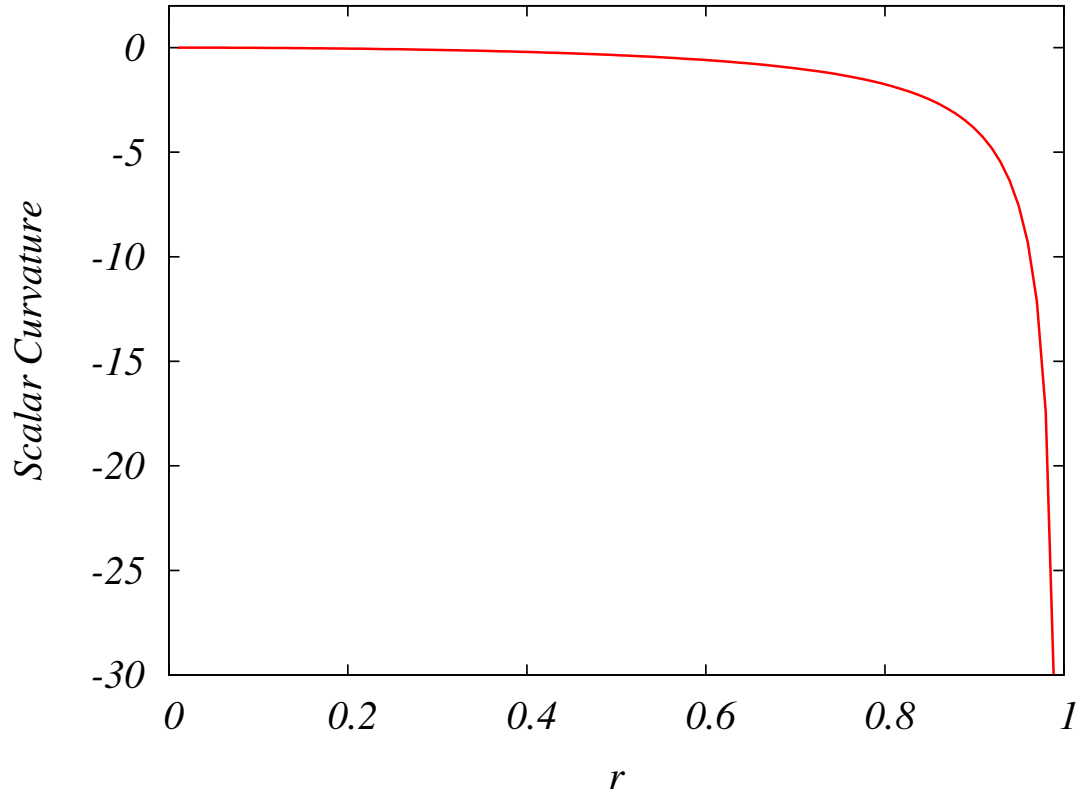
Figure 5.2: The scalar curvature (5.21) for the metric displayed in (5.34) as a function of r, the distance from the centre of the Bloch sphere.

As we can see from Figure 5.2, the metric has a negative scalar curvature and therefore the geodesics Figure 5.3 cannot cross more than once. It follows therefore that any two states, are connected by an unique geodesic. The length of this geodesic gives us a distance on the space of states. This has all the properties expected of a distance function: it is symmetric, strictly positive between distinct points and satisfies the triangle inequality. The scalar curvature is zero near the origin and diverges logarithmically to minus infinity as r goes to unity. The geodesics of this metric are easily worked out from classical mechanics. The metric has spherical symmetry, because

the quantum state space is invariant under unitary transformations.

Setting $r = \sin\alpha$, we rewrite the metric as

$$ds^2 = d\alpha^2 + F(\alpha)\left(d\theta^2 + \sin^2(\theta)d\phi^2\right), \tag{5.22}$$

where $F(\alpha) = \frac{\sin\alpha}{2}\log\left[\frac{1+\sin\alpha}{1-\sin\alpha}\right]$. Because of the spherical symmetry, there is a conserved angular momentum vector $\vec{J}$ and thus the geodesics lie on the plane perpendicular to $\vec{J}$. Thus we can confine our calculations to a plane, reducing the form of the metric to

$$ds^2 = d\alpha^2 + F(\alpha)\left(d\phi^2\right), \tag{5.23}$$

where we have set $\theta = \frac{\pi}{2}$. The Lagrangian of the classical mechanical system is

$$L = \frac{1}{2}\left(\dot{\alpha}^2 + F(\alpha)\dot{\phi}^2\right). \tag{5.24}$$

The constants of motion for this problem are the energy and the angular momentum, which are given by

$$E = \frac{1}{2}\left(\dot{\alpha}^2 + F(\alpha)\dot{\phi}^2\right), \quad P_\phi = J = \frac{\partial L}{\partial\dot{\phi}} = F(\alpha)\dot{\phi}. \tag{5.25}$$

Using the above equations we solve for $\dot{\alpha}$ and $\dot{\phi}$. Our numerical solution gives us the geodesics of interest. A typical geodesic is displayed in Figure 5.3. Given any two points in the state space (for example the red dots of Figure 5.3), the length of the unique geodesic [66] connecting them gives us a distance function. This is very similar in spirit to a construction of Wootters [27], who introduced a metric based on distinguishability for *pure* states and used this to define a metric on pure states, which ultimately yielded the Fubini-Study metric. This work can be viewed as an application of this idea to mixed states.
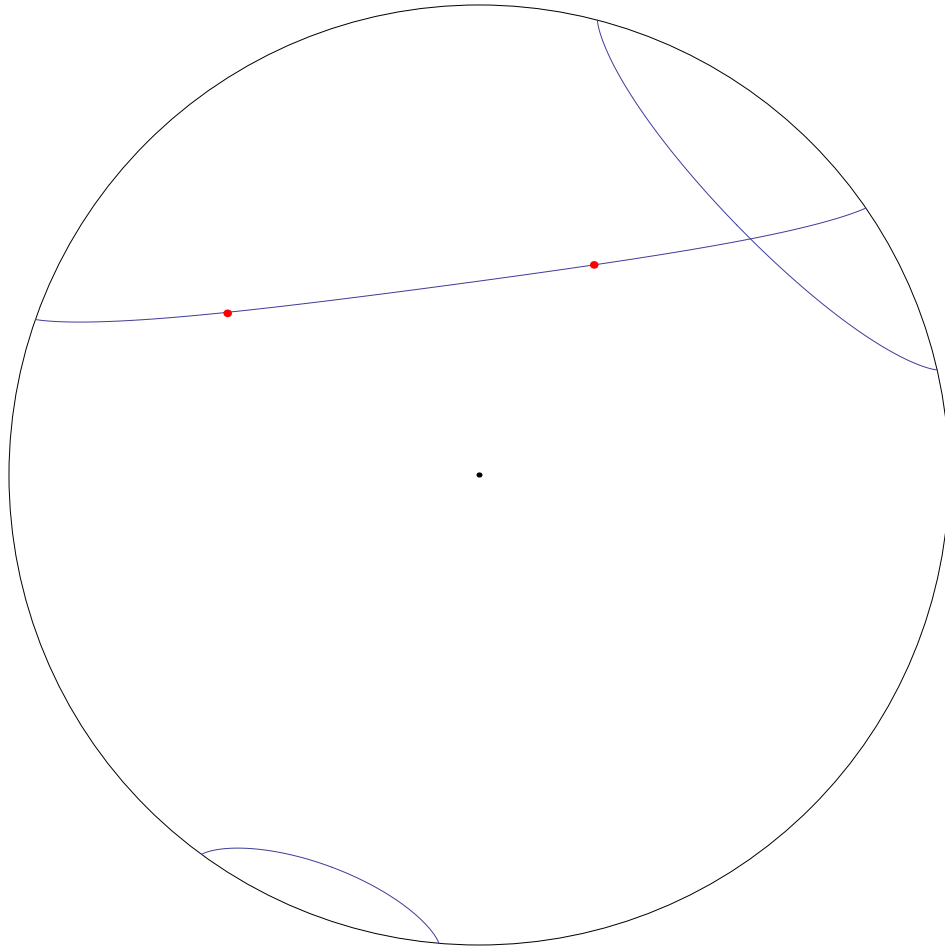
Figure 5.3: The figure shows a geodesic connecting two typical quantum states, indicated by two red dots on the Bloch ball. Two more geodesics are shown with different values of $J = |\vec{J}|$. We also show geodesics crossing each other once. As explained in the text, the metric on quantum state space has negative curvature and so geodesics cannot cross more than once.

5.6   Relation between the metric and fluctuations in the free energy

Any quantum state ρ can be formally viewed as a Gibbs state for the Hamiltonian $H = -(1/\beta) \log \rho$. We will see below that the relative entropy of two quantum states

ρ_1 and ρ_2 is related to the change in the free energy between the two states. If these two states are infinitesimally close together, the second order correction to the free energy is related to the metric defined on the space of quantum states. Thus, the metric (5.7) has a physical interpretation in terms of susceptibility.

Consider a thermal state $\rho_2 = \frac{e^{-\beta H_2}}{Z_2} = e^{-\beta(H_2 - F_2)}$ in the neighborhood of $\rho_1 = \frac{e^{-\beta H_1}}{Z_1} = e^{-\beta(H_1 - F_1)}$ such that $H_2 = H_1 + \epsilon V$ [67]. Here ϵ is a small parameter and F_1 and F_2 are the free energies corresponding to states ρ_1 and ρ_2 respectively. $Z_1 = \mathbf{tr}\left[e^{-\beta H_1}\right]$ and $Z_2 = \mathbf{tr}\left[e^{-\beta H_2}\right]$. Then the relative entropy of the two states is given by:

$$
\begin{aligned}
S(\rho_1 \| \rho_2) &= \mathbf{tr}\left[\rho_1 \log \rho_1 - \rho_1 \log \rho_2\right] \\
&= -\beta[\mathbf{tr}\left[\rho_1(H_1 - F_1)\right]] \\
&\quad + \beta[\mathbf{tr}\left[\rho_1(H_2 - F_2)\right]].
\end{aligned}
\tag{5.26}
$$

Setting $\mathbf{tr}\left[\rho H\right] = U$, the energy and $\mathbf{tr}\left[\rho F\right] = F$, the free energy (5.26) can be simplified as:

$$
-TS(\rho_1 \| \rho_2) = [(U_1 - F_1) - (U_2 - F_2)].
\tag{5.27}
$$

Since $H_2 = H_1 + \epsilon V$, taking the ensemble average on both sides we get $U_2 = U_1 + \epsilon\langle V \rangle$. Substituting this into (5.27) we get:

$$
-TS(\rho_1 \| \rho_2) = (F_2 - F_1) - \epsilon\langle V \rangle.
\tag{5.28}
$$

Since ρ_1 and ρ_2 are infinitesimally close together we can use thermodynamic perturbation theory [68] to show:

$$
F_2 = F_1 + \epsilon F_1' + \frac{\epsilon^2}{2} F_1'' + O(\epsilon^3),
\tag{5.29}
$$

where,

$$F_1' = \frac{d}{d\epsilon}\left(\frac{1}{\beta}\log Z_2\right) = \langle V \rangle. \tag{5.30}$$

From (5.6) we find

$$S(\rho_1 \| \rho_2) = \frac{1}{2}\frac{\partial^2 S}{\partial\lambda^i\partial\lambda^j}\Delta\lambda^i\Delta\lambda^j. \tag{5.31}$$

Substituting (5.29) and (5.30) in (5.28) we get:

$$g_{ij}\Delta\lambda^i\Delta\lambda^j = \frac{\partial^2 S}{\partial\lambda^i\partial\lambda^j}\Delta\lambda^i\Delta\lambda^j = -\beta\epsilon^2 F_1''. \tag{5.32}$$

From the statistical physics perspective, the metric (5.7) is related to the susceptibility of the quantum state to perturbations [60, 61, 69]. The Gibbs state is the state that maximizes its entropy subject to an energy constraint. However, in statistical physics a system makes spontaneous excursions to neighbouring lower entropy states. The size of these fluctuations is determined by the Hessian of the entropy function and thus related to the susceptibility.

5.7 Quantum Cramér Rao bounds

As we have seen, the quantum relative entropy leads us to a metric (the BKM metric) on the tangent space. We notice that the quantum relative entropy dominates over the classically optimized relative entropy in section 4.4 : $S(\rho_1 \| \rho_2) \geq S^*(\rho_1 \| \rho_2)$[65]. This implies that $g_{BKM}(v, v) \geq g_{BH}(v, v)$ for all tangent vectors v. This can be explicitly seen by comparing Eq. (5.15) with Eq. (5.17) and noting that $r/2\log\left[(1 + r)/(1 - r)\right] \geq r^2$. This means that the BKM metric is more *discriminating* than the BH metric in the sense that distances are larger. Figure 5.1 shows a graphical representation of the geometry of state space as given by the BH metric

(in blue) and the BKM metric (in red). Geometrically the unit sphere of the BKM metric is contained within the unit sphere of the BH metric.

The higher discrimination of the BKM metric over the BH metric translates into a *less stringent* Cramér-Rao bound, since the bound is based on the inverse of the metric. Let X be an unbiased estimator for a parameter θ. Then the variance $V = \mathbf{tr}\,[\rho XX] - (\mathbf{tr}\,[\rho X])^2$ has to satisfy $V \geq \frac{1}{g(v,v)}$. This is the well known Cramér-Rao bound.

5.8 Non-uniqueness of the Riemannian metric on the quantum state space

We can construct many more Riemannian metrics on a quantum state space. In fact a theorem due to Morozova-Cencov-Petz[14] states that every function $f(t)$ which satisfies the following conditions

- $f(t)$ is a operator monotone[1]

- $f(1/t) = \frac{f(t)}{t}$

- $f(1) = 1$

define a Riemannian metric on the quantum state space.

Interestingly replacing $\rho(\lambda^i)$ for the $p(x|\lambda^i)$ in Eq.(5.4) gives another metric which is different form the BKM-metric. For example, on a space of qubit parametrized by

---

[1]A function $f : [0, \infty) \to [0, \infty)$ is an operator monotone if for any self adjoint matrices $\mathbf{A}$ and $\mathbf{B}$, $\mathbf{A} \geq \mathbf{B} \geq 0$ implies $f(\mathbf{A}) \geq f(\mathbf{B}) \geq 0$

vector $\boldsymbol{\lambda}$ we get,

$$\left\langle \frac{\partial \log \rho}{\partial \lambda^i} \frac{\partial \log \rho}{\partial \lambda^j} \right\rangle = \mathbf{tr}\left[\rho \frac{\partial \log \rho}{\partial \lambda^i} \frac{\partial \log \rho}{\partial \lambda^j} \right] \tag{5.33}$$

Making use of logarithmic expansion as in section 4.3.3 we find

$$\boxed{g_{ij} = \left\langle \frac{\partial \log \rho}{\partial \lambda^i} \frac{\partial \log \rho}{\partial \lambda^j} \right\rangle = C(r)\frac{x^i x^j}{r^2} + D(r)\{\delta_{ij} - \frac{x^i x^j}{r^2}\}}, \tag{5.34}$$

where $C(r) = \frac{1}{1-r^2}$, $D(r) = \frac{r^2}{4} \log\left(\frac{1+r}{1-r}\right) \log\left(\frac{1+r}{1-r}\right)$ and $r = |\boldsymbol{\lambda}|$.

5.9   Conclusion

The main goal of this chapter is to draw attention to a non-commutativity of limits in the context of quantum state discrimination. In particular, there are two limits — one which we call the "thermodynamic" limit (of N, the number of copies of state available for each of the $\mathbb{N}$ measurements) and the infinitesimal limit (of the separation of states tending to zero) — which do not commute in the quantum case. We show that taking the infinitesimal limit first leads to the BH metric. In contrast, taking the "thermodynamic" limit first leads to the BKM metric. The lack of commutation of limits is a purely quantum phenomenon with no classical counterpart. We have explicitly shown, that one can make use of this lack of commutation of limits to make use of quantum entanglement to get an advantage in state discrimination.

In this Chapter we have tried to answer the question raised by Peres and Wootters [26] regarding the existence of a multi-qubit strategy, better than the single qubit strategy for state discrimination. Later however, it was shown by Hiai and Petz[70, 65] that the multi-qubit strategy is better than the best single-qubit strategy in discriminating two quantum states using C^* algebras. As $N-$ the number of states for each

of the $\mathcal{N}$ measurements– increases we approach the bound set by the BKM metric. Thus the quantum Cramér-Rao bound set by the BKM metric can be approached but not surpassed. In contrast, the BHCR bound can be surpassed.

We have worked out the geodesics of the BKM metric and plotted them numerically. We have noticed that any two points are connected by a unique geodesic. The BKM metric leads to a distance function on the state space that emerges naturally from entropic and geometric considerations. In working out the geodesics, it is easily seen analytically that the geodesics approach the boundary of the state space at right angles. However, this approach is logarithmically slow and is not apparent in Figure 5.3. The form of the geodesics on state space is reminiscent of the geodesics of the Poincaré metric which also meet the boundary at right angles. However, there are serious differences. While both metrics have negative curvature, the Poincaré metric has *constant* negative curvature, unlike the BKM metric that has a varying curvature, which diverges logarithmically at the boundary. It is natural to ask if this is a genuine singularity or one caused by our choice of coordinates. It is easily seen that the singularity is genuine. Consider a radial geodesic starting from $r = r_0$ and reaching the boundary at $r = 1$. Its length is given by $\int_{r_0}^{1} dr/\sqrt{1 - r^2} = \pi/2 - \arcsin r_0$, which is finite. So the geodesic reaches the singularity of R in a finite distance. Since the length of the geodesic and the scalar curvature are independent of coordinates, it follows that the singularity is genuine and not an artifact of the coordinate system. The divergence of the metric as one approaches $r = 1$ has a physical interpretation. It means that pure states offer a much larger quantum advantage than mixed states. Conversely, even a small corruption of the purity of quantum states will seriously

undermine our ability to distinguish between them.

From the statistical physics perspective, the BKM metric can be interpreted as a thermodynamic susceptibility of a quantum state ρ (viewed as a Gibbs state for the Hamiltonian $H = -(1/\beta)\log\rho$ where $\frac{1}{\beta} = \frac{1}{k_B T}$ and T is the temperature of the corresponding system), to perturbations. The Gibbs state is the state that maximizes its entropy subject to an energy constraint. However, in statistical physics, a system makes spontaneous excursions to neighbouring lower entropy states. The size of these fluctuations is determined by the Hessian of the entropy function and thus related to the susceptibility.

In the existing literature[55, 56, 57, 58, 59] researchers have discussed the BKM and other Riemannian metrics on the quantum state space but have mainly focussed on the geometrical and mathematical aspects of the metric. In the context of quantum metrology[71, 72] the idea that a quantum procedure leads to an improved sensitivity in parameter estimation compared to its classical counterpart has been explored.

We go beyond earlier studies in suggesting physical and statistical mechanical interpretations of the geometry.

Chapter 6

Poincaré metric on Statistical Manifolds

As we noticed in the last chapter, the quantum Fisher Rao metric plays a crucial role in quantum state distinguishability. Here we explore a particular aspect of the Fisher Rao metric pertaining to two parameter classical distributions. We show below that for all distributions with two parameters namely location μ and scaling σ the Fisher information metric corresponds to the Poincaré metric on the half plane.

6.1 Poincaré Metric

It is a quadratic form defined on the upper half plane $\mathbf{H}$ $\{(x,y)|y > 0\}$ which defines a distance function on the plane.

$$ds^2 = \frac{dx^2 + dy^2}{y^2} \tag{6.1}$$

where s measures the distance along the curve. Geodesics for this distance function can be obtained by minimizing the distance function of a parametrized curve.

6.1.1 Geodesics

Let's parametrize the curve given by (6.1) in **H** with a parameter t:

$$\frac{ds^2}{dt^2} = \frac{\dot{x}^2 + \dot{y}^2}{y^2} \tag{6.2}$$

By looking at the symmetries of the above equation we can construct constants of integration, and integrate the above expression in terms of these constants. The RHS of (6.2) can be viewed as the Lagrangian $\mathcal{L}(x, \dot{x}, y, \dot{y})$ of an equivalent classical system. We observe that $\mathcal{L}$ is independent of x and t which suggests two constants of motion P(momentum conjugate to x) and E(energy)

$$\frac{\partial \mathcal{L}}{\partial \dot{x}} = P \qquad \text{and} \qquad \frac{\dot{x}^2 + \dot{y}^2}{y^2} = E$$

which gives $dx = y^2 P dt$ and $dt = dy/(y\sqrt{E - P^2 y^2})$. If $P \neq 0$, substituting for dt we can perform the integration to obtain the geodesic(see Figure6.1) equation which turns out to be of the form:

$$\frac{(x + c)^2}{E/P^2} + \frac{y^2}{E/P^2} = 1 \tag{6.3}$$

6.2 Fisher-Rao Metric

The Fisher-Rao metric is a Riemannian metric defined on the space of probability distributions(a statistical manifold) which defines a distance function on the manifold.
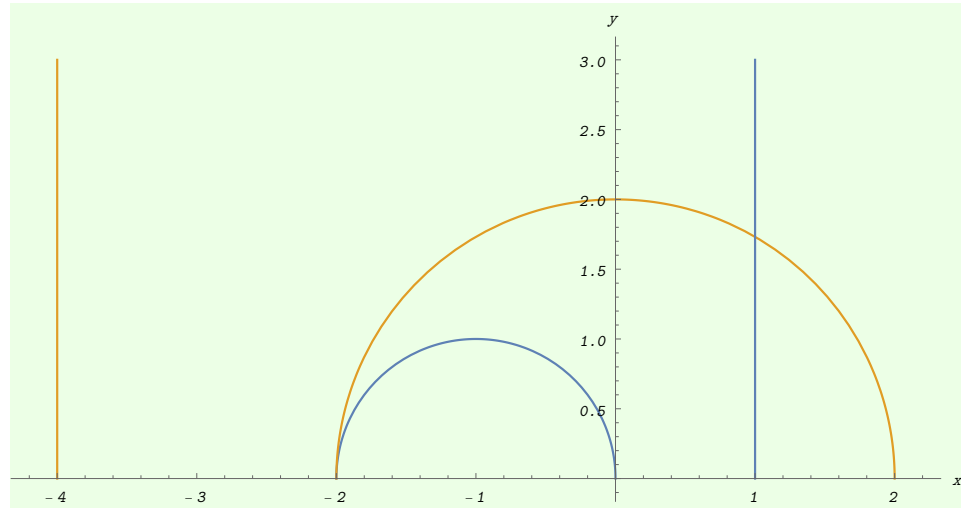
Figure 6.1: Geodesics on the Poincaré Half-Plane

Let $p_{\boldsymbol{\theta}}(X)$ denote a set of distributions parametrized by a parameter $\boldsymbol{\theta} \in \mathbb{R}^d$ then the Fisher-Rao *information metric* is given by:

$$g_{ij} = \int_{-\infty}^{\infty} \frac{\partial p_{\boldsymbol{\theta}}}{\partial \theta_i} \frac{\partial p_{\boldsymbol{\theta}}}{\partial \theta_j} dX \tag{6.4}$$

We would now like to see the explicit form of the Fisher-Rao metric for a set of distributions parametrized by two parameters; μ pertains to translation and σ pertains to dilation.

6.2.1   Gaussian Distribution

Gaussian(see Figure 6.2) distributions are the most ubiquitous distributions that come up naturally in a variety of mathematical and physical situations. A Gaussian distribution has the following form:

$$p(x|\mu, \sigma) = \frac{e^{-\frac{(x-\mu)^2}{2\sigma^2}}}{\sqrt{2\pi}\sigma} \tag{6.5}$$
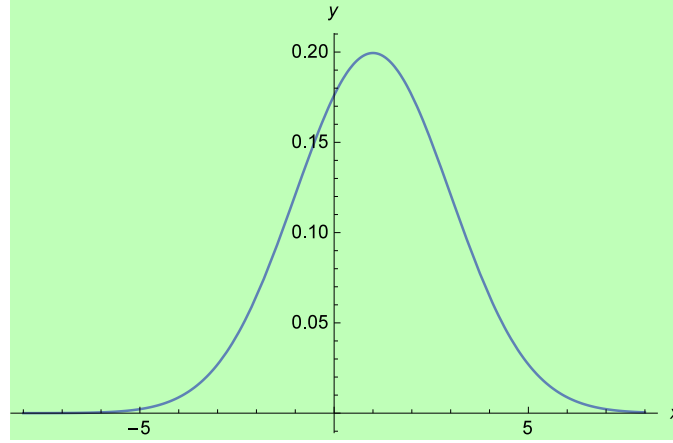
Figure 6.2: A Gaussian distribution with $\mu = 1, \sigma = 2$

where μ is the mean and σ is the standard deviation. The partial derivatives of Equation(6.5) with respect to the parameters are given by

$$\frac{\partial \log p(x|\mu, \sigma)}{\partial \mu} = \frac{(x - \mu)e^{-\frac{(x-\mu)^2}{2\sigma^2}}}{\sqrt{2\pi}\sigma^3} \quad \text{and} \quad \frac{\partial \log p(x|\mu, \sigma)}{\partial \sigma} = \frac{(x - \mu)^2 e^{-\frac{(x-\mu)^2}{2\sigma^2}}}{\sqrt{2\pi}\sigma^4} - \frac{e^{-\frac{(x-\mu)^2}{2\sigma^2}}}{\sqrt{2\pi}\sigma^2}$$

Using the two partial derivatives we calculate the Fisher-Rao metric from the formula (6.4) for this distribution and obtain:
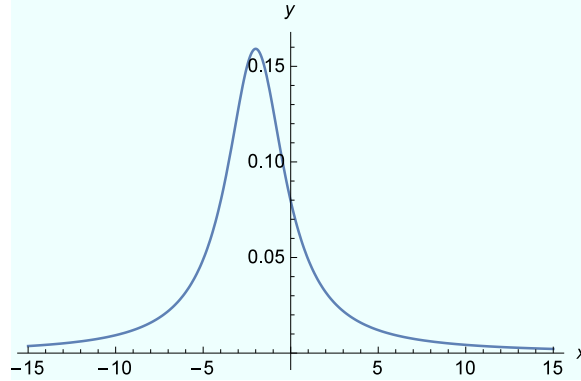
$$g = \begin{pmatrix} \frac{1}{6\sqrt{3}\pi\sigma^4} & 0 \\ 0 & \frac{1}{3\sqrt{3}\pi\sigma^4} \end{pmatrix} \tag{6.6}$$

6.2.2 Cauchy Distribution

It is a two parameter distribution(see Figure 6.3) given by:

$$p(x|\mu, \sigma) = \frac{\sigma^2}{\pi\sigma[(x - \mu)^2 + \sigma^2]} \tag{6.7}$$

such that

Figure 6.3: A Cauchy distribution with $\mu = -2, \sigma = 2$

$$\frac{\partial \log p(x|\mu, \sigma)}{\partial \mu} = -\frac{2(x - \mu)}{[(x - \mu)^2 + \sigma^2]} \quad \text{and} \quad \frac{\partial \log p(x|\mu, \sigma)}{\partial \sigma} = \frac{(x - \mu)^2 - \sigma^2}{\sigma[(x - \mu)^2 + \sigma^2]}$$

Using the two partial derivatives we calculate the Fisher-Rao metric from the formula (6.4) for this distribution and obtain:

$$g = \begin{pmatrix} \frac{1}{2\sigma^2} & 0 \\ 0 & \frac{1}{2\sigma^2} \end{pmatrix} \tag{6.8}$$

6.2.3 Laplace Distribution

The Laplace distribution(shown in Figure 6.4) function is given by:

$$p(x|\mu, \sigma) = \frac{\exp\left\{-\frac{|x - \mu|}{\sigma}\right\}}{2\sigma} \tag{6.9}$$

and

$$\frac{\partial \log p(x|\mu, \sigma)}{\partial \mu} = -\begin{cases} \frac{1}{\sigma} & \text{for} \quad x < \mu \\ -\frac{1}{\sigma} & \text{for} \quad x > \mu \end{cases} \quad \text{and} \quad \frac{\partial \log p(x|\mu, \sigma)}{\partial \sigma} = -\frac{1}{\sigma} + \frac{|x - \mu|}{\sigma}$$

Using the same procedure again we obtain,

$$g = \begin{pmatrix} \frac{1}{\sigma^2} & 0 \\ 0 & \frac{1}{2\sigma^2} \end{pmatrix} \tag{6.10}$$
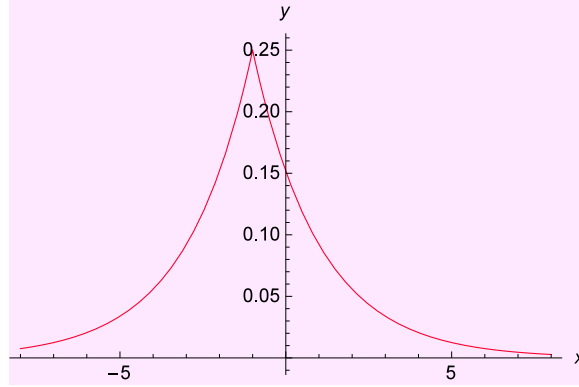
Figure 6.4: A Laplace distribution with $\mu = -1, \sigma = 2$

These examples suggest a general theorem which we state and prove below:

6.3 A General (μ-σ) Distribution

A general $\mu - \sigma$ distribution is of the form:

$$P(x|\mu, \sigma) = \frac{1}{\sigma} f\left(\frac{x - \mu}{\sigma}\right) \tag{6.11}$$

Theorem. *The Fisher-Rao metric on the $\mu - \sigma$ sub-manifold is the Poincaré Half-Plane metric.*

Proof. By making a change of variable $y = \frac{x-\mu}{\sigma}$ and taking partial derivatives with respect to μ and σ of Eq.(6.11) we obtain,

$$\frac{\partial \log P(x|\mu, \sigma)}{\partial \mu} = -\frac{1}{\sigma f(y)} \qquad \text{and} \qquad \frac{\partial \log P(x|\mu, \sigma)}{\partial \sigma} = -\left(\frac{y}{\sigma f(y)} + \frac{1}{\sigma}\right) \tag{6.12}$$

Using these partial derivatives we evaluate all the components of the Fisher-Rao metric (6.4),

$$g_{\mu\mu} = \frac{1}{\sigma^2} \int_{-\infty}^{\infty} \frac{dy}{f(y)} = \frac{A}{\sigma^2}$$

$$g_{\sigma\sigma} = \frac{1}{\sigma^2} \int_{-\infty}^{\infty} f(y) \left(\frac{y}{f(y)} + 1 \right) dy = \frac{B}{\sigma^2}$$

$$g_{\mu\sigma} = g_{\sigma\mu} = \frac{1}{\sigma^2} \int_{-\infty}^{\infty} \left(\frac{y}{f(y)} + 1 \right) dy = \frac{C}{\sigma^2}$$

and hence obtain the following form for the metric

$$g = \frac{1}{\sigma^2} \begin{pmatrix} A & C \\ C & B \end{pmatrix} \tag{6.13}$$

We can diagonalize the metric by a suitable choice of basis. $\square$

6.4 Conclusion

In this chapter we investigated the Fisher-Rao metric on the two dimensional subspace of the probability simplex with location and scaling as the parameters. Each point on the subspace represents a probability distribution with its parameters as the coordinates. This metric defines a distance function which quantifies how distinguishable two distributions are in a given number of trials. We have seen with some specific distributions that the Fisher information metric induces a hyperbolic geometry on the subspace as in the case of Poincaré metric on the half plane[73]. We then state and prove a general theorem for all distributions on this subspace. This metric has a constant negative curvature all over the subspace. We also generate and plot the geodesics on this subspace.

We would like to explore in future the possibility of extending this theorem to a quantum manifold. One of the hurdles in extending this theorem to quantum manifolds is non commutativity.

Chapter 7

Conclusion and future directions

In this chapter, we will conclude the work that formed the basis of this thesis and will give a perspective on future work. The central theme of the thesis has been to study the mathematical and geometrical aspects of entanglement. We also looked at various physical situations where it can be used as a resource. For example, in a *coarse measurement* the extent of entanglement between the spin and the center of mass of the silver atom directly determines the amount of information we can obtain about the spin of the silver atom by making a position measurement of its center of mass. We have also seen that entanglement can be useful in discriminating between two quantum states. An explicit example using projective measurement on multiple qubits demonstrates how entanglement between the qubits can give rise to greater distinguishability between nearby states.

In **chapter 2**, we looked at the entanglement criteria for a two qubit system density matrix, geometrically. A two qubit density matrix can be associated with a second rank tensor($A_{\mu\nu}$) which is like the energy-momentum tensor of relativity.

We have also demonstrated that the positivity of the density matrix is equivalent to the *dominant energy condition*(DEC) on $A_{\mu\nu}$. If the tensor associated with the density operator fails to satisfy the strong energy condition (SEC) for any two timelike vectors, then the density matrix represents an entangled state. Using a Werner state, we have explicitly shown that $A_{\mu\nu}$ associated with the density matrix fails to satisfy the SEC for the parameter range $1/3 \le \alpha \le 1$ implying that the state is entangled for this range of the parameter α.

For a Werner state, we were able to show the violation of the SEC by just optimizing with respect to D (see Section 2.2.3). However, to show the violation for an arbitrary state it would require an optimization over the spinors κ_1 and κ_2 as well. We would like to investigate in future the DEC for an arbitrary state of a two qubit bipartite system. We would also like to explore the transformation of $A_{\mu\nu}$ under positive but not completely positive maps which detect entanglement in a bipartite system.

Chapter 3 presents a Lorentzian geometric framework which has been used to come up with a test for detection of entanglement discussed in 2. We study the relation between qubit entanglement and Lorentzian geometry. In the chapter 2, we had given a recipe for detecting two qubit entanglement. The entanglement criterion is based on Partial Lorentz Transformations (PLT) on individual qubits. Chapter 3 gives the theoretical framework underlying the PLT test. The treatment is based physically, on the causal structure of Minkowski spacetime, and mathematically, on a Lorentzian Singular Value Decomposition. A surprising feature is the natural emergence of "Energy conditions" used in Relativity. All states satisfy a "Dominant Energy Condition"

(DEC) and separable states satisfy the Strong Energy Condition(SEC), while entangled states violate the SEC. Apart from testing for entanglement, this approach also enables us to construct a separable form for the density matrix in those cases where it exists. This approach leads to a simple graphical three dimensional representation of the state space which shows the entangled states within the set of all states (See figure 3.2).

In **chapter 4** we discussed the role of entanglement in a coarse measurement. We looked at the Stern-Gerlach measurement process in the light of the idea that every measurement is performed with a limited resource of resolution and concluded that the apparent loss of unitarity in a measurement process is due to the coarseness of the measurement probe which is unable to discriminate between the successive eigenstates of the system. The main motivation behind this point of view comes from a somewhat familiar concept that *entropy is subjective*[40, 41] depending upon the amount of resource an experimenter has to distinguish between statistical states. We investigated the effect of coarse-graining on the Wigner function associated with the position of the silver atom. We have seen that the Wigner matrix goes to a diagonal form on coarse-graining over the volume of phase space cell of the order of a few $\hbar$.

In future, we would like to explore the same idea –coarse measurement– in another case commonly known as the static Stern-Gerlach setup. In this setup, a spin half particle is placed in a harmonic trap. The coupling between the spin and the magnetic field shifts the energy of the oscillator by an amount depending upon the orientation of the spin. We would like to explore the outcome of a coarse measurement on the energy of the system.

The central observation made in **chapter 5** is that the two limits involved in state discrimination namely the thermodynamic limit and the infinitesimal limit do *not* commute. Taking the thermodynamic limit followed by the infinitesimal limit leads us to the BH metric. However, taking the limits in the opposite order gives us the BKM metric. An improvement in the distinguishability for the BKM metric stems from entanglement. We have shown explicitly that by making use of entanglement between the copies of quantum states, we can improve the distinguishability between states beyond the BH distance. We explored the geometry of the space of quantum states as induced by this metric, and developed a visual representation of the distinguishability measure similar to that of the Mc Adam ellipses on the space of colors. We saw that the metric has a diverging negative curvature towards the boundary of the space, implying that the states on the boundary(pure) are very far apart and can be better distinguished from each other than any other two points in the hull(mixed). We also looked at the thermodynamic connection of the metric with the fluctuation in free energy in a thermal system. We were led to the conclusion that this metric sets a less stringent Crarmér-Rao bound on the variance of the unbiased parameter estimator resulting in a greater distinguishability than the BH metric.

Apart from the BH and the BKM metrics there is an entire family of monotone metrics[14] that can be defined on the state space which gives an improvement over the BKM-metric. In future we wish to investigate these and explore possible strategies for experimentally realizing these.

In **chapter 6**, we stated and proved a theorem on $\mu - \sigma$ subspace of the classical probability simplex. This theorem concerns the distinguishability of two distributions

which are represented as points on the subspace. We argued that this subspace is isomorphic to the Poincaré half plane as the Fisher-Rao information metric defined on the $\mu - \sigma$ plane is the same as the Poincaré metric on the half plane.

We would like to extend this theorem to a quantum manifold, in particular, the space of density matrices with the two parameters as location and scaling.

Appendix A

Used Programs

A.1   PLT : A positive map

```mathematica
In[56]:= ClearAll[Li, R]
Li = {};
m[i_, j_] := KroneckerProduct[PauliMatrix[i], PauliMatrix[j]]
For[i = 0, i ≤ 5000, i++,
  X = Table[RandomReal[], {i, 0, 3}, {j, 0, 3}];
      1
  S = ─ (X + X†); (* Produces a real symmetric matrix. *)
      2
  ρ = (1 / Tr[MatrixExp[S]]) MatrixExp[S]; (* Creates a random density matrix. *)
  AA[i_, j_] := Tr[ρ.m[i, j]];
  AAij = Table[Simplify[AA[i, j]], {i, 0, 3}, {j, 0, 3}];

  η = RandomReal[5];
  φ = RandomReal[2 π];
  θ = RandomReal[π];
  ψ = RandomReal[2 π];

  α = 0.7;
  R1z = {{1, 0, 0, 0}, {0, Cos[φ], Sin[φ], 0}, {0, -Sin[φ], Cos[φ], 0}, {0, 0, 0, 1}};
  Ry = {{1, 0, 0, 0}, {0, Cos[θ], 0, Sin[θ]}, {0, 0, 1, 0}, {0, -Sin[θ], 0, Cos[θ]}};
  R2z = {{1, 0, 0, 0}, {0, Cos[ψ], Sin[ψ], 0}, {0, -Sin[ψ], Cos[ψ], 0}, {0, 0, 0, 1}};
  R = R2z.Ry.R1z; (* Euler Rotations*)
  Λ = {{Cosh[η], Sinh[η], 0, 0}, {Sinh[η], Cosh[η], 0, 0}, {0, 0, 1, 0}, {0, 0, 0, 1}};
  pLtAAij = R.Λ.Rᵀ.AAij;
  pLtAA[i_, j_] := pLtAAij[[(i + 1), (j + 1)]];
           1
  rhopLt = ─ Sum[Simplify[pLtAA[i, j] * m[i, j]], {i, 0, 3}, {j, 0, 3}];
           4
            rhopLt
  ρpLt = ───────────;
          Tr[rhopLt]
  X = Min[Chop[Eigenvalues[ρpLt]]];
  (* Smallest eigenvalue of the partially Lorentz transformed density matrix*)
  Li = Append[Li, {i, X}]
]

plot1 =
 Labeled[ListPlot[Li, PlotMarkers → {Automatic, 3}, BaseStyle -> {FontSize -> 12},
  ImageSize -> Full], {Style["smallest eigenvalue", FontSize -> 15],
    Style["iᵗʰ realization", FontSize -> 15]}, {Left, Bottom}, RotateLabel → True]
```

Appendix A: Used Programs 115

Out[60]=
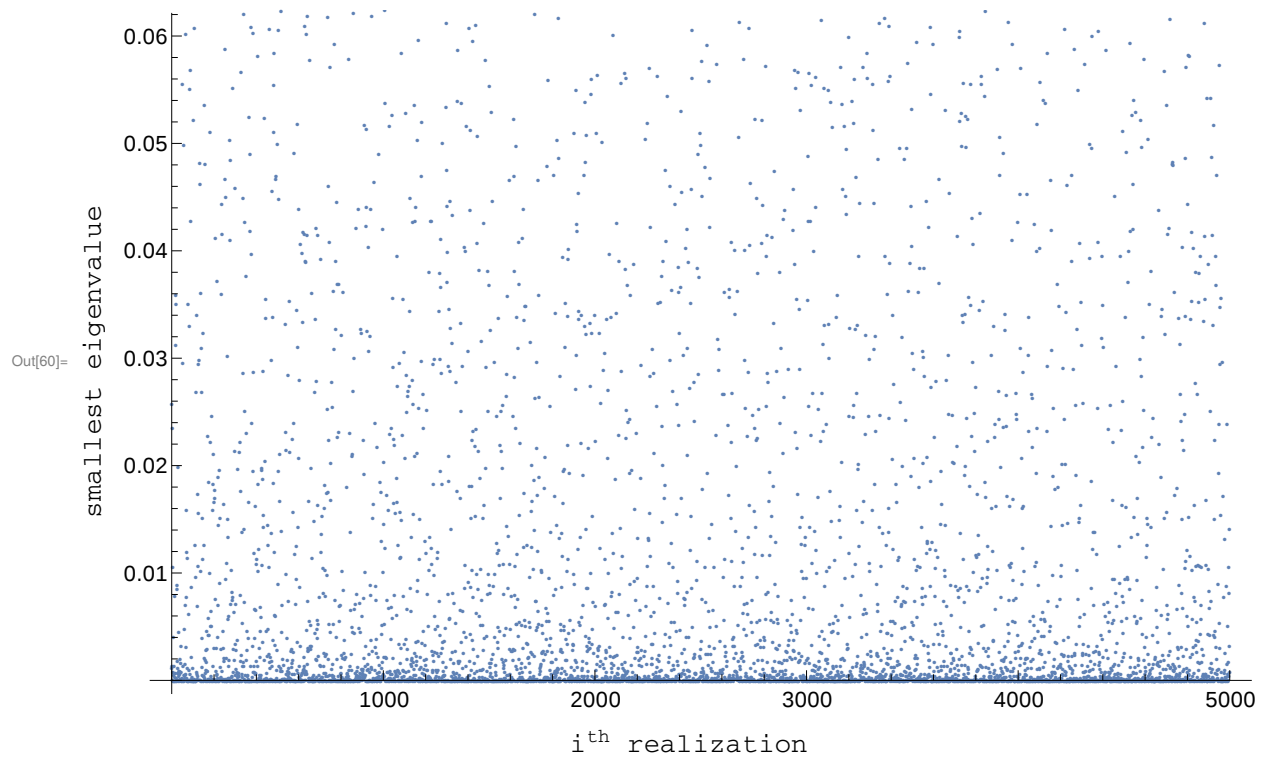
```mathematica
In[63]:= Export["PLTasCPmap.pdf", plot1]
```

Out[63]= PLTasCPmap.pdf

```mathematica
In[62]:= SystemOpen[DirectoryName[AbsoluteFileName["PLTasCPmap.jpg"]]]
```

```mathematica
In[27]:= Chop[Tr[ρpLt]]
PositiveSemidefiniteMatrixQ[ρpLt]
Min[Li[[2]]]
```

Out[27]= 1.

Out[28]= True

Out[29]= 0.0000328789

A.2 Positivity of A_{ij}^{Werner}

```mathematica
In[77]:= α = 0.7; (* α ∈ [0,1],
    0 for maximally mixed state and 1 for a Bell state. *)
    ρ = 1 / 4 * {{1 - α, 0, 0, 0}, {0, 1 + α, -2 * α, 0},
        {0, -2 * α, 1 + α, 0}, {0, 0, 0, 1 - α}}; (* Werner State *)
    ρ̃ = {{ρ[[1, 1]], ρ[[2, 1]], ρ[[1, 3]], ρ[[2, 3]]},
      {ρ[[1, 2]], ρ[[2, 2]], ρ[[1, 4]], ρ[[2, 4]]},
      {ρ[[3, 1]], ρ[[4, 1]], ρ[[3, 3]], ρ[[4, 3]]},
      {ρ[[3, 2]], ρ[[4, 2]], ρ[[3, 4]], ρ[[4, 4]]}};
    (* Partial Transpose of ρ *)
    σ₀ = IdentityMatrix[2];
    σ₁ = PauliMatrix[1];
    σ₂ = PauliMatrix[2];
    σ₃ = PauliMatrix[3];
    m_{i_,j_} := KroneckerProduct[σ_i, σ_j]
    A = Table[Tr[ρ.m_{i,j}], {i, 0, 3}, {j, 0, 3}]; (* Computes A_{ij} for the ρ *)
    At = Table[Tr[ρ̃.m_{i,j}], {i, 0, 3}, {j, 0, 3}];
    (* Computes A_{ij} for the ρ̃ *)
    X = {};
    Xt = {};
    For[q = 0, q < 10 000, q++, ψ = {Normalize[
        {RandomComplex[], RandomComplex[], RandomComplex[], RandomComplex[]}]};
     a = {{ψ[[1, 1]], ψ[[1, 2]]}, {ψ[[1, 3]], ψ[[1, 4]]}};
     (* Random state of a two qubit system *)
     S = SingularValueDecomposition[a];
     u = S[[1]];
     d = S[[2]];
     c1 = d[[1, 1]];
     c2 = d[[2, 2]];
     v = S[[3]];
     i1 = {{u[[1, 1]], u[[2, 1]]}};
     i2 = {{u[[1, 2]], u[[2, 2]]}};
     j1 = {{v[[1, 1]], v[[1, 2]]}};
     j2 = {{v[[2, 1]], v[[2, 2]]}};
     l0 = (i1.PauliMatrix[0].i1†)[[1, 1]];
     l1 = (i1.PauliMatrix[1].i1†)[[1, 1]];
     l2 = (i1.PauliMatrix[2].i1†)[[1, 1]];
     l3 = (i1.PauliMatrix[3].i1†)[[1, 1]];
     l = {{l0, l1, l2, l3}};
     ll0 = (i2.PauliMatrix[0].i2†)[[1, 1]];
     ll1 = (i2.PauliMatrix[1].i2†)[[1, 1]];
     ll2 = (i2.PauliMatrix[2].i2†)[[1, 1]];
     ll3 = (i2.PauliMatrix[3].i2†)[[1, 1]];
     ll = {{ll0, ll1, ll2, ll3}};
     n0 = (j1.PauliMatrix[0].j1†)[[1, 1]];
     n1 = (j1.PauliMatrix[1].j1†)[[1, 1]];
```

```
n2 = (j1.PauliMatrix[2].j1⁺)[[1, 1]];
n3 = (j1.PauliMatrix[3].j1⁺)[[1, 1]];
n = {{n0, n1, n2, n3}};
nn0 = (j2.PauliMatrix[0].j2⁺)[[1, 1]];
nn1 = (j2.PauliMatrix[1].j2⁺)[[1, 1]];
nn2 = (j2.PauliMatrix[2].j2⁺)[[1, 1]];
nn3 = (j2.PauliMatrix[3].j2⁺)[[1, 1]];
nn = {{nn0, nn1, nn2, nn3}};
mA = {{(i1.PauliMatrix[0].i2⁺)[[1, 1]], (i1.PauliMatrix[1].i2⁺)[[1, 1]],
     (i1.PauliMatrix[2].i2⁺)[[1, 1]], (i1.PauliMatrix[3].i2⁺)[[1, 1]]}};
mAc = {{(mA[[1, 1]])*, (mA[[1, 2]])*, (mA[[1, 3]])*, (mA[[1, 4]])*}};
mB = {{(j1.PauliMatrix[0].j2⁺)[[1, 1]], (j1.PauliMatrix[1].j2⁺)[[1, 1]],
     (j1.PauliMatrix[2].j2⁺)[[1, 1]], (j1.PauliMatrix[3].j2⁺)[[1, 1]]}};
mBc = {{(mB[[1, 1]])*, (mB[[1, 2]])*, (mB[[1, 3]])*, (mB[[1, 4]])*}};
(* This part produces four null vector n,
l, m, m̄ as describded in Chapter-1. *)
τ =
  Re[(c1² l.A.nᵀ + c2² ll.A.nnᵀ + c1 * c2 * mA.A.mBᵀ + c1 * c2 * mAc.A.mBcᵀ)[[1, 1]]];
τ̃ = Re[(c1² l.At.nᵀ + c2² ll.At.nnᵀ + c1 * c2 * mA.At.mBᵀ + c1 * c2 * mAc.At.mBcᵀ)[[
     1, 1]]];
X = Append[X, Sign[τ]];
Xt = Append[Xt, Sign[τ̃]]]
plot1 = ListPlot[X, {AxesLabel →
     {Style["iᵗʰ realization", FontSize → 15], Style["τ", FontSize → 15]}},
  BaseStyle → {(*FontWeight→"Bold",*)FontSize → 12}, ImageSize → Large]
plot2 = ListPlot[Xt, {AxesLabel →
     {Style["iᵗʰ realization", FontSize → 15], Style["τ̃", FontSize → 15]}},
  BaseStyle → {(*FontWeight→"Bold",*)FontSize → 12}, ImageSize → Large]
(*ListPlot[Xt,AxesLabel→τ,BaseStyle→{FontWeight→"Bold",FontSize→12}]
  Lmin={Min[X],Min[Xt]}*)
```
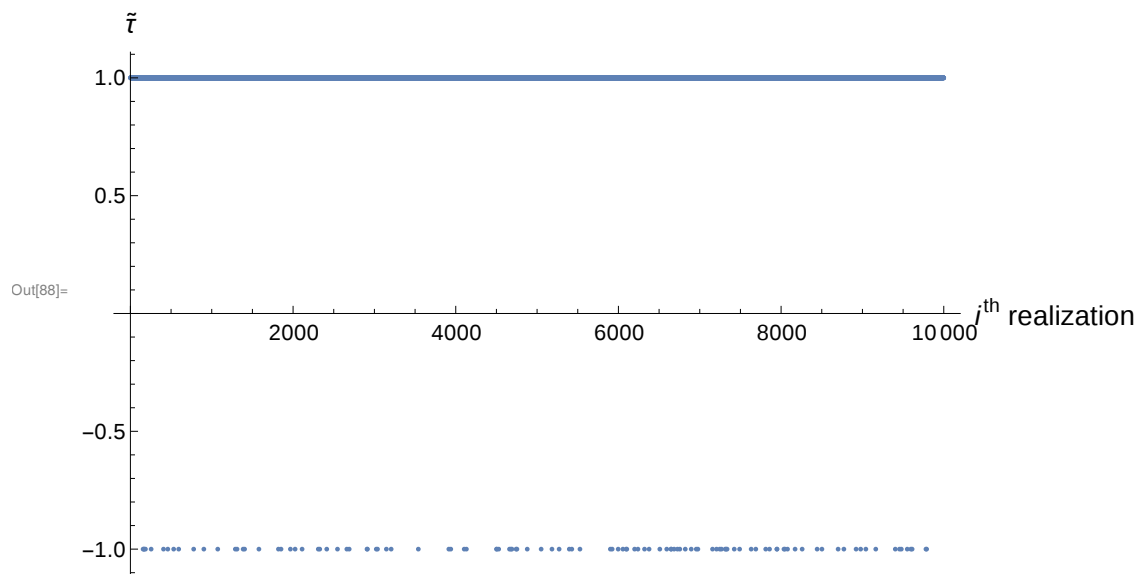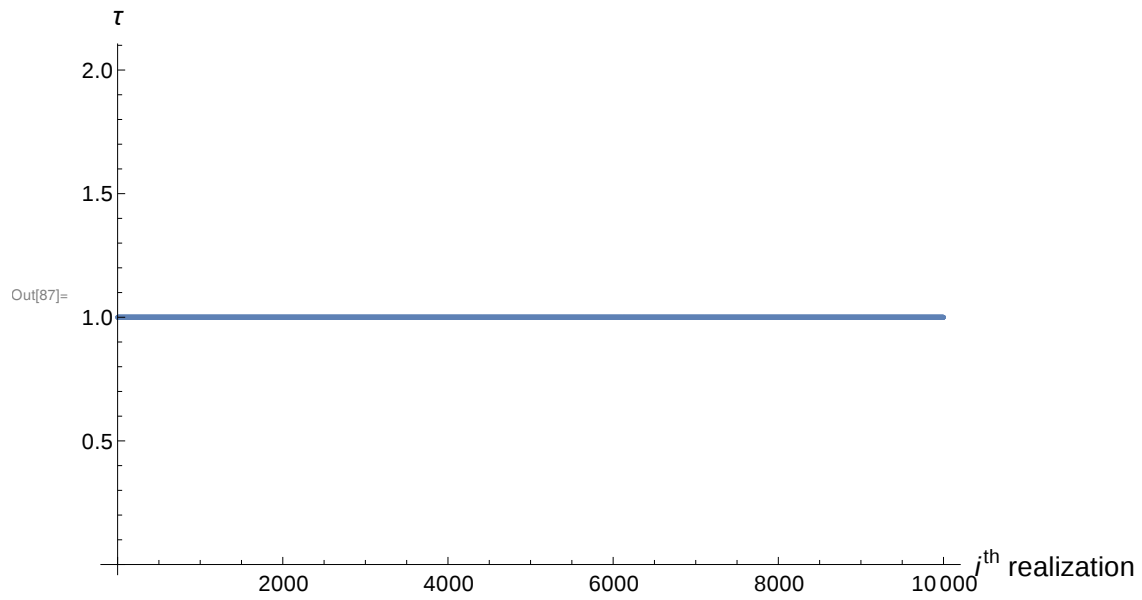
A.3   PPT Vs PLT

Here we give the Mathematica program used in Chapter 2 which numerically generates 2 qubit density matrix randomly and check for entanglement using both PPT and PLT. Here we see that the PLT always agrees with PPT as the sign(PPT×PLT) is always positive.

```
(*This program generates a numerical,
Random density matrix, computes the matrices
 A and its ``square'' B. Then computes the eigenvalues of B,
forms the function T described in the paper. *)
Lplt = {};
Lppt = {};
LBev = {};
(*Initialising the strings Lplt,Lppt, which store the outcomes of the test:
   1=separable,-1=entangled*)
Nmax = 100;
(*Nmax is the number of random density matrices to be tested. try 1000 or higher
  depending on your patience. Nmax=100 takes about 10 seconds to run.*)
For[i = 1, i < Nmax + 1, i++,
  λ1 = RandomReal[];
  λ2 = RandomReal[];
  λ3 = RandomReal[];
  λ4 = RandomReal[];
  (*Eigenvalues chosen at random between 0 and 1*)
  ρ0 = DiagonalMatrix[{λ1, λ2, λ3, λ4}];
  S = Table[RandomComplex[], {i, 1, 4}, {j, 1, 4}];
  H = (S + S†);
  (*H is a Random Hermitean Matrix*)
  ρ = MatrixExp[I * H].ρ0.MatrixExp[-I * H];
  tr = Tr[ρ];
  ρ = ρ / tr;
  (*Normalising ρ, really not necessary for either test*)
  σ0 = IdentityMatrix[2];
  σ1 = PauliMatrix[1];
  σ2 = PauliMatrix[2];
  σ3 = PauliMatrix[3];
  mi_,j_ := KroneckerProduct[σi, σj];
  Ai_,j_ := Tr[ρ.mi,j];
  A = Table[Ai,j, {i, 0, 3}, {j, 0, 3}];
  A1 = Chop[A];
  g = DiagonalMatrix[{1, -1, -1, -1}];
  (*Lorentzian Metric is Crucial for test to work*)
  AT = Transpose[A1];
  B = A1.g.AT.g;
  evb = Eigenvalues[B];
  minb = Min[evb];
  LBev = Append[LBev, minb];
  (*Collecing the smallest eigenvalue of B to show that these are positive*)
  (*Eigenvalues are arranged by mathematica
   in decreasing order evb[[1]] is the dominant eigenvalue*)
  mu = Sqrt[evb];
  mu0 = mu[[1]];
  mu1 = mu[[2]];
```

```
 mu2 = mu[[3]];
 mu3 = mu[[4]];
 If[mu0 - (mu1 + mu2 + mu3) ≥ 0, plttest = 1, plttest = -1];
 (*If ρ passes the partial Lorentz transformation test,
 it is separable and assigned plttest=1, else -1,
 these values are stored in the string Lplt*)
 Lplt = Append[Lplt, plttest];
 rhoAB = ρ;
 Eigenvalues[rhoAB];
 rhoABt = {{rhoAB[[1, 1]], rhoAB[[2, 1]], rhoAB[[1, 3]], rhoAB[[2, 3]]},
    {rhoAB[[1, 2]], rhoAB[[2, 2]], rhoAB[[1, 4]], rhoAB[[2, 4]]},
    {rhoAB[[3, 1]], rhoAB[[4, 1]], rhoAB[[3, 3]], rhoAB[[4, 3]]},
    {rhoAB[[3, 2]], rhoAB[[4, 2]], rhoAB[[3, 4]], rhoAB[[4, 4]]}};
 evrho = Chop[Eigenvalues[rhoABt]];
 min = Chop[Min[evrho]];
 If[min ≥ 0, ppttest = 1, ppttest = -1];
 Lppt = Append[Lppt, ppttest];
 (*If ρ passes the Positive partial transpose test,
 it is separable and assigned ppttest=1,
 else -1. These values are stored in Lppt*)
];
(*These are the outputs of the program. Lplt is a string of 1s and -1s, the 1 s
 represent those passing the plt test. Lppt is a similar string,
with 1 s passing the ppt test. Note
  that both strings have both 1 s and -1s in general.
   However, their product Lplt*Lpptis always 1, which means that the two tests
 always agree. A simple diagnostic is Min[Lplt*Lppt],
which would be -1 if they disagreed in even one case. They never do, proving that
 PLT agrees with PPT in every case *)
Lplt

Lppt
Lplt * Lppt
Min[%]
LBev;
Min[LBev]
(*The smallest the entries of LBev is positive,
showing that they all are. To see LBev,
remove the semicolon appearing after LBev; *)
{1, 1, 1, 1, 1, 1, 1, 1, 1, 1, 1, -1, 1, 1, 1, 1, 1, 1, 1, 1, 1, 1, 1, 1, 1,
 1, 1, 1, 1, 1, 1, 1, 1, 1, 1, 1, 1, 1, 1, 1, 1, 1, 1, 1, 1, 1, 1, 1, 1, 1,
 1, 1, 1, 1, 1, -1, -1, 1, -1, 1, 1, -1, 1, 1, 1, 1, 1, 1, 1, 1, 1, -1, 1, 1,
 1, 1, 1, 1, 1, 1, -1, 1, -1, 1, 1, 1, 1, 1, 1, 1, 1, 1, 1, -1, 1, 1, 1, 1}

{1, 1, 1, 1, 1, 1, 1, 1, 1, 1, 1, -1, 1, 1, 1, 1, 1, 1, 1, 1, 1, 1, 1, 1, 1,
 1, 1, 1, 1, 1, 1, 1, 1, 1, 1, 1, 1, 1, 1, 1, 1, 1, 1, 1, 1, 1, 1, 1, 1, 1,
 1, 1, 1, 1, 1, -1, -1, 1, -1, 1, 1, -1, 1, 1, 1, 1, 1, 1, 1, 1, 1, -1, 1, 1,
 1, 1, 1, 1, 1, 1, -1, 1, -1, 1, 1, 1, 1, 1, 1, 1, 1, 1, 1, -1, 1, 1, 1, 1}
```

Appendix A: Used Programs 123

```
{1, 1, 1, 1, 1, 1, 1, 1, 1, 1, 1, 1, 1, 1, 1, 1, 1, 1, 1, 1, 1, 1, 1,
 1, 1, 1, 1, 1, 1, 1, 1, 1, 1, 1, 1, 1, 1, 1, 1, 1, 1, 1, 1, 1, 1, 1,
 1, 1, 1, 1, 1, 1, 1, 1, 1, 1, 1, 1, 1, 1, 1, 1, 1, 1, 1, 1, 1, 1, 1, 1,
 1, 1, 1, 1, 1, 1, 1, 1, 1, 1, 1, 1, 1, 1, 1, 1, 1, 1, 1, 1, 1, 1, 1, 1, 1}
```

1

1.26855×10^{-7}

Appendix B

Energy Conditions

In this appendix we discuss the energy conditions that come into play in our analysis. Given a stress energy tensor T_{ab} one requires it to satisfy some "reasonable" positivity conditions. If T^a_b has a timelike eigenvector, it can be diagonalised ([21]) and brought to the form $T^a_b = diag(\epsilon, -p_1, -p_2, -p_3) = diag(\mu_0, \mu_1, \mu_2, \mu_3)$, where ϵ is the energy density of matter and p_1, p_2, p_3 the principal pressures of the matter fluid. Note that in our context, the pressures are negative when the μs are positive. The exceptional case, where T has a repeated lightlike eigenvector represents a null fluid and this corresponds to the Type-II density matrices mentioned above. Below is a short primer on energy conditions, giving the formal definition and a physical interpretation. Below we will suppose for illustration that T is Type-I and can be

diagonalised, which is the generic and most interesting case.

$$T_{ab} = \begin{pmatrix} \epsilon & 0 & 0 & 0 \\ 0 & p_1 & 0 & 0 \\ 0 & 0 & p_2 & 0 \\ 0 & 0 & 0 & p_3 \end{pmatrix} \tag{B.1}$$

B.1 Weak Energy Condition:

The weak energy condition (WEC) states that given any timelike vector ξ^a T must satisfy:

$$T_{ab}\xi^a\xi^b \geq 0 \tag{B.2}$$

This yields

$$\epsilon + p_{\hat{a}} \geq 0 \qquad \text{for } \hat{a} = 1, 2, 3 \tag{B.3}$$

The weak energy condition physically represents the idea that all observers must see a postive energy density. There is no negative mass!

B.2 Dominant Energy Condition:

The Dominant Energy Condition(DEC) states that: given any two lightlike vectors ξ_1^a and ξ_2^b

$$T_{ab}\xi_1^a\xi_2^b \geq 0 \tag{B.4}$$

Notice that for $\xi_1 = \xi_2$ we recover the weak energy condition. So, the DEC implies the WEC. It is enough to demand (B.4) for lightlike n, m. Since timelike vectors

are convex combinations of lightlike ones, it follows that (B.4) holds for timelike n, m. For a suitable choice of ξ_1, ξ_2 the DEC gives us: $\epsilon \geq |p_{\hat{a}}|$ for $\hat{a} = 1, 2, 3$. The Dominant energy condition requires that all observers see a non spacelike matter current $j_a = T_{ab}\xi^b$. Matter cannot travel faster than light!

B.3 Strong Energy Condition:

The strong energy condition(SEC) reads:

$$(T_{ab} - \frac{1}{2}Tg_{ab})\xi^a\xi^b \geq 0, \ \forall \text{ time-like } \xi \tag{B.5}$$

We find that the SEC gives us $\epsilon + p_{\hat{a}} \geq 0$ and $\epsilon + p_1 + p_2 + p_3 \geq 0$. The strong energy condition emerges from the focussing property of timelike geodesics with tangent vector ξ^a as described by Raychaudhuri's equation[74]. The focussing of timelike geodesics is determined by the sign of $R_{ab}\xi^a\xi^b$, where R_{ab} is the Ricci tensor. The positivity of $R_{ab}\xi^a\xi^b$ is essentially the SEC via Einstein's equations. These "Energy conditions" are imposed in Relativity as "reasonable". They are obeyed by the known classical forms of matter. However, they are violated by quantum matter and Dark Energy violates the SEC. The point **P** in Fig.2 has a stress energy tensor of the same form as Dark Energy.

Bibliography

[1] Charles H. Bennett, Gilles Brassard, Claude Crépeau, Richard Jozsa, Asher Peres, and William K. Wootters. Teleporting an unknown quantum state via dual classical and einstein-podolsky-rosen channels. *Phys. Rev. Lett.*, 70:1895–1899, Mar 1993.

[2] Charles H. Bennett, Gilles Brassard, Claude Crépeau, Richard Jozsa, Asher Peres, and William K. Wootters. Teleporting an unknown quantum state via dual classical and einstein-podolsky-rosen channels. *Phys. Rev. Lett.*, 70:1895–1899, Mar 1993.

[3] Charles H. Bennett, Gilles Brassard, and N. David Mermin. Quantum cryptography without bell's theorem. *Phys. Rev. Lett.*, 68:557–559, Feb 1992.

[4] Artur K. Ekert. Quantum cryptography based on bell's theorem. *Phys. Rev. Lett.*, 67:661–663, Aug 1991.

[5] Artur K. Ekert. Quantum cryptography based on bell's theorem. *Phys. Rev. Lett.*, 67:661–663, Aug 1991.

[6] Časlav Brukner, Marek Żukowski, Jian-Wei Pan, and Anton Zeilinger. Bell's in-

equalities and quantum communication complexity. *Phys. Rev. Lett.*, 92:127901, Mar 2004.

[7] Richard Jozsa, Daniel S. Abrams, Jonathan P. Dowling, and Colin P. Williams. Quantum clock synchronization based on shared prior entanglement. *Phys. Rev. Lett.*, 85:2010–2013, Aug 2000.

[8] Vlatko Vedral. High-temperature macroscopic entanglement. *New Journal of Physics*, 6(1):102, 2004.

[9] Vlatko Vedral. High-temperature macroscopic entanglement. *New Journal of Physics*, 6:102–102, aug 2004.

[10] Leonid Gurvits. Classical complexity and quantum entanglement. *Journal of Computer and System Sciences*, 69(3):448 – 484, 2004.

[11] Michael A. Nielsen and Isaac L. Chuang. *Quantum Computation and Quantum Information: 10th Anniversary Edition.* Cambridge University Press, New York, NY, USA, 10th edition, 2011.

[12] Ryszard Horodecki, Paweł Horodecki, Michał Horodecki, and Karol Horodecki. Quantum entanglement. *Rev. Mod. Phys.*, 81:865–942, Jun 2009.

[13] Micha Horodecki, Pawe Horodecki, and Ryszard Horodecki. Separability of mixed states: necessary and sufficient conditions. *Physics Letters A*, 223(1):1 – 8, 1996.

[14] I. Bengtsson and K. Zyczkowski. *Geometry of Quantum States: An Introduction to Quantum Entanglement.* Cambridge University Press, 2007.

[15] M Plenio and Shashank Virmani. An introduction to entanglement measures. *Quantum Information and Computation*, 2005.

[16] William K. Wootters. Entanglement of formation of an arbitrary state of two qubits. *Phys. Rev. Lett.*, 80:2245–2248, Mar 1998.

[17] M. Born, E. Wolf, and A.B. Bhatia. *Principles of Optics: Electromagnetic Theory of Propagation, Interference and Diffraction of Light.* Cambridge University Press, 1999.

[18] F.R. Halpern. *Special Relativity and Quantum Mechanics.* Prentice-Hall, 1968.

[19] Andrew M. Steane. An introduction to spinors. 2013.

[20] J. Samuel. Poincaré sphere representation for three state systems. *J. Pramana - J. Phys. (1996) 47: 361*, 1996.

[21] S.W. Hawking and G.F.R. Ellis. *The Large Scale Structure of Space-Time.* Cambridge Monographs on Mathematical Physics. Cambridge University Press, 1973.

[22] S Chandrasekhar. *The mathematical theory of black holes.* Oxford classic texts in the physical sciences. Oxford Univ. Press, Oxford, 2002.

[23] H. Goldstein, C.P. Poole, and J.L. Safko. *Classical Mechanics.* Addison Wesley, 2002.

[24] J. Samuel, K. Shivam, and S. Sinha. Lorentzian geometry of qubit entanglement. *ArXiv e-prints*, 2018.

[25] Oliver Rudolph. Some properties of the computable cross-norm criterion for separability. *Phys. Rev. A*, 67:032312, Mar 2003.

[26] Asher Peres. Separability criterion for density matrices. *Phys. Rev. Lett.*, 77:1413–1415, Aug 1996.

[27] W. K. Wootters. Statistical distance and hilbert space. *Phys. Rev. D*, 23:357–362, Jan 1981.

[28] John Howie, Steven Duplij, Ali Mostafazadeh, Masaki Yasue, Vladimir Ivashchuk, Steven Duplij, Sergey Gukov, Theodore Voronov, Steven Duplij, Christos Kokorelis, George Papadopoulos, JosÉ CariÑena, and Angels Ramos. *Intertwined Operator*, pages 208–208. Springer Netherlands, Dordrecht, 2004.

[29] J.E. Avron and O. Kenneth. Entanglement and the geometry of two qubits. *Annals of Physics*, 324(2):470 – 496, 2009.

[30] Oliver Rudolph. Some properties of the computable cross-norm criterion for separability. *Phys. Rev. A*, 67:032312, Mar 2003.

[31] Mazhar Ali, A. R. P. Rau, and G. Alber. Quantum discord for two-qubit x states. *Phys. Rev. A*, 81:042105, Apr 2010.

[32] K. K. Sabapathy and R. Simon. Quantum discord for two-qubit X-states: A comprehensive approach inspired by classical polarization optics. *ArXiv e-prints*, November 2013.

[33] Roger Penrose and Wolfgang Rindler. *The geometry of world-vectors and spin-*

vectors, volume 1 of *Cambridge Monographs on Mathematical Physics*, page 167. Cambridge University Press, 1984.

[34] J. Samuel, K. Shivam, and S. Sinha. Detecting qubit entanglement : an alternative to the PPT test. *ArXiv e-prints*, December 2017.

[35] R.P. Feynman and A.R. Hibbs. *Quantum mechanics and path integrals.* International series in pure and applied physics. McGraw-Hill, 1965.

[36] R. Shankar. *Principles of Quantum Mechanics.* Springer US, 1995.

[37] Anirudh Reddy, Joseph Samuel, Kumar Shivam, and Supurna Sinha. Coarse quantum measurement: An analysis of the sterngerlach experiment. *Physics Letters A*, 380(11):1135 – 1140, 2016.

[38] P. Gomis and A. Pérez. A study of decoherence effects in the Stern-Gerlach experiment using matrix Wigner functions. *arXiv preprint quant-ph/1507.08541*, July 2015.

[39] Johannes Kofler and Caslav Brukner. Classical world arising out of quantum physics under the restriction of coarse-grained measurements. *Phys. Rev. Lett.*, 99:180403, Nov 2007.

[40] E. T. Jaynes. Information theory and statistical mechanics. *Phys. Rev.*, 106:620, 1957.

[41] *Entropy and the Time Evolution of Macroscopic Systems.* International Series of Monographs on Physics. OUP Oxford, 2008.

[42] B. P. et.al. Abbott. Observation of gravitational waves from a binary black hole merger. *Phys. Rev. Lett.*, 116:061102, Feb 2016.

[43] Aravind Chiruvelli and Hwang Lee. Quantum cramer-rao bound and parity measurement, 2010.

[44] S. Amari. *Information Geometry and Its Applications.* Applied Mathematical Sciences. Springer Japan, 2016.

[45] Yong Siah Teo. *Introduction to Quantum-State Estimation.* World Scientific, 2015.

[46] Anthony Chefles. Quantum state discrimination. *Contemporary Physics,* 41(6):401–424, 2000.

[47] Masao Osaki, Masashi Ban, and Osamu Hirota. Derivation and physical interpretation of the optimum detection operators for coherent-state signals. *Phys. Rev. A*, 54:1691–1701, Aug 1996.

[48] Stephen M. Barnett and Sarah Croke. Quantum state discrimination. *Adv. Opt. Photon.*, 1(2):238–278, Apr 2009.

[49] Thomas M. Cover and Joy A. Thomas. *Elements of Information Theory (Wiley Series in Telecommunications and Signal Processing).* Wiley-Interscience, 2006.

[50] Joseph W. Weinberg. The geometry of colors. *General Relativity and Gravitation,* 7(1):135–169, 1976.

[51] David L. MacAdam. Visual sensitivities to color differences in daylight∗. *J. Opt. Soc. Am.*, 32(5):247–274, May 1942.

[52] Hisaharu Umegaki. Conditional expectation in an operator algebra. iv. entropy and information. *Kodai Math. Sem. Rep.*, 14(2):59–85, 1962.

[53] Jonathon Shlens. Notes on kullback-leibler divergence and likelihood. *CoRR*, abs/1404.2000, 2014.

[54] Paolo Facchi, Ravi Kulkarni, V.I. Man'ko, Giuseppe Marmo, E.C.G. Sudarshan, and Franco Ventriglia. Classical and quantum fisher information in the geometrical formulation of quantum mechanics. *Physics Letters A*, 374(48):4801 – 4803, 2010.

[55] Dnes Petz. Geometry of canonical correlation on the state space of a quantum system. *Journal of Mathematical Physics*, 35(2), 1994.

[56] Dnes Petz. Covariance and fisher information in quantum mechanics. *Journal of Physics A: Mathematical and General*, 35(4):929, 2002.

[57] Hiroshi Hasegawa. Exponential and mixture families in quantum statistics: Dual structure and unbiased parameter estimation. *Reports on Mathematical Physics*, 39(1):49 – 68, 1997.

[58] Anna Jencova. Geodesic distances on density matrices. *Journal of Mathematical Physics*, 45(5), 2004.

[59] M. R. GRASSELLI and R. F. STREATER. On the uniqueness of the chentsov metric in quantum information geometry. *Infinite Dimensional Analysis, Quantum Probability and Related Topics*, 04(02):173–182, 2001.

[60] Dénes Petz and Gabor Toth. The bogoliubov inner product in quantum statistics. *Letters in Mathematical Physics*, 27(3):205–216, 1993.

[61] R. Kubo, M. Toda, and N. Hashitsume. *Statistical Physics II, Nonequilibrium Statistical Mechanics*. Berlin:Springer, 1991.

[62] C.W. Helstrom. Minimum mean-squared error of estimates in quantum statistics. *Physics Letters A*, 25(2):101 – 102, 1967.

[63] E. Ercolessi and M. Schiavina. Symmetric logarithmic derivative for general n-level systems and the quantum fisher information tensor for three-level systems. *Physics Letters A*, 377(3436):1996 – 2002, 2013.

[64] I. Contreras, E. Ercolessi, and M. Schiavina. On the geometry of mixed states and the fisher information tensor. *Journal of Mathematical Physics*, 57(6), 2016.

[65] V. Vedral. The role of relative entropy in quantum information theory. *Rev. Mod. Phys.*, 74:197–234, Mar 2002.

[66] Martin Bridson and Andre Haeflinger. *Metric Spaces of Non-Positive Curvature*. Springer, 2013.

[67] Noam Erez. Thermodynamics of projective quantum measurements. *Physica Scripta*, 2012(T151):014028, 2012.

[68] L.D. Landau and E.M. Lifshitz. *Statistical Physics*. Elsevier Science, 2013.

[69] John C. Baez. Renyi Entropy and Free Energy. *arXiv e-prints*, page arXiv:1102.2098, Feb 2011.

[70] Fumio Hiai and Dnes Petz. The proper formula for relative entropy and its asymptotics in quantum probability. *Comm. Math. Phys.*, 143(1):99–114, 1991.

[71] Vittorio Giovannetti, Seth Lloyd, and Lorenzo Maccone. Quantum metrology. *Phys. Rev. Lett.*, 96:010401, Jan 2006.

[72] Marcin Zwierz, Carlos A. Pérez-Delgado, and Pieter Kok. General optimality of the heisenberg limit for quantum metrology. *Phys. Rev. Lett.*, 105:180402, Oct 2010.

[73] Sueli I.R. Costa, Sandra A. Santos, and Joo E. Strapasson. Fisher information distance: A geometrical reading. *Discrete Applied Mathematics*, 197:59 – 69, 2015. Distance Geometry and Applications.

[74] Amalkumar Raychaudhuri. Relativistic cosmology. i. *Phys. Rev.*, 98:1123–1126, May 1955.